Characterizing the effect of amylase inhibitors on glycan metabolism by gut bacteria using fluorescent glycan labeling

Olivia Lui

Department of Pharmacology & Therapeutics
McGill University, Montreal

February 2022

A thesis submitted to McGill University in partial fulfillment of the requirements of the degree of Master of Science

TABLE OF CONTENTS

Abstract

Background: The human gut microbiota is an ecosystem of microorganisms which reside in the human gastrointestinal tract (GIT) and play an integral role in host health. Perturbation of the normal composition and function of the gut microbiota, known as dysbiosis, has been linked to chronic illnesses like inflammatory bowel disease, obesity, and type 2 diabetes (T2D). Furthermore, some gut microbes confer health benefits through carbohydrate fermentation and subsequent production of metabolites like short-chain fatty acids. It is thus important to consider the effect of drugs—particularly, oral drugs that pass through the GIT—on the gut microbiota. Amylase inhibitors, for instance, are used to treat T2D by inhibiting human α-amylase, a glycosyl hydrolase (GH) involved in starch metabolism. However, many gut bacteria also possess α-amylases and can be affected by amylase inhibitors. Acarbose is an amylase inhibitor that has been shown to inhibit the growth of certain bacterial species on starch. Another amylase inhibitor, montbretin A (MbA), has been reported to be specific for human α-amylase based on a panel of isolated bacterial amylases. Yet, the extent of both amylase inhibitor's effect on glycan metabolism in the gut microbiota remains to be fully appreciated.

Hypothesis: Given that bacterial uptake of polysaccharides, such as starch, requires extracellular hydrolysis by GHs into smaller oligosaccharides, we hypothesized that gut bacteria affected by amylase inhibitors can be identified by metabolic labeling with fluorescent glycan probes combined with flow cytometry and 16S rDNA sequencing.

Methods: Bacteria isolated from stool samples were incubated for one hour with fluorescein-conjugated maltodextrin (Mal-Fl)—a polysaccharide derived from starch—in the absence or presence of amylase inhibitor (acarbose or MbA). Mal-Fl^+ bacteria were sorted from non-labeled bacteria by fluorescence activated cell sorting and identified through 16S rDNA sequencing. To

validate our findings, labeling with Mal-Fl in the absence and presence of amylase inhibitor was performed on bacterial isolates presumed to be impacted in the metabolic labeling of stools. The effect of amylase inhibitors on metabolism and growth on maltodextrin was further investigated in these identified bacteria through growth assays.

Results: The overall uptake of Mal-Fl by stool bacteria was found to be affected by both acarbose and MbA in a manner that varied between stools of different individuals. Interestingly, we observed an increase in Mal-Fl labeling in the presence of amylase inhibitor in two different stool samples, contrary to what we would predict from GH inhibition by amylase inhibitors. We identified several bacteria in which the labeling by Mal-Fl was affected by amylase inhibitor, including *Agathobacter rectalis*, *Bacteroides vulgatus*, *Bacteroides xylanisolvens* and *Bifidobacterium adolescentis*. Growth of these bacteria on maltodextrin was indeed inhibited by amylase inhibitor, more often by acarbose than by MbA.

Conclusion: We demonstrated that our functional method of probing bacteria from stool samples with a fluorescently-labeled glycan can pinpoint members of the gut microbiota affected in their starch metabolism by amylase inhibitors. Further investigation into the growth of these identified bacteria underscored how these amylase inhibitors can create unforeseen effects on glycan metabolism of certain gut bacteria which can ultimately lead to broader consequences in the gut microbiota.

Résumé

Contexte: Le microbiote intestinal humain est un écosystème de micro-organismes qui résident dans le tractus gastro-intestinal et jouent un rôle essentiel dans la santé de l'hôte. La perturbation de la composition et de la fonction du microbiote intestinal est associée à des maladies chroniques telles que l'obésité et le diabète de type 2 (DT2). De plus, certaines bactéries intestinales confèrent des bienfaits pour la santé grâce à la production de métabolites comme les acides gras à chaîne courte. Il est donc important de considérer l'effet des médicaments oraux qui traversent le tractus gastro-intestinal sur le microbiote intestinal. Les inhibiteurs d'amylase, par exemple, sont utilisés pour traiter le DT2 en inhibant l'α-amylase humaine, une glycosyl hydrolase (GH) impliquée dans le métabolisme de l'amidon. Cependant, de nombreuses bactéries intestinales possèdent également des α-amylases et peuvent être affectées par les inhibiteurs d'amylase. Acarbose est un inhibiteur de l'amylase qui inhibe la croissance de certaines espèces bactériennes sur l'amidon. Montbretin A (MbA), un nouvel inhibiteur d'amylase sous étude, a lui été décrit comme étant spécifique à l'α-amylase humaine sur la base d'un panel d'amylases bactériennes isolées. Pourtant, l'étendue de l'effet des inhibiteurs de l'amylase sur le métabolisme des glycanes dans le microbiote intestinal reste à apprécier pleinement.

Hypothèse: Étant donné que l'absorption bactérienne de l'amidon nécessite une hydrolyse extracellulaire par les GHs en oligosaccharides plus petits, nous avons émis l'hypothèse que les bactéries intestinales affectées par les inhibiteurs d'amylase peuvent être identifiées par un marquage métabolique avec des glycanes fluorescentes combinées à la cytométrie en flux et au séquençage de l'ADNr 16S.

Méthodes: Les bactéries isolées à partir d'échantillons de selles ont été incubées pendant une heure avec de la maltodextrine conjuguée à la fluorescéine (Mal-Fl) - un polysaccharide dérivé de

l'amidon - en l'absence ou en présence d'acarbose ou MbA. Les bactéries Mal-Fl$^+$ ont été triées par tri cellulaire activé par fluorescence et identifiées par séquençage d'ADNr 16S. Pour valider nos résultats, des marquages avec Mal-Fl en l'absence et en présence d'inhibiteur d'amylase ont été réalisés sur des isolats bactériens présumés impactés dans le marquage métabolique de selles. L'effet des inhibiteurs de l'amylase sur le métabolisme et la croissance de la maltodextrine a été étudié plus en détail chez ces bactéries identifiées avec des courbes de croissance.

Résultats: L'absorption globale de Mal-Fl par les bactéries fécales s'est avérée être affectée à la fois par l'acarbose et le MbA d'une manière qui variait entre les selles des individus. Fait intéressant, nous avons observé une augmentation de marquage avec Mal-Fl en présence d'inhibiteur d'amylase dans deux échantillons de selles différents, contrairement à ce que nous prévoyions à partir de l'inhibition de la GH par les inhibiteurs d'amylase. Nous avons identifié plusieurs bactéries chez lesquelles le marquage par Mal-Fl était affecté par un inhibiteur de l'amylase, notamment *Agathobacter rectalis, Bacteroides vulgatus, Bacteroides xylanisolvens* et *Bifidobacterium adolescentis*. La croissance de ces bactéries sur la maltodextrine était en effet inhibée par l'inhibiteur d'amylase, plus souvent par acarbose que par MbA.

Conclusion: Nous avons démontré que notre méthode fonctionnelle de sondage des bactéries fécales avec un glycane marqué par fluorescence peut identifier les membres du microbiote intestinal affectés dans leur métabolisme de l'amidon par les inhibiteurs de l'amylase. Une enquête plus approfondie sur la croissance de ces bactéries identifiées a souligné comment ces inhibiteurs d'amylase peuvent créer des effets imprévus sur le métabolisme des glycanes de certaines bactéries intestinales, ce qui peut finalement entraîner des conséquences plus larges sur le microbiote intestinal.

Acknowledgements

I would first like to thank my supervisor, Dr. Bastien Castagner, for his invaluable guidance and continuous support of my learning and growth as a scientist. I am extremely grateful for his kindness and encouragements throughout my studies. I would like to thank my advisor, Dr. Anne McKinney, and my committee members, Dr. Corinne Maurice and Dr. Terry Hébert, for their insightful feedback. I am further grateful to Dr. Lharbi Dridi for training me on stool labeling, flow cytometry, and bacterial culturing, and for all the technical advice he has provided me to help shape my experimental methods. I am thankful for all my wonderful past and present lab members for always being helpful, especially Reilly, Rebecca, and Ryszard. I would also like to acknowledge Mark Hancock for his help with MALDI spectroscopy, and Camille Stegen and Julien Leconte for their assistance with flow cytometry. My gratitude extends to the Department of Pharmacology & Therapeutics for providing me with the opportunity to learn amongst the brightest individuals. I am deeply thankful for Leo, Helen, and Jenn, who have been my rocks throughout this entire experience. Finally, I am eternally grateful to my family for their love, encouragement, and support in all my endeavours.

Contribution of authors

Olivia Lui: synthesis, purification, and characterization of Mal-Fl. Stool labeling assays with Mal-Fl and flow cytometry of Mal-Fl labeled bacteria. DNA extraction and quantification of sorted cells, labeled with Mal-Fl. Culture of bacterial isolates and growth assays of isolates. Bacterial isolate labeling assays with Mal-Fl and flow cytometry of Mal-Fl labeled bacteria. DNA extraction, quantification, and PCR of 16S rDNA in bacterial isolates. Gram staining of bacterial isolates. Experimental design. Writing of this thesis.

Bastien Castagner: experimental design and project supervision.

Lharbi Dridi: method optimization of stool labeling, flow cytometry of labeled stool bacteria, DNA extraction and quantification of sorted cells and bacterial isolates, PCR of 16S rDNA in bacterial isolates, and gram staining of bacterial isolates. Isolation of *Bacteroides xylanisolvens*, *Bifidobacterium adolescentis* C6, and *Bifidobacterium adolescentis* C5 from VF74 stool and identification by MALDI-TOF. Project advising (microbiology).

Corinne Maurice: project advising (microbiology).

Emmanuel Gonzalez: project advising (bioinformatics) and 16S rDNA sequence analysis of labeled stools.

Ryszard Kubinski: synthesis, purification, and characterization of the first batch of Mal-Fl.

Reilly Pidgeon: Isolation of *Bifidobacterium adolescentis* C5 from VF74 stool and identification by MALDI-TOF.

1 Introduction

1.1 The human gut microbiota (GM)

1.1.1 Structure of the human GM

Hundreds of trillions of microorganisms reside in the human gastrointestinal tract (GIT)[1,2]; collectively, these microbes are known as the GM. The gene set of the GM, the microbiome, is estimated to be over 100 times that of the human genome[3]. While the GM comprises bacteria, fungi, archaea, and viruses, most studies on the GM to date have focused on bacteria due to their largest functional contribution in relative genomic content[4]. A given individual can harbour over 1000 species-level phylotypes (or 16S rRNA gene sequences that are usually ≥ 97% identical in sequence identity)[5]. Amongst the gut bacterial kingdom, two phyla dominate: the Firmicutes and the Bacteroidetes— together making up at least 90% of the microbial members[6]. The remaining proportion comprises Actinobacteria, Cyanobacteria, Fusobacteria, Proteobacteria and Verrucomicrobia phyla. The composition of GM can vary considerably between individuals due to interpersonal, geographical, lifestyle, and temporal factors[7]. Though, recurrent compositional patterns in the GM have been observed independent of age, gender, nationality, and body mass index, and have been termed "enterotypes"[8]. While three enterotypes—*Bacteroides*-, *Prevotella*- and *Ruminococcus*-enriched—were identified and did not differ in functional richness, the number and even the existence of enterotypes has been controversial[9].

1.1.2 Functions of the human GM

The GM, in conjunction with its host, has further been termed a "superorganism" due to the great species diversity, stability and resilience of a healthy GM, and its symbiotic interaction with the host[3]. Indeed, the GM carries out immune and metabolic functions that influence host health. Beginning from rapid colonization of the GIT at birth, the GM supports the development of the

intestinal mucosal and systemic immune system[2]. Major deficiencies in immune cell types and lymphoid organs, and impaired epithelial homeostasis are seen in germ-free (GF) animals[10-12]. Moreover, certain intestinal commensal bacteria, known as segmented filamentous bacteria, can stimulate the release of serum amyloid A1 by epithelial cells, the differentiation of Th17 cells, and IgA response[13,14]. The host further benefits from gut microbial *de novo* synthesis of vitamins that humans require but cannot produce themselves, including vitamins B_1, B_2, B_5, B_6, B_7, B_{12}, and K[15-17]. Bile acid (BA) biotransformation is another vital function carried out by the GM that can confer a protective effect on the liver against BA toxicity and suppress germination of pathogenic *Clostridioides difficile* spores[18,19]. The GM produces a number of other metabolites from dietary or host-derived substrates which include undigested or incompletely digested carbohydrates, dietary proteins, plant polyphenols, host mucins, desquamated epithelial cells and digestive enzymes[6,20]. Indeed, environmental factors like diet play a significant role in shaping the GM, even more so than host genetics[21]. Though some studies in healthy adults have remarked that an individual's GM composition remains stable over a long period of time[22,23] and can be resilient to antibiotics and pathogens to a certain extent[24], other studies have shown that diet alone can rapidly and distinctly influence GM composition and subsequent effects on the host[25-28]. Even subtle differences in dietary glycan structure can produce vastly different outcomes in GM composition and metabolic output[29].

1.2 Glycan metabolism

1.2.1 Metabolism of starch by the host

Owing to the large variety of linkage patterns and types of sugar monomers, polysaccharides are the most structurally diverse molecules in a biological system[30]. There are over twenty common monosaccharides with variable ring conformations (i.e., six-atom pyranose or five-atom furanose);

polysaccharides can have α- and/or β-glycosidic bonds, with multiple branching points from a single substituent, and/or covalent coupling to other biological molecules (i.e., proteins and lipids)[31]. The human body is genetically equipped with only the enzymes to digest the complex polysaccharide starch (e.g., amylose and glycogen), which consist of glucose substituents linked by α1,4 and α1,6 bonds. Human digestion of starch begins in the mouth where the complex polysaccharides are partially hydrolyzed by salivary α-amylases. Principal degradation of starch is achieved in the gut lumen by human pancreatic α-amylase (HPA), where linear and branched oligosaccharides (maltose, maltotriose, and dextrins) are produced from the hydrolysis of α1,4 bonds[32]. These oligosaccharides are further hydrolyzed into glucose monomers by α-glucosidases anchored to the gut epithelium. Within the brush border of the small intestine, lactases also break down lactose into glucose and galactose, sucrases hydrolyze sucrose into glucose and fructose, and α-dextrinases cleave the α1,6 glycosidic bonds in dextrins. The monosaccharides are ultimately absorbed into the bloodstream via enterocytes[33]. Under healthy conditions, starch molecules are almost fully digested[34].

1.2.2 Dietary fibers (DFs) and resistant starch (RS) are substrates for gut bacteria

DF and RS are polysaccharides that escape human digestion and become a major source of nutrients for colonic bacteria. Through a mutualistic role, gut bacteria ferment these DFs and RS into metabolites in which the host and syntrophic partners can utilize as an energy source, among other beneficial effects[31]. Derived from plant cell walls (i.e., of fruits, vegetables, and cereals), DFs can be soluble or insoluble. Insoluble DFs, such as cellulose and lignin, are highly fermentable whereas soluble DFs, like pectins or gums, have a relatively low fermentability but increase fecal bulking and decrease transit time[35]. RS is considered the most powerful substrate for the production of the short-chain fatty acid (SCFA) butyrate, and can be further classified into four

types: physically trapped starch (in coarse grains); starch granules rich in amylose; retrograded starch; and chemically modified starch[36]. In comparison to the limited array of digestive enzymes encoded in the human genome, some gut bacteria can individually produce hundreds of carbohydrate-active enzymes (CAZymes)[7]. Among these highly-capable degraders are the gram-negative *Bacteroides* spp. including *B. thetaiotaomicron* (*B. theta*), *B. ovatus*, *B. cellulosilyticus* and *B. xylanisolvens*[31]. CAZymes that cleave glycosidic bonds within polysaccharides are classified into either GHs or polysaccharides lyases (PLs). GHs hydrolyze glycosidic bonds[37] whereas PLs cleave bonds via an elimination mechanism[38]. According to the Carbohydrate Active Enzymes (CAZy) database (www.CAZy.org), there are currently 173 sequence-based families of GHs and 42 families of PLs[39]. Catalytic mechanism and stereochemical outcome are usually conserved within a family; however, substrate specificity can vary[7].

1.2.3 CAZymes involved in starch metabolism

Starch is one of the most abundant polysaccharides in a Western diet, with foods such as potatoes, bananas, rice, and cereal grains being particularly rich in starch[40,41]. Of the GH families 3, 13-15, 57, 119, and 126, which are associated with starch degradation[42], GH13s are among the most represented enzyme families in the GM[7,43]. The GH13 family is most often associated with initial degradation of starch through endo-hydrolysis[7,42]. While there are 41 subfamilies which are differentiated by sequence and activity of GH13 enzymes, there are two general subtypes: α-amylases and pullulanases[41]. α-amylases like HPA target α1,4 linkages whereas pullulanases hydrolyze α1,6 glycosidic bonds. Some enzymes can have a GH13 catalytic domain with carbohydrate binding modules (CBMs) that allow the enzymes to dock on the substrate, improving catalytic efficiency[41].

1.2.4 The starch utilization system (Sus) of Bacteroidetes

The digestion of complex polysaccharides like starch requires the concerted action of multiple enzymes along with transporters and glycan-binding proteins. In gut bacteria, glycan-specific targeting proteins are usually encoded in a multigene locus known as a polysaccharide utilization locus (PUL)[44]. One of the most well-known PULs is the prototypic Sus discovered in *B. theta* by Abigail Salyers' group[44]. This PUL comprises eight adjacent genes SusRABCDEFG that encode proteins involved in starch uptake and catabolism. On the outer membrane of the gram-negative bacterium, SusCDEFG capture and import soluble starch molecules[45,46] (Figure 1). The lipoproteins SusDEF bind starch molecules to the surface of the cell to facilitate hydrolysis of the glycosidic bonds by the membrane-tethered α-amylase SusG, producing maltooligosaccharides[47]. SusG has a GH13 catalytic domain, along with a CBM58—though, this CBM is more important for accessing insoluble starch[48]. Because starch is a large polymer of 105-108 Da in size, extracellular degradation by SusG is essential for starch utilization[41,47]. Furthermore, SusG has a unique ability to accommodate both α1,4 and α1,6 glycosidic bonds of branched and linear starch[49]. Once imported into the periplasm by the TonB-dependent transporter SusC[50], maltooligosaccharides are further broken down by the neopullulanase SusA and α-glucosidase SusB[51] (Figure 1). Glucose monomers produced can then be transported across the inner membrane into the cytoplasm. Within the periplasm, SusR, an inner membrane-spanning sensor/regulator, recognizes maltose and rapidly upregulates the expression of Sus genes[51] (Figure 1). All PULs in Bacteroidetes encode homologous SusCD proteins, glycan-binding lipoproteins like SusEF, and the appropriate GHs for a specific glycan, and thus have been termed "Sus-like" systems[44]. These systems have been identified for the uptake and catabolism of distinct polysaccharides such as arabinoxylan, rhamnogalacturonans, *O*-glycans, fructans, α-mannan, and porphyrin, to name a few[52-56].

1.2.5 Starch metabolism by Firmicutes and Actinobacteria

While the Sus and Sus-like systems are limited to the Bacteroidetes phylum, starch-specific PULs are also encoded within the genomes of gram-positive Firmicutes and Actinobacteria[41]. PULs among these bacteria are much more diverse in locus organization and in the genes involved. For instance, the uptake of hydrolyzed starch can be carried out through a variety of transport systems like ATP-binding cassette (ABC) transporters, major facilitator superfamily or phosphotransferase systems, and can be encoded within a PUL with one or more extracellular GH13s[41,57]. Leitch *et al.*[58] revealed through 16S rRNA sequencing of human fecal samples that 80% of sequences recovered from RS particles belonged to the Firmicutes species *Bifidobacterium* spp., *Ruminococcus bromii*, and *Eubacterium rectale*. These bacteria were indeed able to utilize ^{13}C-labelled starch[59].

1.2.5.1 Starch metabolism by *Bifidobacterium* spp.

Bifidobacteria are known to be one of the colonizers of the gut in early life due to their ability to utilize human milk oligosaccharides and intestinal mucins[60,61]. In starch-degrading bifidobacteria, various CBMs can be encoded with multimodular GH13 enzymes[62,63]. *Bifidobacterium adolescentis* L2-32, for example, encodes seven starch-specific GH13s in its genome with enzymatic activity for both α1,4 and α1,6 linkages (an amylopullanase)[41].

1.2.5.2 Starch metabolism by *R. bromii*

While *B. adolescentis* completely utilizes RS, *R. bromii* has been shown to be a primary degrader or a "keystone species", who provides starch by-products for secondary degraders like *B. theta* and *E. rectale*[64]. In accordance, it seems that *R. bromii* specializes in starch degradation as a majority of the identified GHs in its genome encode for GH13s[65]. Moreover, five out of seventeen of its GH13 enzymes contain a C-terminal dockerin domain[64,66]. Dockerins bind to cohesin

domains that are often found on structural proteins known as scaffoldins[67]. The dockerin-cohesin interaction is known to be one of the strongest protein-protein interactions in nature[68]. Discovered in cellulosomes—multiprotein cellulose-degrading complexes—of cellulolytic bacteria[67], RS-degrading multiprotein complexes in *R. bromii* have been termed amylosomes and allow for highly efficient degradation of RS[41,64,65] (Figure 1).

1.2.5.3 Starch metabolism by *Clostridium* cluster XIVa spp.

E. rectale, along with *Roseburia inulinovorans* and *Butyrivibrio fibrisolvens*, are butyrate-producing secondary RS-degraders belonging to the *Clostridium* cluster XIVa[41]. Each of these bacteria possess a cell-wall anchored GH13 α-amylase with various CBMs that is encoded in a PUL with ABC transporter genes[69-71] (Figure 1).

1.2.5.4 Starch metabolism by *Lactobacillus* spp.

Other secondary degraders outside of the *Clostridium* cluster XIVa include lactobacilli[72] who can utilize maltooligosaccharides released from RS. Amylopullulanase is the only extracellular GH that has been identified in *Lactobacillus* species including *L. fermentum*, *L. plantarum*, *L. mannihotivorans*, *L. amylovorans*, and *L. gasseri*[72]. The four-component ABC transporter system, encoded by genes MalEFG and MsmK, imports maltodextrins into the cytosol[72]. Then, intracellular amylopullulanases, dextranase and maltose phosphorylase work together to process imported maltodextrins[72]. The genes for these proteins are organized in a maltodextrin operon in most lactobacilli. Though, the MalEFG/MsMK transport system is absent in lactobacilli that grow rapidly on maltose as a sole carbon source[72]. One such bacterium is *L. sanfranciscensis* which has an alternative transport system for maltose uptake: the maltose-H+ symporter[73].

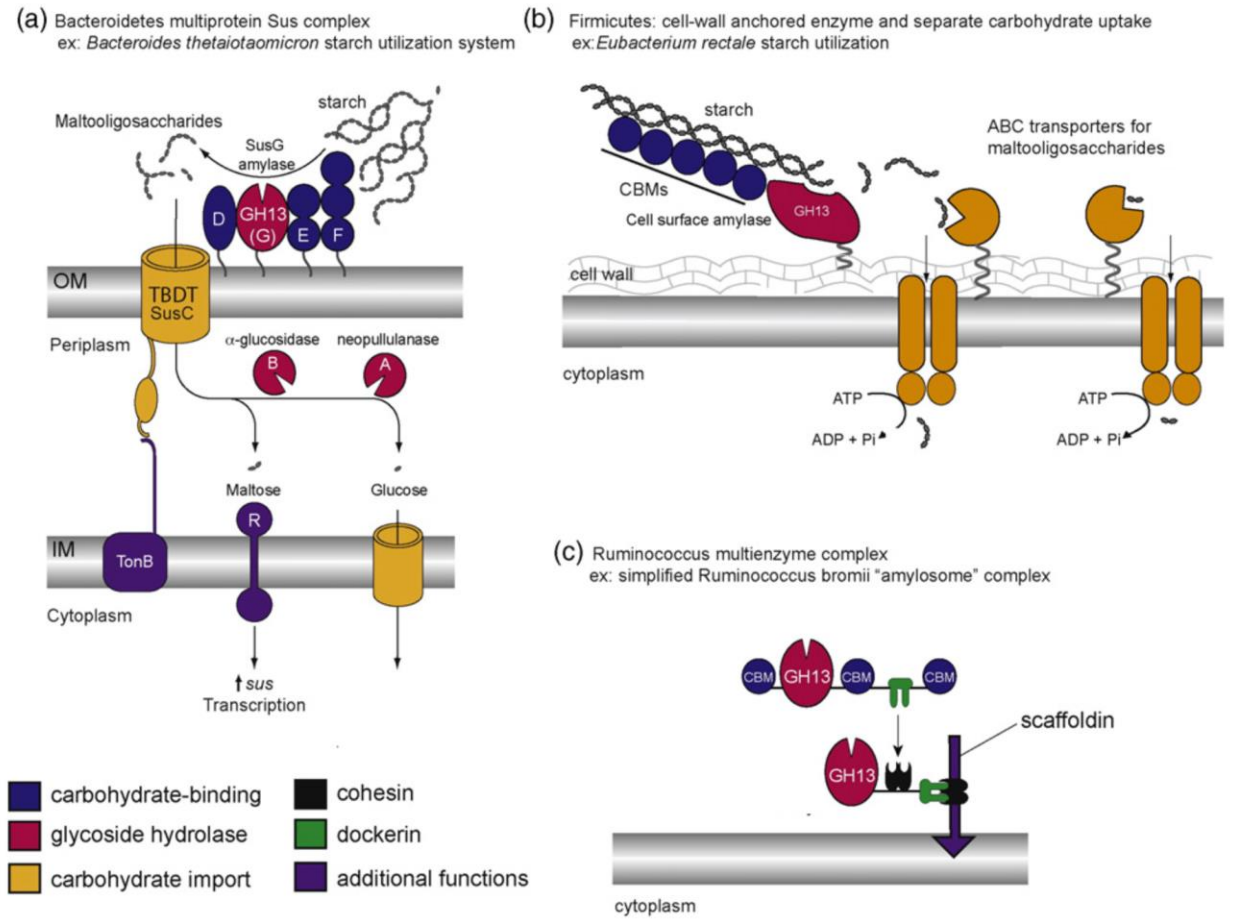

Figure 1. **Bacterial systems for maltodextrin uptake.** Adapted from Cockburn & Koropatkin[74]. A) *B. theta* starch utilization system. OM = outer membrane, IM = inner membrane, TBDT = TonB-dependent transporter. B) *E. rectale* starch uptake system. C) *R. bromii* amylosome.

1.3 SCFAs

Contributing around 10% of caloric requirements to the host[75], SCFAs—saturated fatty acids of six or less carbon atoms—are the major fermentation products of DFs and RS. The most abundant SCFAs, including butyrate (four carbon atoms), propionate (three carbon atoms) and acetate (two carbon atoms), are produced in the proximal colon[76]. Butyrate is mainly metabolized by colonocytes, providing around 60-70% of the energy needed for these cells to proliferate and

differentiate[77], while acetate and propionate travel through the portal vein to the liver. Propionate is then metabolized by hepatocytes and acetate can remain in the liver or is released to the peripheral venous system[78]. Indeed, many of the GM's effects on host health, particularly related to gut and immune homeostasis, are mediated by SCFA action through signalling pathways[35]. There are two main signalling mechanisms of SCFAs: inhibition of histone deacetylases (HDACs) and activation of G-protein coupled receptors (GPCRs). The effects of SCFAs on the host are broad, ranging from modulation of chemotaxis, reactive oxygen species production, cell proliferation and function, and gut intestinal barrier integrity, to anti-inflammatory, antitumorigenic, anorexigenic and antimicrobial effects[2,35,79,80].

1.3.1 HDAC inhibition by SCFAs

The acetylation of histones induces gene transcription by promoting access of transcription factors to promoter regions[81]. Since HDACs remove acetyl groups from histones, inhibition of HDACs by SCFAs increases gene activation. Relative to propionate and acetate, butyrate is considered the most potent inhibitor of HDACs[82-84]. The main effect resulting from SCFA-mediated HDAC inhibition is an anti-inflammatory immune response, particularly via suppression of the NF-κB pathway that leads to the release of inflammatory cytokines[85]. Butyrate and propionate have been shown to decrease the activity of NF-κB in human peripheral blood mononuclear cells, thus decreasing a lipopolysaccharide (LPS)-induced TNFα proinflammatory response[86]. Acetate has also been shown to decrease HDAC activity in human macrophages, decreasing the production of inflammatory cytokines IL-6, IL-8 and TNFα[87]. Furthermore, SCFA-mediated inhibition of HDAC9 enhanced the expression of the forkhead box P3 transcription factor, which increased proliferation and function of regulatory T cells (Tregs)[88,89].

1.3.2 Activation of GPCRs by SCFAs

Of the body's GPCRs, GPR43, GPR41, and GPR109A are the major ones with which SCFAs interact. GPR43, or free fatty acid receptor 2, is the most selective for acetate[90]. GPR43 is expressed along the entire GIT, particularly on intestinal peptide YY (PYY)- and glucagon-like peptide 1 (GLP-1)-producing endocrine L-cells[91,92], colonocytes and enterocytes[35]. Secretion of PYY and GLP-1 leads to insulin release and reduction of food intake, and so SCFAs can regulate body weight by acting on endocrine cells and mediating the release of these hormones[91,93]. SCFAs can further inhibit lipolysis[94] and stimulate adipocyte differentiation[95] via GPR43 on adipocytes. Within the GIT, GPR43 is also expressed on various immune cells[90,96,97] such as eosinophils, basophils, neutrophils, monocytes, dendritic cells and mucosal mast cells, and so immunomodulatory effects by SCFAs may occur not only via HDAC inhibition but also through GPR43 signalling[35]. GPR41, or free fatty acid receptor 3, is expressed in colonic mucosa and smooth muscle cells. Through GPR41 activation, SCFAs can induce phasic contractions of colonic smooth muscles and activate sympathetic ganglia to regulate body energy expenditure (i.e., via intestinal gluconeogenesis)[98-100]. The third main GPCR activated by SCFAs is GPR109A, a high affinity niacin receptor. GPR109A is highly expressed in adipocytes[101], and on immune cells like dermal dendritic cells, monocytes, macrophages and neutrophils[102]. Activation of GPR109A on adipocytes leads to reduced lipolysis and plasma free fatty acid levels[103]. In macrophages and dendritic cells, activation of GPR109a stimulates differentiation of Tregs and IL-10-producing T cells, suppressing inflammation and carcinogenesis[104].

1.4 Diet, dysbiosis and disease

Perturbations of the GM such that microbial diversity is decreased and proinflammatory or pathogenic species are increased, is characteristic of dysbiosis[105]. Loss of bacterial diversity in the

GM and increased incidence of inflammatory disease is often seen in populations of industrialized countries in which the quantity and diversity of complex glycans in the Western diet is also reduced[106-108]. In contrast, diets from rural areas of Africa are higher in DF and RS, and levels of SCFAs and its producers are high while the prevalence of inflammatory diseases is low[106,109]. One study found an inverse correlation between the consumption of DF and premature death associated with cardiovascular, infectious and respiratory diseases[110]. Thus, it has been suggested that diet can play a key role in dysbiosis and dysbiosis-associated diseases including but not limited to inflammatory bowel disease (IBD), obesity and T2D[108].

1.4.1 IBD

IBD, namely Crohn's disease and ulcerative colitis, are characterized by chronic and relapsing inflammation in the intestine[111]. Although the precise etiology of the disease remains under investigation, it is widely accepted that pathogenesis arises from intricate interplay of genetics, environmental factors, and the host immune system[112]. The GM has been thought to be implicated in IBD pathogenesis due to a number of IBD associated-susceptible genes that are involved in mediating host responses to GM[113,114], as well as an association of dysbiosis with IBD[115-117]. IBD-associated dysbiosis is generally observed as a lower microbial diversity, a decrease of Firmicutes and SCFA-producing bacteria (i.e., *Faecalibacterium prausnitzii* and *Clostridium* clusters IV, XIVa, and XVII), and an increase of mucolytic bacteria (i.e., *Ruminococcus gnavus* and *Ruminococcus torques*), sulfate-reducing bacteria (i.e., *Desulfovibrio*), and pathogenic bacteria (i.e., *Escherichia coli*)[112]. Furthermore, SCFA levels are reduced in IBD, which may contribute to abnormal intestinal and immune homeostasis[118,119].

1.4.2 Obesity

Obesity is a complex, multifactorial, and mostly preventable disease, chiefly associated with excess adiposity[120,121]. The obese GM has an increased ability to harvest energy from the diet[122]. Thought it remains unclear which specific bacteria are implicated in obesity pathogenesis, a decreased abundance of Bacteroidetes[123] and *Bifidobacterium* spp.[124,125] and an increase in *Enterobacteriaceae*[126] have been observed in obese compared to lean individuals. There is evidence that a dysbiotic GM may be linked to obesity through chronic low-grade inflammation and endotoxemia. Inflammation can be triggered by the LPS of gram-negative bacterial cell walls, binding to the toll-like receptor-4 (TLR-4) complex on innate immune cells[127]. High-fat diet (HFD)-induced obesity in mice led to increased circulating LPS levels[128]. Further, deletion of TLR-4 prevented insulin resistance induced by a HFD[129]. In humans, a high-fat and high-carbohydrate meal can similarly produce high plasma LPS levels and is associated with insulin resistance[130]. Further evidence implicating the GM in obesity pathology comes from a study by Ridaura *et al*.[131] Transplantation of the fecal microbiota from an obese co-twin into GF mice led to obese and abnormal metabolic phenotypes. When mice were co-housed with the microbiota from the lean co-twin, the invasion of *Bacteroides* spp. into the obese microbiota correlated with a protection against the obese phenotype. Importantly, this rescue was dependent on a low fat, high fiber diet. Among the *Bacteroides* spp. that contributed to the prevention of the obese phenotype was *B. theta*, which is markedly depleted in the obese GM. Another study showed that gavage with *B. theta* in specific-pathogen-free (SPF) mice decreased serum glutamate, body weight gain, and adiposity induced by HFD[132].

1.4.3 T2D

According to the World Health Organization, diabetes affected over 422 million people worldwide in 2014[133] and was among the top ten leading causes of death in 2019[134]. By 2030, it is estimated that the number of individuals with diabetes will rise to 552 million[135]. Accounting for 90-95% of all cases of diabetes, T2D is characterized by the body's inefficient use of insulin. It is most often clinically presented as hyperglycemia, hypertension and abnormal cholesterol levels[127]. Patients with T2D typically also have chronic inflammation and abnormal activation of the innate immune system, including upregulation of inflammatory factors like TNF-α and C-reactive protein[136-138]. Over time, life-threatening complications arise from damage to various organs such as the heart, blood vessels, eyes, kidneys and nerves. Considering lack of physical activity, high-sugar diets, and obesity are the major contributors of T2D, lifestyle changes are effective in preventing or delaying the onset of this syndrome. Metagenome-wide association studies suggest that there is a link between dysbiosis and T2D development[139,140]. Across both populations studied, opportunistic pathogens belonging to the *Clostridium clostridioforme* metagenomic cluster (*C. bolteae*, *C. hathewayi* and *C. clostridioforme*) were increased whereas butyrate-producing *Roseburia* were decreased in T2D microbiomes[139,140]. A more recent study in mice showed that the transplant of *Prevotella copri*, a bacterium associated with insulin resistance, into SPF mice can lead to the insulin-resistant phenotype in these mice[141]. Indeed, regulation of energy harvest and storage via SCFAs is likely a key function of the GM in countering the development of T2D[142]. As has been discussed above, SCFAs can stimulate intestinal gluconeogenesis, induce satiety, and reduce adiposity. In mice, dietary supplementation with butyrate prevented and treated HFD-induced insulin resistance by increasing energy expenditure and mitochondrial function[143]. BA metabolism has further been implicated in metabolic disease pathogenesis. Changes in the composition of

plasma BAs have been observed in diabetic patients[144,145]. Interactions between the host and GM indeed play an important role in BA metabolism and signalling.

1.5 Drugs and the GM

Recently, more emphasis has been placed on the topic of the GM in pharmacology as a target, a modifier, and a source of drugs[146-148]. However, when the GM becomes an unintended target or modifier of medications, consequences on the host can ensue. For example, proton pump inhibitors, used to treat gastric reflux, can alter the GM composition and increase susceptibility to gut infections[149,150]. In fact, a meta-analysis demonstrated associations between 17 drug categories and the relative abundances of individual microbial taxa[147]. Among these drug categories, proton-pump inhibitors, antidiabetic drugs (particularly metformin) and laxatives had the strongest associations to relative abundances of microbial taxa[147]. It is therefore important to consider how these xenobiotics interact with the GM. In this section, a few key examples of drug-GM interactions will be explored.

1.5.1 Metabolism of drugs by the GM

The GM plays a significant role in the metabolism of drugs[151]. Several prodrugs with azo bonds have been designed to be bioactivated by microbial azoreductases[146]. One such prodrug is sulfasalazine, a sulfonamide sulfapyridine linked with an azo bond to the anti-inflammatory compound salicylic acid[152]. The liberated salicylic acid can be, in turn, metabolized and inactivated by microbial arylamine, affecting the bioavailability of the drug[146]. Toxicity can be another outcome of microbial metabolism of xenobiotics. For example, microbial β-glucuronidases can re-activate anti-cancer and anti-inflammatory drug metabolites produced from the liver's detoxification pathway of glucuronidation[146].

1.5.2 Treatments for T2D

When lifestyle changes are not successful in lowering blood sugar levels, pharmacological interventions must be used to manage T2D[153]. Different organs influence glycemic levels: the brain via appetite, the kidney via glucose reabsorption, the liver via gluconeogenesis, muscle and adipose tissue via glucose uptake, the pancreas via insulin production and secretion, and the gut via sugar uptake and gut hormones[127]. As such, different anti-diabetic medications regulate blood glucose levels through action in these organs[127]. There is increasing evidence suggesting that T2D medications, particularly metformin, exert anti-diabetic effects via amelioration of gut dysbiosis. Unraveling the impacts of these drugs on the GM could suggest ways to improve the efficacy of current treatments for T2D.

1.5.2.1 Metformin

Metformin, the first-line treatment in newly diagnosed T2D patients, has multiple mechanisms of action including reducing hepatic gluconeogenesis and intestinal glucose absorption, and increasing glycogenesis and glucose uptake by muscle and adipose cells[127,154]. The most widely studied action of metformin is its ability to inhibit Complex I of the respiratory chain in mitochondria to suppress gluconeogenesis in the liver[154]. A multitude of studies have also highlighted a link between metformin's antidiabetic effects and the GM[155-160]. Notably, transplantation of metformin-treated fecal microbiota into GF mice increased glucose tolerance[157]. Numerous studies on metformin-treated T2D patients and rodents identified an increased abundance of *Akkermansia muciniphila*[155,156,159,161,162]. In fact, administration of *A. muciniphila* alone can increase glucose tolerance in HFD-fed mice[159]. It has been postulated that *A. muciniphila*'s cell wall contains a component that mimics metformin's antidiabetic action and improves the gut barrier[163]. Metformin also enriched the *Lactobacillus* genus[156,161,164], and other

SCFA-producing bacteria[157,162], including *Bifidobacterium adolescentis*[157]. Supplementation with *B. adolescentis* in rats with metabolic syndrome indeed recovered insulin sensitivity[165]. Bifidobacteria are thought to have anti-inflammatory effects and are associated with reduced endotoxemia and proinflammatory cytokine levels[166]. Biguanides like metformin also have anti-microbial properties. Metformin inhibits *Alistipes*, *Oscillibacter* and *Bacteroides* genera, which is significantly correlated with improved glucose homeostasis[167]. In T2D patients treated with metformin, abundance of *Bacteroides fragilis* and its bile salt hydrolase (BSH) were decreased while the BA glycoursodeoxycholic acid (GUDCA) was increased[160]. Antagonism of intestinal farnesoid X receptor (FXR), a nuclear receptor involved in BA metabolism, by GUDCA was found to improve metabolic outcomes in obese mice, suggesting one of metformin's modes of action is mediated through a *B. fragilis*—GUDCA—intestinal FXR axis[160].

1.5.2.2 Acarbose

α-glucosidase inhibitors like acarbose exert an anti-diabetic effect by inhibiting α-glucosidases required for glucose absorption in the intestine. Of all the current T2D medications, α-glucosidase inhibitors seem to most effectively reduce postprandial hyperglycemia[168]; the inhibition of carbohydrate catabolism directly modulates blood glucose levels and can even help with weight loss in T2D and prediabetic individuals[169]. Compared to the other two α-glucosidase inhibitors, miglitol and voglibose, acarbose is the most widely studied and has additional effects in decreasing inflammation[170] and stabilizing atherosclerotic plaques[171]. Produced by *Actinoplanes* sp., acarbose is a pseudo-tetrasaccharide made up of acarviosin bound to maltose[172] (

Figure *2*). Unlike other α-glucosidase inhibitors like voglibose and miglitol, acarbose can also reversibly and competitively inhibit α-amylases[172]. Acarbose binds the active site of α-amylase as

a transition state analog, with the protonated nitrogen of acarbose forming electrostatic interactions with the carboxylic acid residues (D197, E233, D300) within the active site[173].

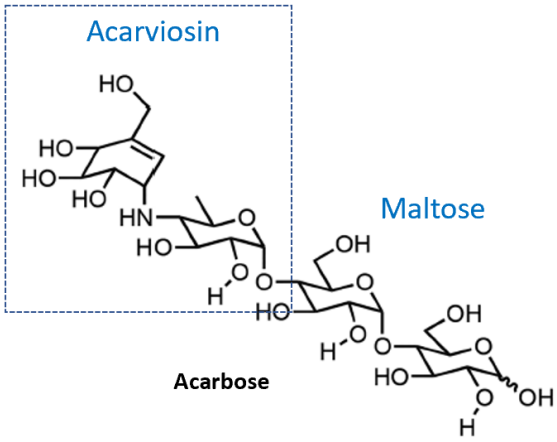

Figure 2. **Structure of acarbose**. Adapted from Santilli *et al*[174].

As acarbose, and other α-glucosidase inhibitors hinder the absorption of glucose in the upper intestinal epithelium, an increased concentration of oligosaccharides transits to the lower colon[175]. Rapid fermentation of these oligosaccharides by gut bacteria can lead to gastrointestinal side effects such as flatulence, bloating and diarrhea, which negatively impacts patient compliance.

Less than 2% of an oral dose of acarbose is absorbed into the bloodstream[176]; the drug acts locally in the GIT and is either excreted intact in the feces or is metabolized by bacterial and digestive enzymes in the gut[177]. Interestingly, α-amylases and cyclodextrin glycosyltransferases, in which the latter is commonly found in the genus *Bacillus*[178], can convert acarbose into longer-chain derivatives with additional acarviosyl residues. This creates a more active inhibitor such that acarbose can be considered a prodrug[179]. Another metabolite, formed by cleavage of a glucose unit from the tetrasaccharide, can remain active as an α-glucosidase inhibitor[176]. Other metabolites can be absorbed into the bloodstream and are then excreted by the kidneys.

In addition to generating an influx in dietary starch for microbes in the distal colon, acarbose can directly affect the GM through inhibition of bacterial amylases. Santilli *et al*.[174], showed that acarbose can inhibit the growth of two *Bacteroides* spp., *B. theta* and *B. fragilis*, on potato starch. This growth phenotype was postulated to be a result of SusG inhibition, as the two bacteria's growth with acarbose treatment were not affected on glucose. Interestingly, miglitol and voglibose did not affect the growth of these two species on starch. Furthermore, this growth inhibition by acarbose was selective since the growth of *Ruminococcus bromii* on starch was not affected by acarbose. With these findings, an important question remains: could acarbose cause potentially beneficial or detrimental compositional changes in the GM; for instance, by reducing the competition for a keystone starch utilizer like *R. bromii*, and other starch-metabolizing members?

Many research groups have utilized 16S sequencing to identify changes to the GM structure from acarbose treatment, in conjunction with measures of metabolites and physiological markers of T2D or other metabolic diseases. Restructuring of the GM in T2D by acarbose is often accompanied by a decrease in α-diversity[164,180,181]. Though the specific taxa affected vary between studies, the most consistent finding across studies with different animal models and patient populations is that *Lactobacillus* and *Bifidobacterium* taxa are enriched by acarbose, as seen in mice[182], rats[164], T2D patients[180,183], prediabetic individuals[181], and hyperlipidemic patients[184]. There is generally also an increase in SCFA production, particularly of butyrate[182,185-191]. This may be a direct consequence of the enrichment of butyrate-producing lactobacilli and bifidobacteria[192] and other SCFA-producing taxa. Often, an increased ratio of Firmicutes to Bacteroidetes[164] is observed, which is positively correlated with fecal SCFA levels[193]. Metagenomic prediction of sequenced fecal samples from Zucker diabetic fatty rats treated with acarbose showed that functional profiles

related to carbohydrate transport and metabolism, and energy production and conversion were enriched[164].

In a human supplementation study with prediabetic individuals, *Butyricicoccus*, *Phascolarctobacterium* and *Ruminococcus* genera were inhibited by acarbose treatment[181]. In contrast, operational taxonomic units (OTUs; i.e., sequences clustered based on similarity) that were increased by acarbose treatment belong to SCFA-producing taxa including *Lactobacillus*, *Faecalibacterium*, and *Dialister*. The genus *Dialister* was furthermore negatively correlated with HbA1c (glycated haemoglobin), and thus may play a role in glucose metabolism. Interestingly, this genus is non-fermentative, but some *Dialister* species can be stimulated by the intermediate metabolite succinate[194,195], hinting at the enrichment of this genus via increased SCFA production brought on by acarbose.

In T2D patients, it was also shown that acarbose increased the amounts of unconjugated primary BAs, cholic acid and chenodeoxycholic acid, and decreased amounts of plasma secondary BAs, mainly conjugated deoxycholic acids[180]. These changes in plasma BAs were not only correlated with metabolic improvements (related to body mass index, lipid profiles, and insulin resistance), but were also associated with increased relative abundances of BSH-expressing species *Lactobacillus gasseri* and *Bifidobacterium longum*, and decreased relative abundances of secondary BA producers *Bacteroides plebeius*, *Bacteroides vulgatus* and *Clostridium bolteae*. Indeed, the degree of BA metabolism alteration by acarbose depended on the baseline microbiota composition – those with *Bacteroides*-driven enterotypes showed greater changes in plasma BA composition and clinical benefits. The increase of *B. longum* after acarbose treatment was corroborated in another study in T2D patients, along with cardiovascular protective effects through decreases in proinflammatory cytokines, LPS and prothrombin activator inhibitor-1[183]. The notion

that acarbose lowers the risk of cardiovascular disease related to T2D is further supported by a decreased incidence of acute coronary syndrome, particularly myocardial infarction, due to acarbose treatment[196,197].

Acarbose further seems to have anti-inflammatory and immunomodulatory effects[198-200]. In collagen-induced arthritic mice, bacterial diversity that was lost as a result of arthritis was restored by acarbose treatment[198]. In particular, *Oscillospira*, *Desulfovibrio* and *Ruminococcus* genera were enriched in the acarbose-treated group, and *Lactobacillus*, *Anaeroplasma*, *Adlercreutzia*, *RF39* and *Corynebacterium* genera were decreased compared to the control group. When compared with miglitol, which is completely absorbed into the bloodstream, acarbose had more potent anti-arthritic effects, suggesting that the GM plays a role in mediating these effects.

Structural changes in murine GM due to acarbose treatment have even been associated with increased lifespan[190,201,202]. 16S sequencing of feces of treated mice showed an increase in the *Bacteroidales* family *Muribaculaceae* (historically called the S24-7), along with an increase in fecal propionate concentrations. Although, this increase was attributed to two main *Muribaculaceae* OTUs; other OTUs in this family decreased in abundance in treated mice.

Baxter and colleagues also highlight the diet-dependence of GM structural changes observed *in vivo* following acarbose treatment[182]. They found that a high dose of acarbose (400 ppm) affected the microbiota of mice fed a high starch diet such that *Bacteroidaceae* and *Bifidobacteriaceae* became enriched while *Verrucomicrobiaceae* (mainly *Akkermansia muciniphila*) and *Bacteroidales* S24-7 taxa decreased. When the mice were fed a high DF diet, the community structure was distinct with increased *Bifidobacteriaceae* and *Lachnospiraceae* levels by acarbose. These GM structure changes were furthermore reversible following cessation of acarbose treatment. Despite these precise differences, the overall metabolic outcome of increased butyrate

levels was conserved between diets. In other studies, acarbose treatment has been shown to increase acetate concentrations in human feces[188] and serum[185], and in rat portal blood and cecum[186]. Propionate has also been shown to be increased in mice feces[190] and in rat portal blood and cecum[186]. However, a decrease in propionate concentrations in the human feces[187,188,191] or serum[185] have also been found. Undoubtedly, there are a plethora of factors in the varying outcomes on GM composition and SCFA output between studies, including differences in microbial communities between humans and animal models and between different human populations.

1.5.2.3 MbA

To circumvent the undesirable gastrointestinal effects brought on by α-glucosidase inhibitors, researchers at the University of British Columbia sought a molecule to selectively inhibit HPA, the enzyme at the top of the starch degradation pathway[203]. A water-soluble flavonol glycoside, known as MbA was isolated from the underground corms of the plant *Crocosmia* sp. and was identified to have therapeutic potential for diabetes and obesity as a potent inhibitor of HPA (K_i = 8 nM)[203]. Its structure is made up of a myricetin and a caffeic acid moiety linked via a glucose-rhamnose disaccharide and flanked by terminal sugars (Figure 3). Compared to α-glucosidase inhibitors, MbA has a novel mechanism of glycosidase inhibition that involves internal π-stacking of the moieties, permitting optimal hydrogen bonding to HPA's active site carboxylic acid residues D197 and E233[173]. In Zucker diabetic fatty rats, MbA was shown to be effective and decreased plasma glucose and free fatty acid levels, as well as improved the oxidative stress levels and decreased markers of cardiovascular complications that are associated with diabetes[204]. Given its potential as a more pleasant therapeutic treatment for T2D, phase 1 clinical trials have recently been approved for MbA.

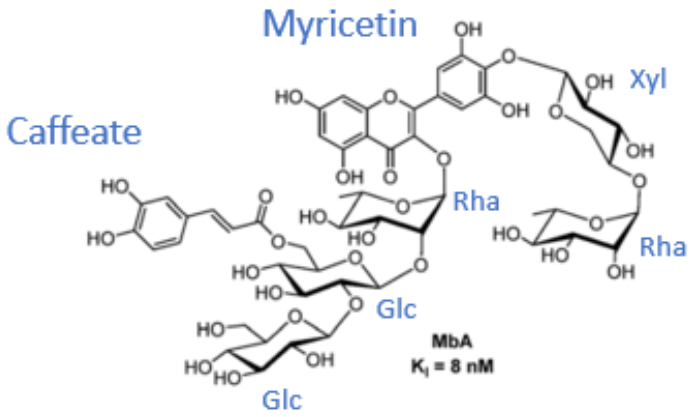

Figure 3. **Structure of MbA**. Adapted from Tysoe *et al*[205]. Glc = glucose, Rha = rhamnose, and Xyl = xylose.

Due to its complex structure, MbA uptake in the gut is limited, restricting the compound to its main site of action. Although this means that adverse effects from systemic bioavailability is minimized, there can be unintended consequences within the gut, as has been demonstrated by α-glucosidase inhibitors. Specificity for HPA has been the main strategy to reduce unwanted effects. Among a panel of host enzymes, including human α-glucosidase, maltase-glucoamylase and sucrose-isomaltase, MbA did not have inhibitory effects at 500 µM[173]. MbA was further shown to be specific for HPA among other GH13s from various sources, such as β-glucosidase (*Agrobacterium* sp.), β-galactosidase (*E. coli*), β-hexosaminidase (jack bean), α-mannosidase (jack bean), α-galactosidase (green coffee bean), and α-glucosidase (brewers' yeast)[203]. Finally, MbA was tested against bacterial amylases from *Clostridium* cluster XIVa spp., demonstrating that MbA (500 µM) does not inhibit the amylase from *Roseburia inulinivorans*, and only weakly inhibits the amylase from *Butyrivibrio fibrisolvens* (K_i = 1600 nM)[173]. These studies indeed provide a foundation for claiming MbA's specificity for HPA. However, the GM is a diverse and complex community that cannot be represented by a few isolated species. Given that the GM is intimately linked to host health, it is important to investigate how MbA, and other amylase inhibitors like acarbose, affect GM function.

1.6 Functional methods to study glycan metabolism by the GM

Traditional laboratory experiments to study the GM have relied on the laborious process of culturing isolates, of which only a small fraction of gut microbial taxa thus far have been successfully cultured[206]. Advances in higher-throughput metagenomic sequencing have allowed for greater understanding of GM diversity in relation to host health and disease[7]. However, genomic data alone, is not sufficient to infer *in vivo* functions nor whether bacteria are active, damaged, or responsive[207]. Function-driven genomics, where some form of functional sifting in combination with sequencing, is a key strategy to explore dynamic functional diversity[208]. With this approach, we can connect information from the population level (i.e., via flow cytometry), cell-level (i.e., using microscopy) and gene-level (i.e., from sequencing) to study cellular heterogeneity, phenotype, and genotype[209]. This section summarizes some examples of function-driven genomics applied to study glycan metabolism in the GM.

Fluorescently-labeled substrates have been shown to be a useful and versatile tool that can be applied to investigate the uptake of various glycans by bacteria from diverse samples. Martinez-Garcia *et al*. showed that their method of using fluorescently-labeled laminarin and xylan, fluorescence activated cell sorting (FACS) and single cell genomics, can rapidly recover the genomes of polysaccharide-degrading *Verrucomicrobia* from coastal and freshwater samples without the need for cultivation[210]. Reintjes and colleagues further employed epifluorescence microscopy and fluorescence in situ hybridisation (FISH) to visualize and identify uptake of fluorescently-labeled polysaccharides (FLA-PS) by marine bacteria from seawater samples. They were able to demonstrate a "selfish" polysaccharide uptake mechanism by the marine Bacteroidetes *Gramella forsetii* with incubation of FLA-PS in pure culture. Hehemann and colleagues also used epifluorescence microscopy to show the uptake of fluorescently-labeled α-

mannan and rhamnogalacturonan-II by *B. theta* isolate into the periplasm[211]. They further quantified the level of uptake using flow cytometry and revealed that ablation of the α-mannan and rhamnogalacturonan-II PULs results in a lack of fluorescence signal. More recently, Doud e*t al*. captured and characterized cellulose-degrading bacteria from geothermal springs using fluorescently-labeled cellulose, FACS and metagenomic sequencing[208]. Amplicon sequencing was done before cell sorting to survey the community, whereas whole genome amplification and shotgun sequencing were carried out on sorted cells to focus on differences in gene content of cellulose-degrading organisms.

Other techniques being developed involve the pairing of substrate-independent isotopic labeling (usually ^{18}O, ^{13}C, ^{15}N, ^{2}H) with various detection methods to follow the fate of the isotope label through the host and/or microbiota after administration[212]. For instance, Berry *et al*. used stable isotope probing (SIP) with heavy water, coupled with Raman microspectroscopy to detect active microbial cells that incorporated D_2O-derived D into their biomass[213]. Using this technique in conjunction with FISH, they characterized the activity of two dominant members of the mouse cecal microbiota, *Akkermansia muciniphila* and *Bacteroides acidifaciens*, on four different polysaccharides. Moreover, they identified novel mucin/glucosamine-degraders through Raman-based sorting and 16S rDNA sequencing. In another study, SIP coupled with 16S rRNA sequencing (RNA-SIP) has been used to identify members of the *Prevotellaceae* and *Ruminococcaceae* families from murine stool to be the primary assimilators of ^{13}C-labeled RS[214]. High-performance liquid chromatography-isotope ratio mass spectrometry was further carried out to examine the main fermentation products. In another study with an *in vitro* model of the human colon, RNA-SIP with ^{13}C-labeled starch and terminal-restriction fragment length polymorphism uncovered the interactions between starch-degraders[215]. Through this method, *Ruminococcus*

bromii was shown to be a primary degrader of starch, while *Prevotella* spp., *Bifidobacterium adolescentis* and *Eubacterium rectale* were involved further down the trophic chain through cross-feeding.

More recently, Patnode *et al.* studied the metabolism of polysaccharides by a consortium of bacteria associated with a lean phenotype[131] colonized into gnotobiotic mice[216]. Community-wide proteomics and forward genetic screens via transposon mutagenesis identified polysaccharide-processing genes required for the metabolism of bioactive fiber components that led to species expansion. They further demonstrated their use of magnetic beads coated with dietary polysaccharides as *in vivo* biosensors of bacterial degradation of polysaccharides. By deliberately manipulating the community, they revealed the nutrient-harvesting strategies and competition between species that underlie the selective effects of DFs.

1.7 Metabolic labeling with fluorescent glycan probes coupled to FACS and 16S rDNA sequencing

Our research group has used a functional and culture-independent method to identify glycan consumers from a human gut microbiota sample. The method involves using fluorescently-labeled glycans to metabolically label bacteria which are then sorted by FACS and identified by 16S rDNA sequencing. In Figure 4, taken from our submitted manuscript[217], we showed that cultured isolates are indeed labeled by fluorescein-conjugated cyclodextrin (CD-F) and fluorescein-conjugated nystose (NYST-F) after one hour of incubation with the probes (500 nM). Moreover, we used FACS on CD-F labeled cells from a stool sample to show that the labeling is a specific and energy-dependent process (Figure 5). Indeed, FACS is a powerful tool that allows us to study cellular phenotypes and physiology in a non-destructive manner. When coupled to sequencing, it further allows us to highlight specific traits, such as metabolism, in individual cells within complex

communities. In our submitted manuscript, we demonstrated the value of our method by identifying bacteria—from the stool samples of three unrelated individuals—that took up three different fluorescently-labeled glycan probes. Some of these identified bacteria had not been biochemically characterized for their metabolism of the specific glycan that they were labeled with, such as the metabolism of fructooligosaccharides by *Collinsella aerofaciens* and *Blautia wexlerae*. Still, we were able to find the appropriate CAZymes in their genomes that support their ability to metabolize these glycans. In this proof-of-concept study, we uncovered a method to deepen our knowledge of glycan metabolism in the GM. Going beyond basic understanding of the metabolic roles of specific GM members, we can apply this pipeline to examine the effect on these metabolic capabilities by various disease states, lifestyles, and diets.

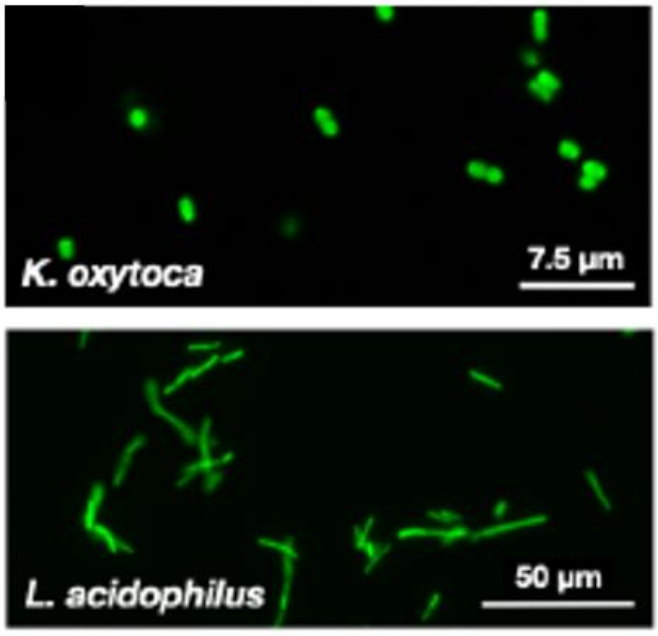

Figure 4. **Confocal microscopy image of *K. oxytoca* and 2-photon microscopy image of *L. acidophilus* after 1 h incubation with 500 nM CD-F and NYST-F respectively.** Adapted from our submitted manuscript[217].

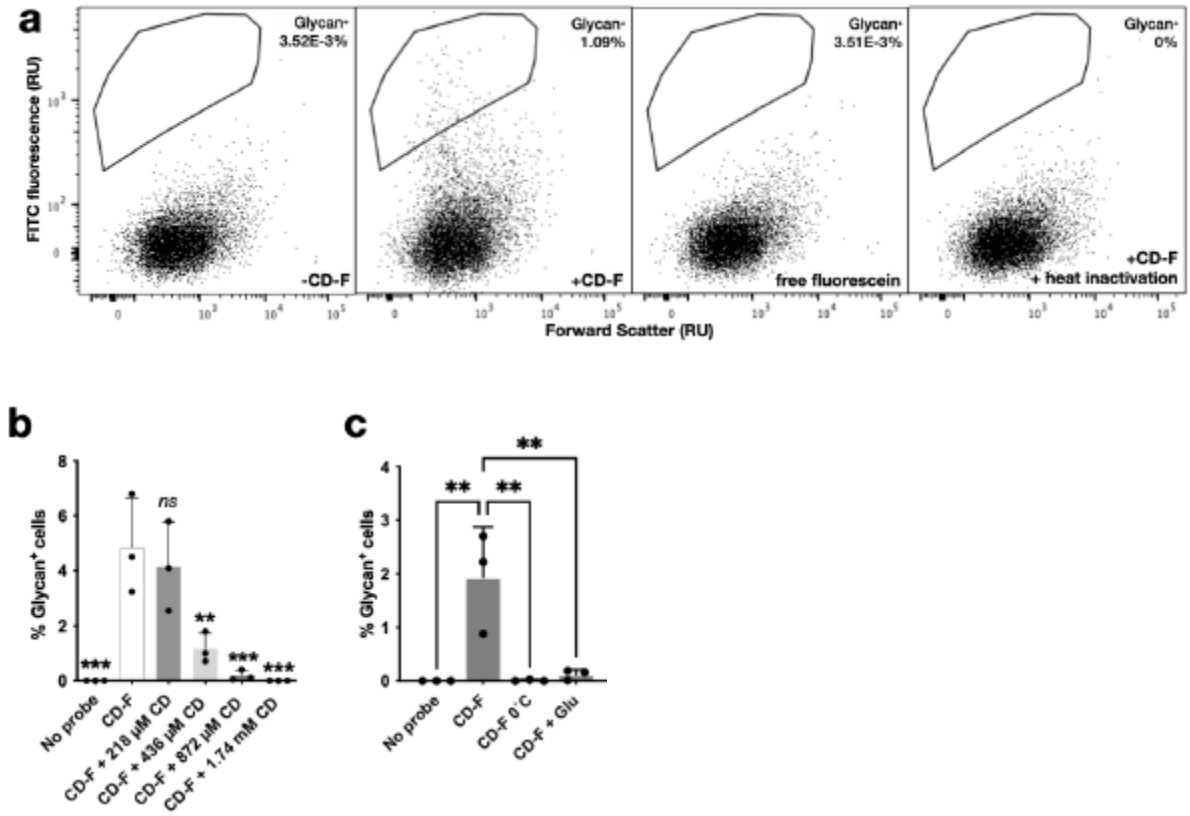

Figure 5. **Stool sample labeled with CD-F.** Adapted from our submitted manuscript[217]. A) Representative flow cytometric dot plots of bacteria labeled with 4.4 µM CD-F, with or without heat inactivation, or 4.4 µM free fluorescein. B) Percentage of CD-F+ cells labeled with increasing concentrations of free β-cyclodextrin (CD). C) Percentage of CD-F+ cells labeled when isolated bacteria are pre-incubated at 0ºC or in the presence of 0.1% glucose.

1.8 Hypothesis

Extracellular starch hydrolyzing enzymes of GH13 are commonly found in many different gut bacteria[7] and could be an unintended target of amylase inhibitors. We hypothesized that we could investigate the effect of amylase inhibitors on gut bacteria and their metabolism of starch through metabolic labeling with fluorescein-conjugated maltodextrin. Bacterial amylases that are inhibited by acarbose or MbA are expected to be unable to take up the Mal-Fl probe, and subsequent FACS and 16S rDNA sequencing can identify the affected bacteria (Figure 6). To test this hypothesis, the following specific aims were carried out:

1. Evaluate the level of Mal-Fl labeling in human stool samples with and without amylase inhibitor by flow cytometry.
2. Analyse sorted bacteria by 16S rDNA sequencing and differential abundance analysis.
3. Validate stool labeling results with Mal-Fl labeling in bacterial isolates with and without amylase inhibitor.
4. Assess the effects of amylase inhibitors on the growth of identified bacteria on maltodextrin.

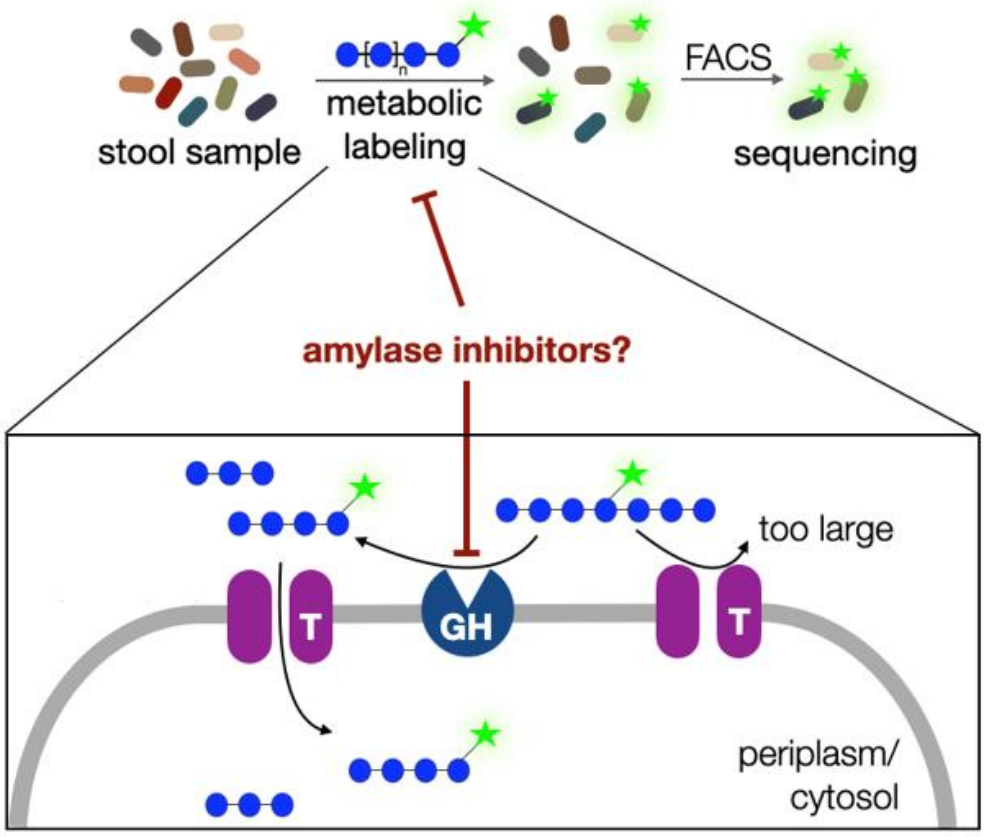

Figure 6. **Bacterial uptake of fluorescently-labeled maltodextrins inhibited by amylase inhibitors (acarbose or MbA) will be identified by FACS and 16S rDNA sequencing.** Rods = stool bacteria, blue circle = glucose unit, green star = fluorescent tag, GH = glycosyl hydrolase, T = transporter.

2 Methods

2.1 Synthesis of Mal-Fl probe

2.1.1 Synthesis, purification, and characterization of Mal-Fl

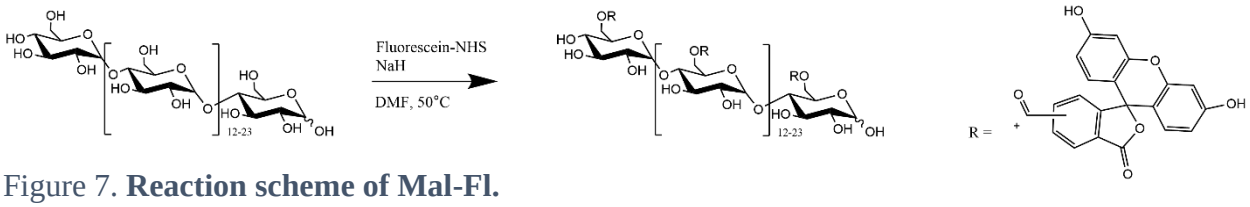

Figure 7. **Reaction scheme of Mal-Fl.**

2.5-3.0 mg (1 eq.) of maltodextrin (dextrose equivalent 4.0-7.0, Sigma-Aldrich) was dissolved in 200 µL of *N*,*N*-dimethyl formamide (DMF; 99.8% extra dry, anhydrous, ACROS Organics) at 50ºC while shaking at maximum speed for 30 minutes. After cooling, 6-8 beads of molecular sieves (4Å, ACROS Organics) were added, and the solution was gently shaken overnight at room temperature. The following day, the supernatant was transferred to a new 1.5 mL Eppendorf tube with 0.5 mg of sodium hydride (NaH; 60% in mineral oil). 3.6-3.9 mg (2 eq.) of 5/6-carboxyfluorescein *N*-hydroxysuccinimidyl ester (fluorescein-NHS; Thermo Fisher Scientific) was added and the mixture was shaken overnight at room temperature, covered in aluminum foil. In a new 1.5 mL Eppendorf tube, Dowex 50WX8 resin (ACROS Organics) was added to cover the bottom of the tube and was washed with 200 µL of DMF twice. The reaction mixture was transferred to the Dowex resin for acidification by rocking at room temperature for at least 3 hours under aluminum foil. The crude sample (supernatant) was diluted in 200-600 µL of aqueous acetonitrile (ACN; 25% v/v, Fisher Scientific, HPLC grade) and loaded onto a column packed with Sephadex LH-20 resin (1 cm x 17 cm) that was swelled overnight in aqueous ACN (25% v/v) and equilibrated with at least 1.5 column volumes of solvent. The sample was eluted with aqueous ACN (25% v/v), separating the functionalized sugars from the unreacted fluorescein. The fractions presumed to contain conjugated glycan (bright orange) and 3 subsequent fractions (presumed to

contain a mixture of functionalized sugar and unreacted fluorescein; less bright and more yellow) were filtered through cotton in a Pasteur pipette. These fractions were analysed by reverse-phase analytical liquid chromatography coupled to mass spectrometry (LC-MS) by injecting into an Agilent 1260 Infinity LC-MS system with a Waters XSelect CSH C18 column (5 µm, 3 mm x 150 mm). Solvents used include aqueous formic acid (mobile phase A; 0.1% v/v) and ACN (mobile phase B) with the following elution profile at a flow rate of 0.425 mL/min: 0-2 min, 100% A; 2-20 min, 100% B in A; 20-23 min, 100% A. Functionalized maltodextrins were observed as a broad mountain in the 280 nm absorption spectrum with a retention time between 9.5 and 12.5 minutes. Unconjugated fluorescein eluted between 12.5 and 13 minutes. The purity of fractions containing the functionalized sugar was approximated by peak integration of the 280 nm absorption spectrum and fractions with at least 85% purity were lyophilized and pooled (see Appendix A, Figure 25). The purified product was further characterized by matrix-assisted laser desorption/ionization-time of flight (MALDI-TOF) mass spectrometry using a Bruker UltrafleXtreme MALDI-TOF-TOF mass spectrometer calibrated with a bovine serum albumin tryptic digest standard in a universal matrix.

2.1.2 Quantification of Mal-Fl probe

The fluorescence intensity of 1/5 and 1/10 dilutions of probe (each in triplicate), and 0, 1, 5, 10, 25, 50, 75 and 100 µM of fluorescein sodium salts (Sigma-Aldrich) in H_2O were measured by a Tecan Spark 10M plate reader with excitation at 485 nm and emission at 535 nm. The blank (0 µM) value was subtracted from each measurement and the blank-subtracted fluorescence intensity of fluorescein samples were plotted against concentration. The standard curve was fitted to a linear equation. The average blank-subtracted fluorescence values of diluted probe were used to determine probe concentration from the standard curve equation and adjusted by dilution factor.

2.2 Labeling of human stool samples with Mal-Fl probe

Fresh human stools were collected by the Maurice Lab at McGill University, following the McGill Committee on Human Research Protocol (protocol A04-M27-15B). The screening criteria of stool donors included 18-60 years of age, no diagnosed gastrointestinal diseases, and abstinence from antibiotics for 6 months prior. Upon collection, stools were immediately introduced into an anaerobic chamber, aliquoted and frozen at -80ºC. Phosphate buffered saline (PBS; gibco) and minimum medium (MM; see Appendix A) were prepared and sterile filtered through a 0.2 µM filter. The PBS and MM were reduced in an anaerobic chamber overnight before each experiment. On the day of the experiment, an aliquot of stool was introduced into the anaerobic chamber and thawed at 37ºC for a few minutes. The following procedure was carried out in the anaerobic chamber. 1 mL of MM per 0.1 g of stool was added to homogenize the stool. The tube was vortexed to break up large particles, then mixed with a sterile inoculating loop to break up small particles, and vortexed once more. The tube was centrifuged at 700 g for 3 minutes and the pellet containing fecal mass was disposed. The supernatant containing the bacteria was centrifuged at 6500 g for 5 minutes and the bacterial pellet was washed with the same volume of MM previously added. The tube was centrifuged again at 6500 g for 5 minutes and the bacterial pellet was resuspended in 195 µL of MM per 0.1 g of stool. The appropriate volume of stool suspension was transferred to 1.5 mL Eppendorf tubes so that the total volume with probe and treatment was 200 µL per tube. Acarbose (TCI), MbA (generously provided by Dr. Stephen Withers at the University of British Columbia) and Mal-Fl probe were added to appropriate tubes, which were then incubated at 37ºC for one hour. The following are the final concentrations of treatments and probes: acarbose, 80 µM; MbA, 80 µM; and Mal-Fl, 0.4 µM. After the incubation period, the tubes were centrifuged at 6500 g for 5 minutes, the supernatant was discarded, and each pellet was washed with 1 mL of

PBS. This wash step was repeated once more to ensure any residual probe and MM were removed. The bacterial pellet was resuspended in 500 μL of PBS for flow cytometry.

2.3 Flow cytometry

Labeled samples were diluted in PBS for optimal resolution (1/50 or 1/100 dilution for stool samples, no dilution or 1/10 dilution for isolated bacteria). Flow cytometry analysis was performed on a BD FACSCantoII flow cytometer and cell sorting of labeled stool samples was performed on BD FACSAria-III or BD FACSAria Fusion flow cytometers. FITC fluorescence was measured with excitation at 488 nm and emission at 535 nm. A non-labeled sample of stool bacteria (negative control) was used to determine the basal fluorescence and 50,000 events were recorded for each sample. Analysis was done using FlowJo software. Gates were designed to include fluorescent-glycan positive (Mal-Fl^+) cells, and to exclude auto-fluorescent cells (based on B585/42 PE:B530/30 FITC detector filters; see Appendix A, Figure 26). For cell sorting, at least 400,000 Mal-Fl^+ cells of each sample and at least 1,000,000 non-labeled cells of the negative control were sorted through a 70 μm nozzle at 70 psi and collected for sequencing.

2.4 DNA extraction and sequencing

2.4.1 DNA extraction, quantification and 16S rDNA sequencing of sorted cells

DNA extraction of sorted cells was performed according to the protocol and with materials provided in the Qiagen AllPrep PowerFecal DNA/RNA Kit. The concentration of extracted DNA was determined using the Thermo Fisher Scientific Qubit dsDNA HS Assay Kit. DNA extracted from sorted cells was sent to Génome Québec where amplification and sequencing of the V4 region of the 16S rDNA gene was carried out on the Illumina MiSeq PE250 platform. Amplicon analysis

was done by Dr. Emanuel Gonzalez, at the Canadian Computational Centre for Genomics, using the ANCHOR pipeline.

2.4.2 DNA extraction and 16S rDNA amplification and sequencing of bacterial isolates

To confirm the purity of bacterial cultures, DNA was extracted, and the 16S rDNA gene was amplified and sequenced. DNA extraction of isolated bacterial cultures was performed according to the protocol and with materials provided in the BioBasic One-4-All Genomic DNA MiniPrep Kit. The concentration and purity of extracted genomic DNA were assessed by a Thermo Scientific NanoDrop 2000c spectrophotometer. The V1-V9 region of the 16S rDNA gene was then amplified by polymerase chain reaction (PCR). For *Bacteroides vulgatus, Agathobacter rectalis*, and *Ruminococcus bromii*, the PCR reaction mix was composed of Master Mix (abm), 100-250 ng of DNA, 27F and 1492R primers (0.4 μM each; AGAGTTTGATCMTGGCTCAG and TACGGYTACCTTGTTAYGACTT respectively), and nuclease-free water (Invitrogen) to bring the total volume up to 100 μL. For *Bacteroides xylanisolvens* and *Bifidobacterium longum* subsp. *infantis,* the PCR reaction mix contained ThermoPol Reaction Buffer (New England BioLabs), dNTPs (200 μM), 100-250 ng of DNA, 27F and 1492R primers (10 μM each), 0.5 μL of Taq DNA polymerase (New England BioLabs), and nuclease-free water (Invitrogen) to bring the total volume up to 100 μL. All reactions were carried out with 1 cycle at 94ºC for 30 seconds; 40 cycles at 94ºC for 30 seconds, 58ºC for 15 seconds, and 72ºC for 20 seconds; 1 cycle at 72ºC for 10 minutes; and held at 4ºC. To verify the success of the amplification, gel loading dye (Biolabs) was added to the PCR product and the sample was run through an agarose gel (1% w/v) containing SafeView Classic (0.01% v/v, abm). QuickLoad Purple 1 kb ladder (BioLabs) was used to determine the size of the PCR product, expected to be ~1.5 kb. The gel was visualized on a BioRad Molecular Imager Gel Doc XR system. Following the protocol from BioBasic EZ-10 Spin Column

DNA Gel Extraction Kit, the PCR product was isolated and purified from the gel, and the concentration and purity of PCR product were determined by a Thermo Scientific NanoDrop 2000c spectrophotometer. The V1 forward and V9 reverse complement sequences were obtained via Sanger sequencing of amplified 16S rDNA done by Génome Québec. Sequence ends were trimmed wherever the Phred quality score was below 10. Bases identified with an N within the trimmed sequences were replaced with the nucleotide observed in the chromatogram trace, if distinguishable. The full 16S rDNA sequence was assembled by combining the trimmed V1 forward sequence with the reverse complement of the trimmed V9 sequence and removing overlapping sequence. The identity of the full 16S sequence was finally confirmed by searching the NCBI 16S ribosomal RNA sequences (Bacteria and Archaea) database with BLASTn.

2.5 Culture of bacterial isolates

Isolated bacterial stocks were stored at -80ºC. Culture and manipulation of these bacteria were done in an anaerobic chamber. All media were pre-reduced overnight. *Bacteroides vulgatus* ATCC 8482, *Bacteroides xylanisolvens* (isolated from VF74 stool and identified by MALDI-TOF), *Bifidobacterium adolescentis* C6 (isolated from VF74 stool and identified by MALDI-TOF), *Eubacterium eligens* ATCC 27750, and *Agathobacter rectalis* ATCC 33656 were cultured on tryptic soy agar (TSA) with 5% sheep blood (remel). *Ruminococcus bromii* ATCC 27255 was cultured on M2 agar (see Appendix A). *Bifidobacterium adolescentis* DSM 20083 and *Bifidobacterium adolescentis* C5 (isolated from VF74 stool and identified by MALDI-TOF), and *Bifidobacterium longum* subsp. *infantis* ATCC 15697 were cultured on De Man, Rogosa and Sharpe (MRS; Sigma-Aldrich) agar supplemented with 0.05% cysteine. The cultures were incubated at 37ºC for 48-72 hours, then kept at room temperature for a maximum of one week (from inoculation date) before discarding or transferring colonies to fresh media.

2.6 Gram staining of *B. adolescentis* strains

For *B. adolescentis* DSM 20083, C6 and C5, amplification of the 16S rDNA by PCR was unsuccessful, and a gram stain was performed to verify the purity and cell morphology of the cultures. A few colonies of bacteria were homogenized in 200 µL of PBS. 10 µL of the bacterial suspension was smeared onto a microscope slide, and fixed by passing through a flame, then washing the smear in ethanol for 30 seconds and passing through a flame again. Gram staining was performed according to the protocol and with materials provided in the BD BBL Gram Stain Kit. The gram-stained smears were imaged using a Leica DM1000 microscope with 100X objective immersed in oil.

2.7 Labeling of *B. vulgatus* and *A. rectalis* isolates with Mal-Fl probe

Colonies of *B. vulgatus* from TSA with 5% sheep blood culture were inoculated in custom anaerobe basal broth (cABB; see Appendix A) supplemented with maltodextrin (0.2% w/v), and colonies of *A. rectalis* from TSA with 5% sheep blood culture were inoculated in cABB supplemented with sodium acetate (NaOAc; 4% w/v) and maltodextrin (0.2% w/v), Liquid cultures were incubated at 37ºC for 24-48 hours until growth (turbidity) was visible. Sterile filtered (through a 0.2 µM filter) PBS (1x) and MM were prepared the day before the experiment and reduced in an anaerobic chamber overnight. The following day, bacterial cultures were diluted with fresh media (dilutions of 1/25 and 1/50 for *B. vulgatus*; 1/20, 1/40 and 1/80 for *A. rectalis*), and 200 µL of diluted culture is transferred to each well in a 96-well plate. The optical density (OD) at 600 nm was recorded with an Epoch 2 microplate reader until bacterial growth reached mid-exponential phase (OD = 0.5-0.8). To ensure sufficient bacteria for the labeling, 4-5 wells (4 wells if OD = 0.7-0.8 and 5 wells if OD = 0.5-0.6) were pooled in a 1.5 mL Eppendorf tube per labeling condition. Each tube was centrifuged at 6500 g for 5 minutes and washed with 1 mL MM

each to remove residual carbohydrates. The bacterial pellet was resuspended in an appropriate volume of MM so that the total volume with probe and treatment was 200 μL per tube. Acarbose, MbA and Mal-Fl were added to appropriate tubes, which were then incubated at 37ºC for one hour. The following are the final concentrations of treatments and probes: acarbose, 80 μM; MbA, 80 μM; and Mal-Fl, 0.4 μM. After the incubation period, the tubes were centrifuged at 6500 g for 5 minutes, the supernatant was discarded, and each pellet was washed with 1 mL of PBS. This wash step was repeated once more to ensure any residual probe and MM were removed. The bacterial pellet was resuspended in 500 μL of PBS for flow cytometry.

2.8 Growth assessment of bacterial isolates

24-72 hours prior to the experiment, bacterial colonies were inoculated in liquid culture until visible growth (turbidity) was observed: *B. vulgatus*, *E. eligens* and *R. bromii* were inoculated in cABB supplemented with 0.2% w/v carbon source (glucose and/or maltodextrin); *A. rectalis* was inoculated in cABB supplemented with NaOAc (4% w/v) and maltodextrin (0.2% w/v); *B. adolescentis* DSM 20083, C6 and C5, and *B. longum* subsp. *infantis* were inoculated in semi-synthetic MRS (ssMRS; see Appendix A) supplemented with 0.75% maltodextrin (0.75% w/v); and *B. xylanisolvens* was inoculated in MM supplemented with maltodextrin (0.2% w/v). Depending on the turbidity of the culture, bacteria were diluted 1/10, 1/20 or 1/40 for the growth experiment. Growth on maltodextrin or glucose was assessed in cABB for *E. eligens* and *R. bromii*; cABB supplemented with NaOAc (4% w/v) for *A. rectalis*; MM for *B. vulgatus* and *B. xylanisolvens*; and ssMRS for *B. adolescentis* DSM 20083, C6 and C5, and *B. longum* subsp. *infantis* in a 96-well plate, with 200 μL of diluted culture and appropriate treatment per well. The OD at 600 nm was recorded with an Epoch 2 microplate reader for 72 hours. Maximum slope (growth rate), and lag time of growth curves were calculated by BioTek Gen5 software.

3 Results

3.1 Characterization of Mal-Fl probe

1 eq. of maltodextrin (dextrose equivalent 4.0-7.0, Sigma-Aldrich) was reacted with 2 eq. of fluorescein-NHS in the presence of NaH. The crude sample was acidified by Dowex 50WX8 resin and then purified by Sephadex LH-20 size exclusion chromatography. The fractions were assessed by reverse-phase analytical LC-MS to determine approximate purity. Fractions with at least 85% purity were pooled and further characterized by MALDI-TOF mass spectrometry. Mass spectra of purified Mal-Fl show m/z corresponding to $(M+Na)^+$ of monofunctionalized maltodextrins with a degree of polymerization (DP) between 7 and 24 (Figure 8 and Table 1), confirming the presence of the desired product. Specific masses of $(M+Na)^+$ and $(M+K)^+$ of non-functionalized maltodextrins with DP 6 to 14 are also observed (see Appendix B, Figure 27).

A)

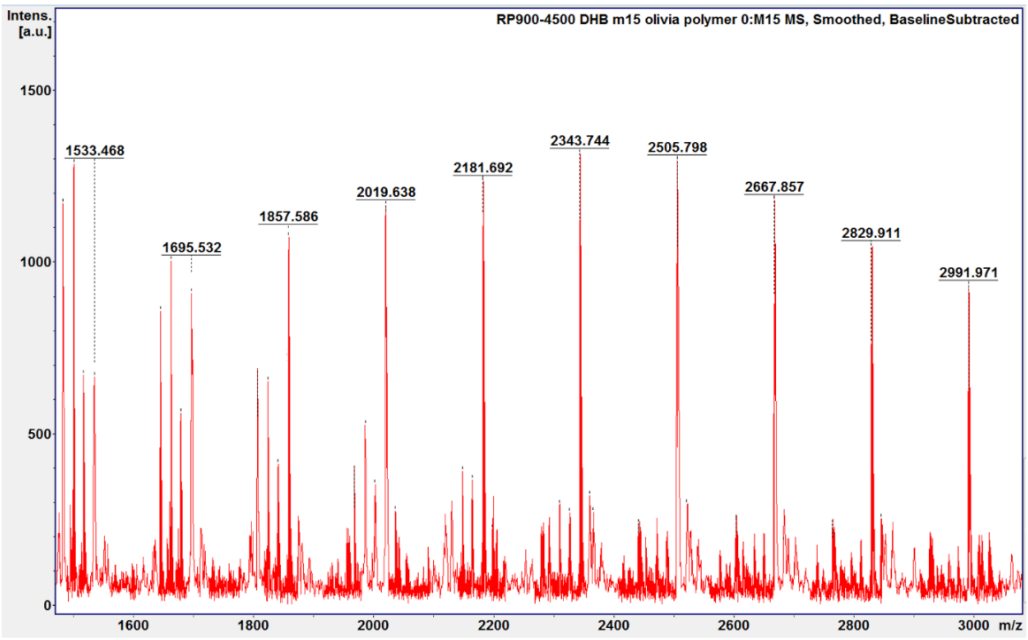

B)

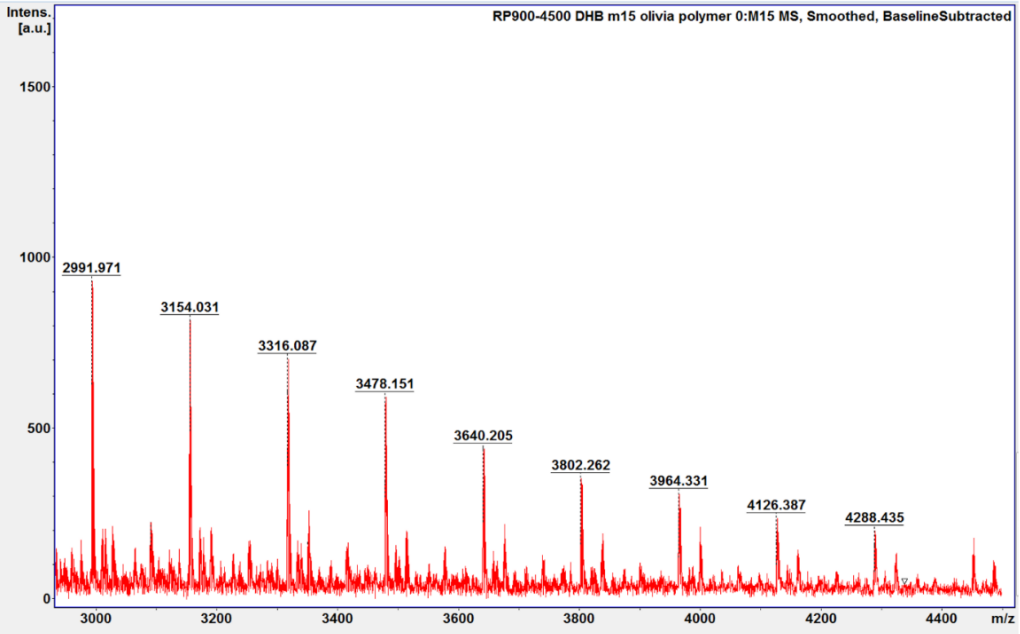

Figure 8. **MALDI mass spectra of purified Mal-Fl.** m/z $(M+Na)^+$ corresponding to monofunctionalized maltodextrins with DP A) 7 to 16 and B) 16 to 24.

Table 1. **Specific masses of monofunctionalized maltodextrins.**

Degree of polymerization	**Chemical formula**	**m/z $(M+Na)^+$ calculated**	**m/z $(M+Na)^+$ found**
7	$C_{63}H_{82}O_{42}$	1533.41	1533.468
8	$C_{69}H_{92}O_{47}$	1695.46	1695.532
9	$C_{75}H_{102}O_{52}$	1857.52	1857.586
10	$C_{81}H_{112}O_{57}$	2019.57	2019.638
11	$C_{87}H_{122}O_{62}$	2181.62	2181.692
12	$C_{93}H_{132}O_{67}$	2343.67	2343.744
13	$C_{99}H_{142}O_{72}$	2505.73	2505.798
14	$C_{105}H_{152}O_{77}$	2667.78	2667.857
15	$C_{111}H_{162}O_{82}$	2829.83	2829.911
16	$C_{117}H_{172}O_{87}$	2991.88	2991.971
17	$C_{123}H_{182}O_{92}$	3153.94	3154.031
18	$C_{129}H_{192}O_{97}$	3315.99	3316.087
19	$C_{135}H_{202}O_{102}$	3478.04	3478.151
20	$C_{141}H_{212}O_{107}$	3640.09	3640.205
21	$C_{147}H_{222}O_{112}$	3802.15	3802.262
22	$C_{153}H_{232}O_{117}$	3964.20	3964.331
23	$C_{159}H_{242}O_{122}$	4126.25	4126.387
24	$C_{165}H_{252}O_{127}$	4288.30	4288.435

3.2 Labeling of human stools with Mal-Fl in the absence and presence of amylase inhibitor

Bacteria isolated from the stool samples of three healthy volunteers were incubated with 0.4 µM Mal-Fl in MM for one hour at 37ºC in the absence and presence of 80 µM acarbose or MbA. Labeled cells were washed twice with PBS and then diluted in PBS for flow cytometry. A non-labeled and non-treated negative control sample was used to adjust forward (FSC) and side scatter (SSC), and fluorescent detectors. Mal-Fl$^+$ cells were gated on a PE (582/42 bandpass filter) vs. FITC (530/30 bandpass filter) dot plot designed to exclude auto-fluorescent cells. In YM54 stool, the mean proportion of Mal-Fl$^+$ cells significantly decreased with either amylase inhibitor treatment ($p = 0.0247$ for acarbose; $p = 0.0219$ for MbA) compared to the non-treated control (Figure 9). Interestingly, in VF74 and JD98 stools, a significant increase in the mean proportion of labeled cells was observed with acarbose treatment in VF74 stool ($p = 0.0422$) and with MbA treatment in JD98 stool ($p = 0.0056$) compared to the non-treated controls. We sought to investigate this effect in VF74 and JD98 stools, and to identify, in particular, which bacteria were directly impacted by the amylase inhibitors.

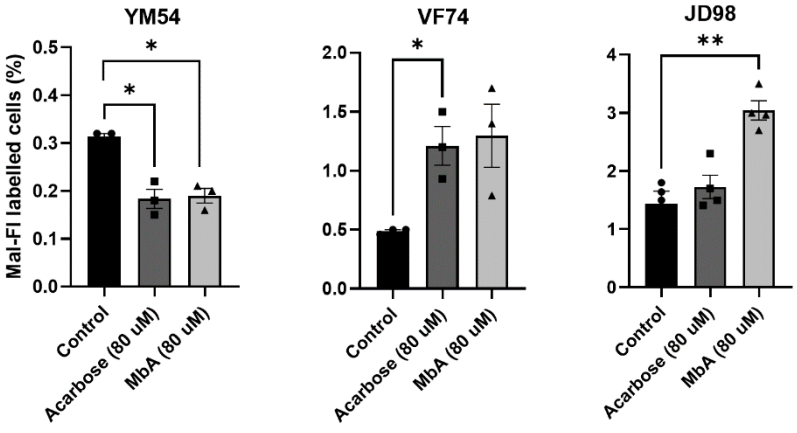

Figure 9. **Percentage of cells from human stool samples metabolically labeled with Mal-Fl in the absence and presence of amylase inhibitor.** Mean ± SEM shown (n = 3 in YM54, VF74; n = 4 in JD98). Paired t-tests were conducted between the non-treated control and each treatment group; * $p < 0.05$, ** $p < 0.01$.

3.3 16S rDNA sequence analysis in JD98 stool

To identify the bacteria impacted by the amylase inhibitor, we performed the same metabolic labeling experiments on JD98 stool with Mal-Fl in the presence and absence of the amylase inhibitors. Using FACS, we then sorted Mal-Fl^{+} cells from Mal-Fl^{-} cells through a 70 μm nozzle at 70 psi. At least 400,000 Mal-Fl^{+} cells from labeled samples and 1,000,000 non-labeled cells from the negative control (i.e., non-labeled and non-treated) were collected after sorting. DNA was extracted from the collected cells using the Qiagen AllPrep PowerFecal DNA/RNA Kit. The V4 region of 16S rDNA of these samples were amplified and sequenced by Génome Québec through the Illumina MiSeq PE250 platform. Analysis of the amplicon data was done using the ANCHOR pipeline by our collaborator, Dr. Emmanuel Gonzalez. Essentially, amplicons were assembled and dereplicated sequences were annotated against four major sequence repositories (NCBI-curated bacterial and Archaea RefSeq, NCBI nr/nt, SILVA and Ribosomal Database Project) with identity and coverage thresholds of >99%[218]. Annotated sequences with the same database accession ID were grouped into exact sequence variants (ESVs). A total of 92 ESVs were identified; 44 of these could be unambiguously assigned to a species with 100% coverage and identity.

The four sample types sorted and sequenced from JD98 stool include non-labeled cells from the negative control samples (Ctrl), and Mal-Fl labeled cells in the absence (MAL-F) and presence of acarbose (MAL-F + ACAR) or MbA (MAL-F + MbA). Redundancy analysis (RDA) of the sample compositions shows that the replicates of the same sample type cluster together (Figure 10). Notably, there are three distinct clusters: the first cluster comprises replicates of Ctrl samples, the second is made up of MAL-F + ACAR samples, and the third cluster encompasses both MAL-F and MAL-F + MbA samples. These results show that the composition of non-labeled cells from negative control samples is distinct from the composition of Mal-Fl labeled cells from all groups.

Furthermore, the composition of the Mal-Fl$^+$ population from MbA-treated samples is more similar to the Mal-Fl$^+$ population of the non-treated samples, than the composition of the Mal-Fl$^+$ population from acarbose-treated samples is to the non-treated group.

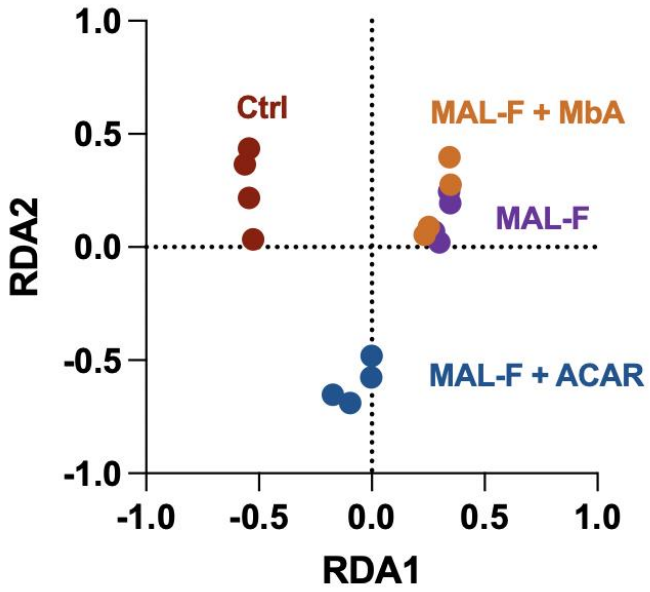

Figure 10. **RDA of sequenced JD98 samples composition (n = 4).** Samples of the non-labeled cells from the negative control are in red (labeled as Ctrl), samples of Mal-Fl$^+$ cells from the non-treated group are in purple (labeled as MAL-F), samples of Mal-Fl$^+$ cells with acarbose treatment are in blue (labeled as MAL-F + ACAR), and samples of Mal-Fl$^+$ cells with MbA treatment are in orange (labeled as MAL-F + MbA).

DESeq2 differential abundance analysis (DAA) was performed on ESVs from non-labeled cells of the negative control compared to Mal-Fl$^+$ ESVs of the non-treated control. Each data point in the volcano plot represents an ESV, with the colour depicting the phylum (Figure 11). The ESVs in the top left quadrant are significantly over-represented in the non-labeled population. In the top right quadrant, ESVs are significantly over-represented in the Mal-Fl$^+$ population, and those that are identified are ESVs assigned to a species. Here, we identified in JD98 stool *Agathobacter*

rectalis (synonymous with *Eubacterium rectale*; adjusted $p < 0.0001$), *Bifidobacterium adolescentis* (adjusted $p < 0.0001$ for ESVs 1 and 2; adjusted $p = 0.000254$ for ESV 3), *Bifidobacterium bifidum* (adjusted $p = 0.001315$), *Blautia massiliensis* (adjusted $p < 0.0001$), *Dialister invisus* (adjusted $p < 0.0001$), and *Faecalibacterium prausnitzii* (adjusted $p = 0.002109$) as significantly labeled by our Mal-Fl probe (Figure 11).

For each of the identified bacteria in Figure 11, the $\log_2$ fold change values in Mal-Fl^+ samples (non-treated, acarbose- and MbA-treated) relative to non-labeled samples are plotted in Figure 12. DESeq2 DAA was further carried out between the Mal-Fl^+ populations of non-treated and amylase inhibitor-treated samples. *A. rectalis* and *B. adolescentis* (ESVs 2 and 3) were significantly over-represented in the Mal-Fl^+ populations of the non-treated control compared to acarbose-treated samples ($p = 0.042263$ for *A. rectalis*; $p = 0.012333$ for *B. adolescentis* 2; $p = 0.024891$ for *B. adolescentis* 3; Figure 12). *F. prausnitzii* was significantly under-represented in the Mal-Fl^+ populations of the non-treated control compared to acarbose-treated samples ($p = 0.044381$; Figure 12). Moreover, *A. rectalis* was significantly over-represented in the Mal-Fl^+ populations of the non-treated control compared to MbA-treated samples (adjusted $p = 0.000649$; Figure 12).

DESeq2 DAA comparing Mal-Fl^+ ESVs from MbA-treated vs. acarbose-treated samples identified *B. adolescentis* 1 as significantly over-represented in the MbA-treated samples ($p = 0.03111$; Figure 13). ESVs found to be over-represented in the acarbose-treated samples are *Veillonella atypica* (adjusted $p = 0.001376$), *A. rectalis* ($p = 0.007711$), *Bacteroides vulgatus* ($p = 0.005633$) and *Bacteroides xylanisolvens* ($p = 0.037187$; Figure 13).

These bacteria that we have identified are potentially affected by amylase inhibitors. Thus, we sought to validate our findings through further *in vitro* experimentation with bacterial isolates.

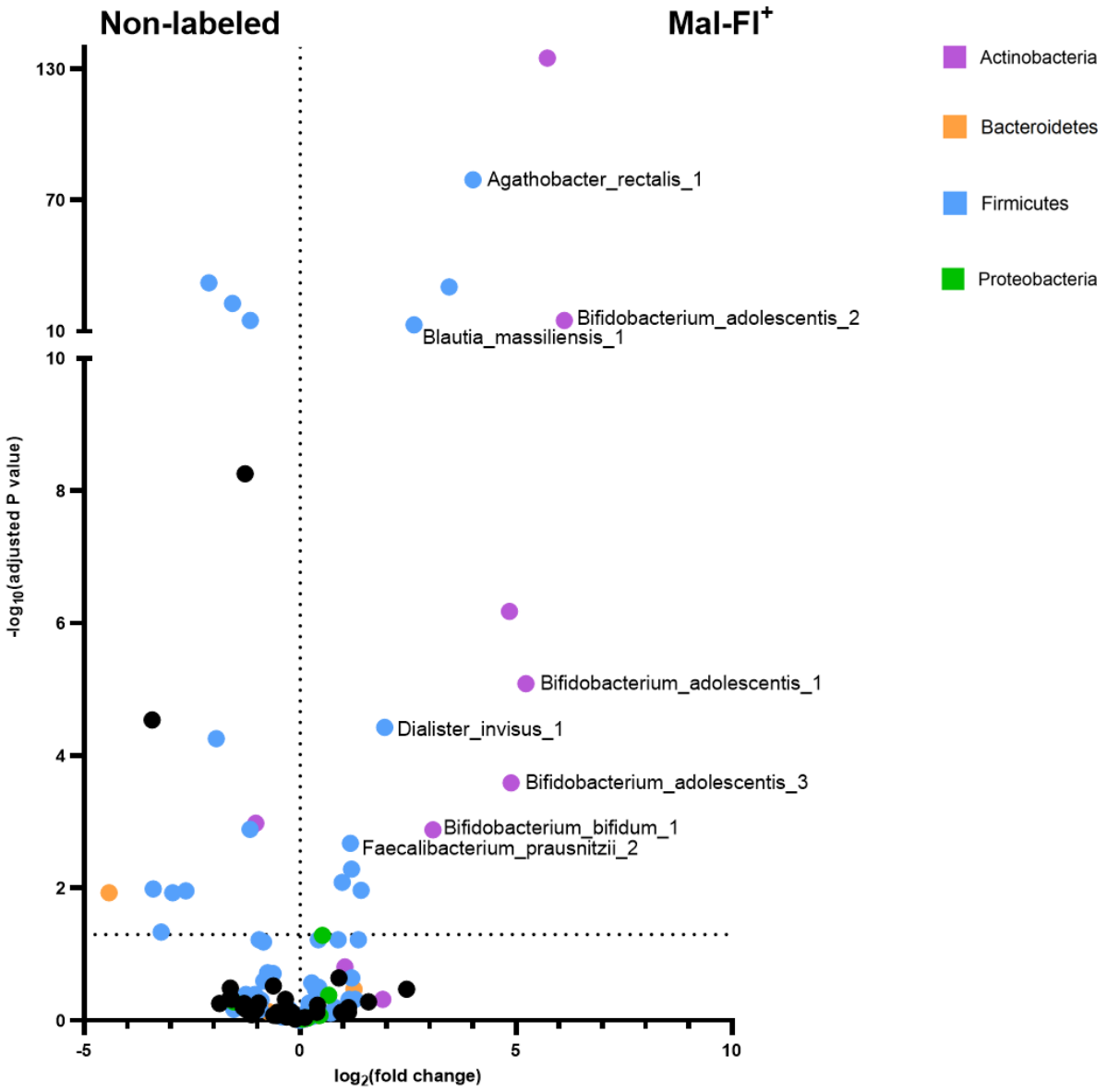

Figure 11. **DESeq2 DAA comparing the ESV abundance between non-labeled (left) and Mal-Fl$^+$ (right) JD98 samples.** ESV abundance in non-labeled negative control samples vs. Mal-Fl$^+$ of non-treated control samples presented in a volcano plot of adjusted p value vs. $\log_2$ fold change. The horizontal line represents the threshold for statistical significance with adjusted $p < 0.05$. Bacteria over-represented in the Mal-Fl$^+$ population compared to non-labeled population are identified at the species level.

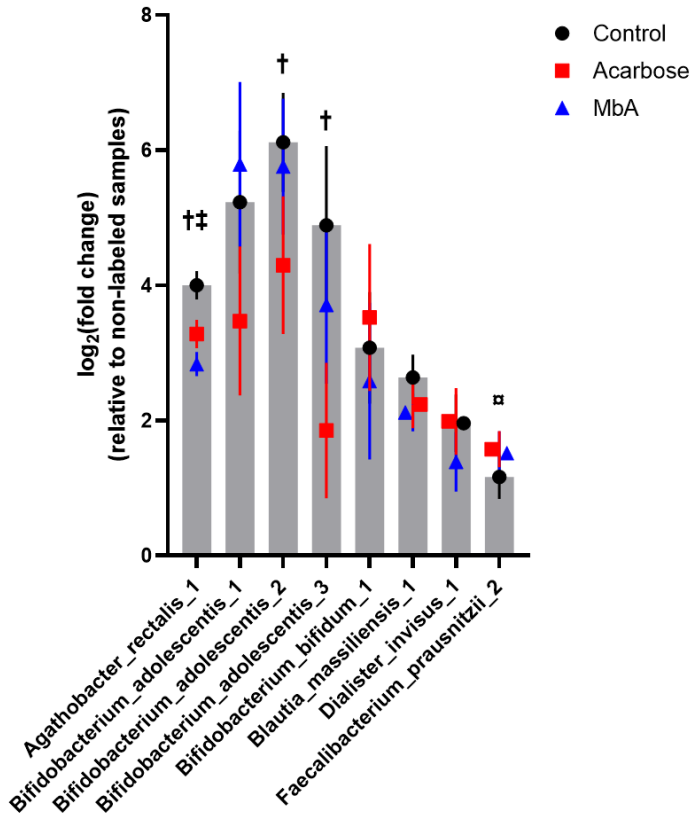

Figure 12. **log_2 fold change of abundances in Mal-Fl$^+$ (non-treated control, acarbose- and MbA-treated) samples relative to abundances in non-labeled negative control for ESVs significantly labeled with Mal-Fl**. † denotes ESV abundance over-represented in Mal-Fl$^+$ of non-treated control vs. acarbose-treated ($p < 0.05$) in DESeq2 DAA, ‡ denotes ESV abundance over-represented in Mal-Fl$^+$ of non-treated control vs. MbA-treated (adjusted $p < 0.001$) in DESeq2 DAA, ¤ denotes ESV abundance over-represented in Mal-Fl$^+$ of acarbose-treated vs. non-treated control ($p < 0.05$) in DESeq2 DAA.

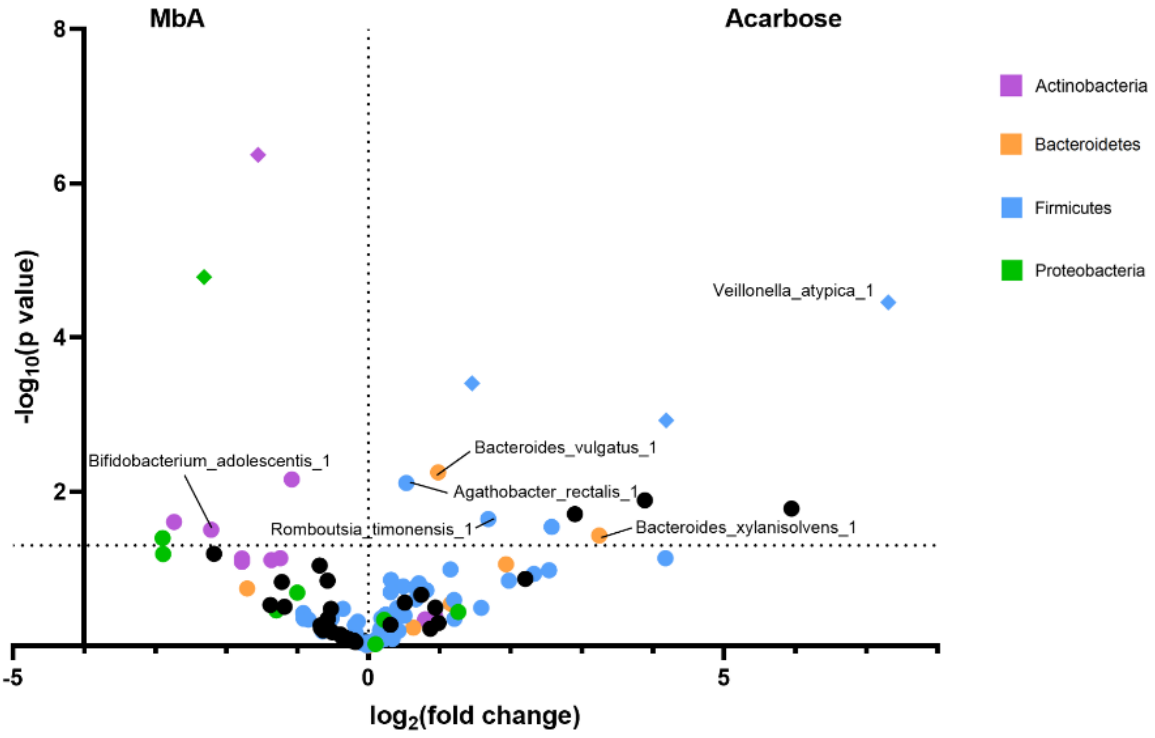

Figure 13. **DESeq2 DAA comparing the ESV abundance between Mal-Fl$^+$ MbA-treated (left) and Mal-Fl$^+$ acarbose-treated (right) JD98 samples.** Circles above the horizontal threshold are statistically significant with $p < 0.05$, diamonds are statistically significant with adjusted $p < 0.05$. Bacteria are identified at the species level.

3.4 16S rDNA sequence analysis in VF74 stool

Since Mal-Fl labeling was also increased in VF74 stool bacteria treated with acarbose, the labeling, sorting and 16S rDNA sequencing of the Mal-Fl$^+$ bacteria in VF74 stool was carried out in the same manner as was done in JD98 stool. However, due to a low level of labeling, the number of sorted Mal-Fl$^+$ cells in the non-treated control samples was not sufficient for amplicon sequencing. DESeq2 DAA comparisons of ESV abundances were done only between Mal-Fl$^+$ populations of acarbose- and MbA-treated samples (Figure 14). *Bacteroides vulgatus* was again identified to be over-represented in the Mal-Fl$^+$ population of acarbose-treated samples compared to MbA-treated samples, corroborating what was seen in the JD98 sequencing analysis.

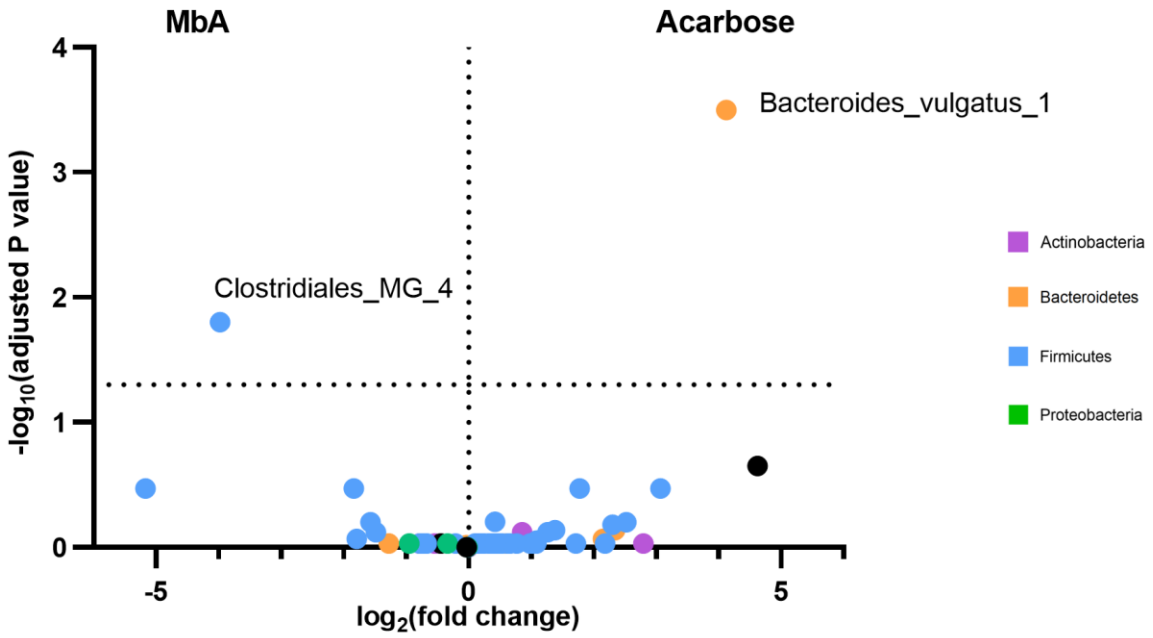

Figure 14. **DESeq2 DAA comparing the ESV abundance between Mal-Fl$^+$ MbA-treated (left) and acarbose-treated (right) VF74 samples.** Circles above the horizontal threshold represent statistical significance with adjusted $p < 0.05$.

3.5 Growth of *E. eligens* and *R. bromii* on maltodextrin in the presence of amylase inhibitors

In unpublished work produced by a former lab member, Suraya Yasmine, the 16S rDNA of ten different stool samples (including VF74 and JD98) labeled with Mal-Fl were sequenced. These results identified *Eubacterium eligens* and *Ruminococcus bromii* as Mal-Fl labeled bacteria. While starch metabolism has not yet been characterized in *E. eligens, R. bromii* is a well-known keystone starch degrader (Figure 1)[64]. We assessed the growth of both bacteria on maltodextrin in the absence and presence of amylase inhibitor. The goals of this assay were to 1) validate our fluorescent glycan labeling method and 2) test the effect of acarbose and MbA on maltodextrin metabolism and growth. *E. eligens* ATCC 27750 and *R. bromii* ATCC 27255 were cultured in cABB supplemented with 0.1% maltodextrin and 0.1% glucose for 72 hours before the growth experiment to ensure that stationary phase had been achieved. The bacteria were then diluted into fresh cABB supplemented with 0.2% maltodextrin, with or without amylase inhibitor, in a 96-well plate. The OD at 600 nm was recorded every 10 minutes for 72 hours to monitor growth. From the resulting mean growth curves, both bacteria were able to grow in media with maltodextrin as the sole carbon source, albeit the growth of *E. eligens* was slight (Figure 15). Moreover, the mean growth curves are nearly identical across the non-treated control and treated groups in *E. eligens* and are similar between non-treated and treated groups in *R. bromii*. No significant differences were found in the mean maximum OD (ODmax) between any of the amylase inhibitor groups and the non-treated controls for either *E. eligens* or *R. bromii* (see Appendix B, Figure 28A and B). Neither the mean maximum growth rate (MGR), calculated by the maximum slope of the curve, nor the lag time of *R. bromii* were significantly different between the non-treated control and treated groups (see Appendix B, Figure 28A and B). The amylase inhibitors did not affect the growth of either bacterium on maltodextrin.

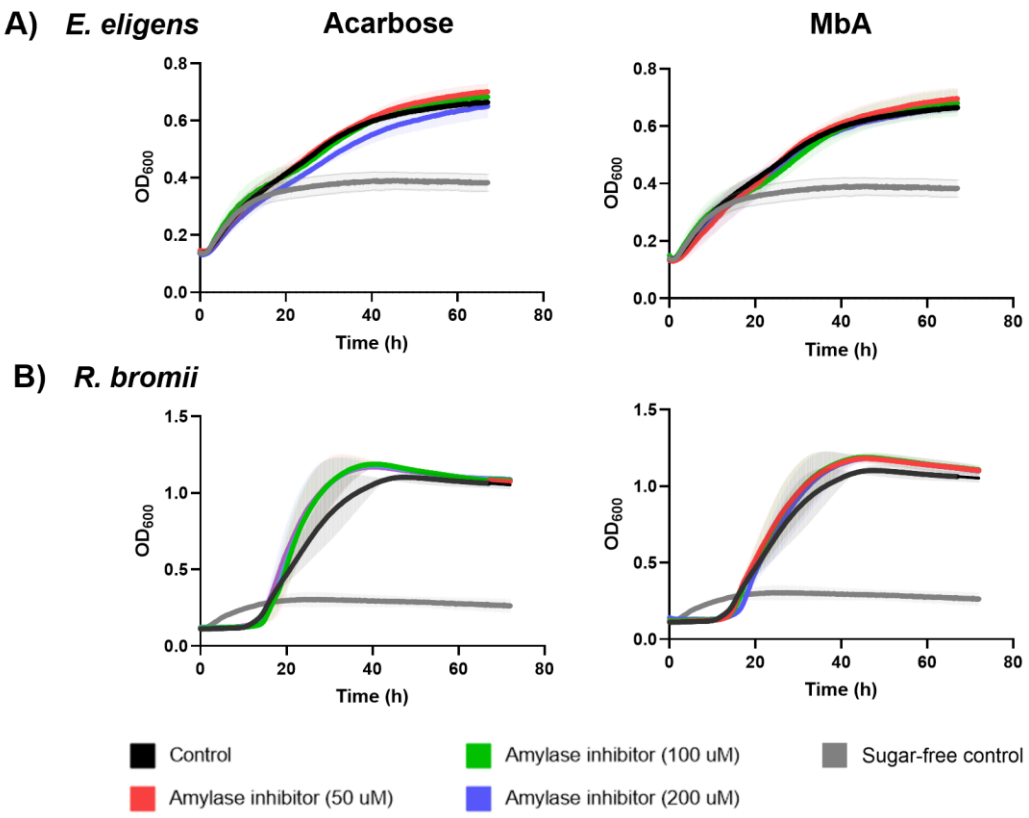

Figure 15. **Growth of A) *E. eligens* ATCC 27750 and B) *R. bromii* ATCC 27255 in cABB supplemented with 0.2% maltodextrin.** Treatment with acarbose (50, 100 and 200 µM) are on the left; treatment with MbA (50, 100 and 200 µM) are on the right. Curves show mean ± SEM of *E. eligens* (n = 4 for controls; n = 3 for amylase inhibitor groups) and *R. bromii* (n = 3). Each replicate was performed on a different day.

3.6 Labeling of *B. vulgatus* with Mal-Fl in the presence of amylase inhibitor

B. vulgatus was identified by 16S sequencing (with 100% identity and coverage) in VF74 and JD98 stools to be significantly over-represented in the acarbose-treated Mal-Fl^+ populations compared to MbA-treated Mal-Fl^+ populations (Figure 13 and Figure 14). To validate these results, we labeled *B. vulgatus* ATCC 8482 with Mal-Fl in the absence and presence of the amylase inhibitors. The full 16S rDNA sequence of *B. vulgatus* ATCC 8482 matched the 16S V4 region sequence of B. *vulgatus* from the stools with 100% identity and coverage. *B. vulgatus* was cultured in MM supplemented with 0.2% maltodextrin until it reached mid-exponential phase. The bacteria were incubated with 0.4 µM of Mal-Fl in MM for one hour at 37ºC. After washing twice and diluting in PBS, flow cytometry was carried out on labeled bacteria. The same gating approach that was used for the stool labeling assay was applied here to quantify Mal-Fl^+ cells. The percentage of Mal-Fl^+ cells are presented as a fold change (FC) relative to the same-experiment non-treated control (Figure 16). While the mean FC with MbA treatment was close to 1, the mean FC was dramatically larger (over 100-fold) with acarbose treatment, though neither difference was statistically significant. In addition to measuring the proportion of labeled cells, the median fluorescence intensity (MFI) of Mal-Fl^+ cells in each sample is reported in Figure 16 as a percentage of the same-experiment non-treated control. To determine if the fluorescence intensity of labeled cells was altered by amylase inhibitors, the mean MFI was compared to a mean MFI of 100%. No significant differences were found for acarbose-treated samples nor for MbA-treated samples. However, there is a positive trend in the MFI of Mal-Fl^+ cells treated with acarbose (with a mean MFI of over 200% of the control). These results are consistent with the findings from the VF74 and JD98 stool sequencing that shows over-representation of fluorescent *B. vulgatus* in the acarbose samples (Figure 13 and Figure 14).

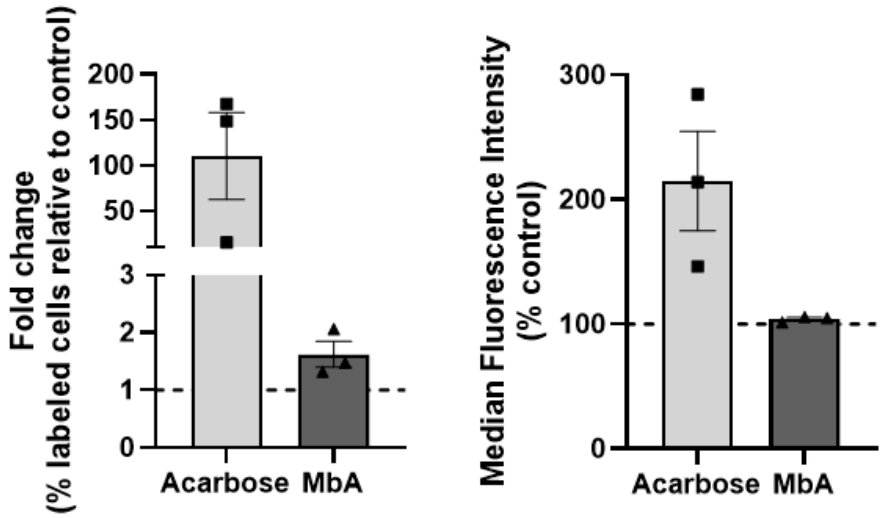

Figure 16. **Labeling of *B. vulgatus* ATCC 8482 with Mal-Fl in the presence of amylase inhibitor.** Mean ± SEM (n = 3) of A) FC of the % labeled cells relative to the non-treated control, and B) MFI as a % of the non-treated control. One sample t-tests with a hypothetical mean of 1 for FC and 100% for MFI were conducted for each treatment group.

3.7 Growth of *B. vulgatus* on maltodextrin and glucose in the presence of amylase inhibitors

We further probed how these increases in the level of Mal-Fl uptake by acarbose treatment would consequently affect metabolism and growth. Therefore, we assessed the growth of *B. vulgatus* ATCC 4842 in MM with 0.2% maltodextrin in the absence and presence of amylase inhibitors for 72 hours. The mean growth curves show complete inhibition of growth by all concentrations of acarbose but not MbA treatments (Figure 17). Mean ODmax of all acarbose-treated groups were significantly decreased by approximately 0.8 OD compared to the control (adjusted $p = 0.0036$ for 50 µM; adjusted $p = 0.0026$ for 100 µM; adjusted $p = 0.0029$ for 200 µM; see Appendix B, Figure 28B). Interestingly, the effects of acarbose on the growth of *B. vulgatus* on maltodextrin appear to contradict the increase in the level of labeling of the isolate with Mal-Fl (Figure 16). To determine if this inhibition of growth by acarbose was specific for maltodextrin, we evaluated the bacteria's growth on glucose, in the presence of amylase inhibitor. No inhibition of growth on glucose was observed by any of the amylase inhibitor treatments (Figure 17). Inhibition of growth on maltodextrin is indeed due to inhibition of metabolism, and not a result of antimicrobial activity by acarbose.

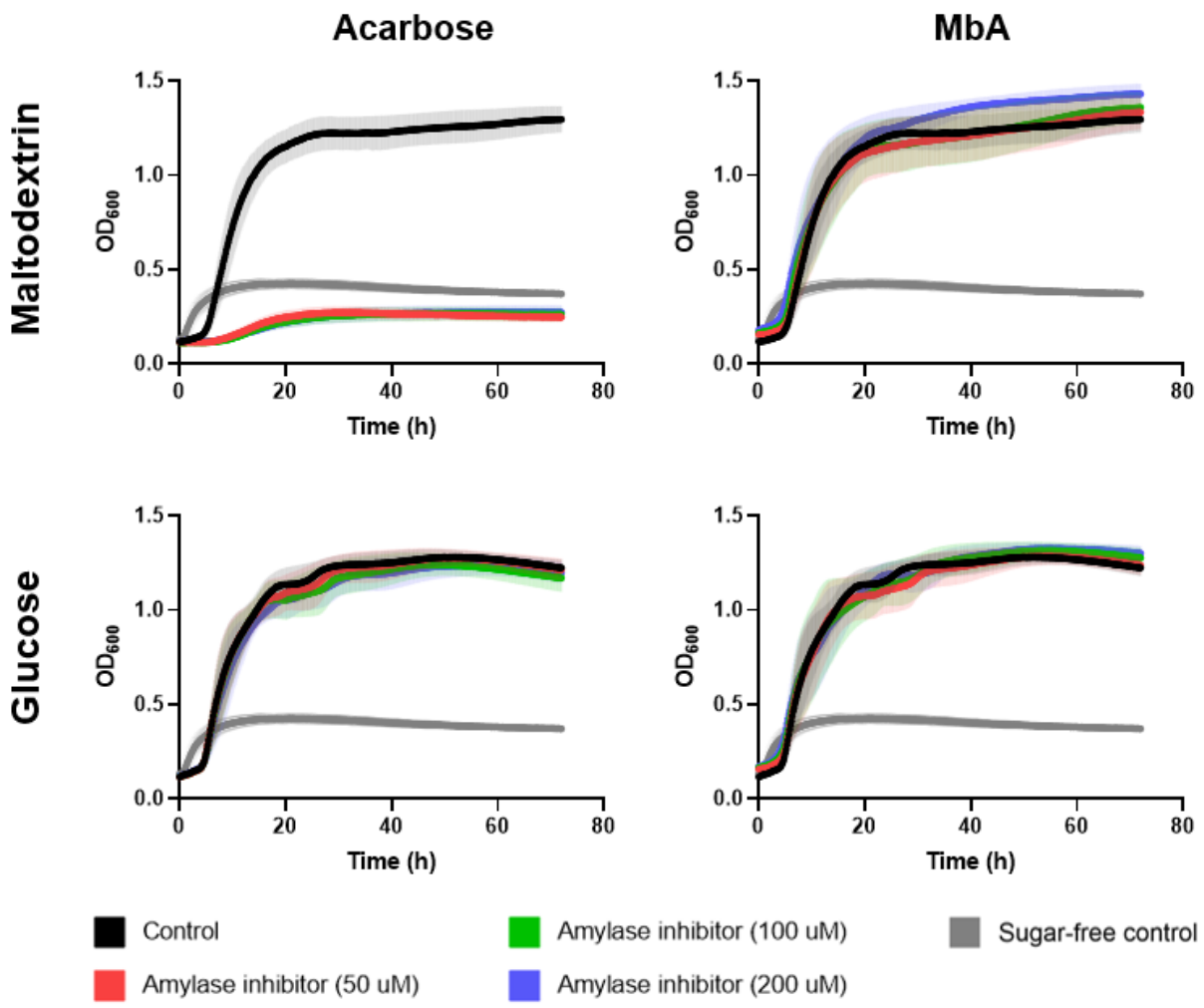

Figure 17. **Growth of *B. vulgatus* ATCC 4842 in MM supplemented with 0.2% maltodextrin (top) or 0.2% glucose (bottom).** Treatment with acarbose (50, 100 and 200 µM) are on the left; treatment with MbA (50, 100 and 200 µM) are on the right. Curves show mean ± SEM (n = 3). Each replicate was performed on a different day.

3.8 Labeling of *A. rectalis* with Mal-Fl in the presence of amylase inhibitors

A. rectalis was another species identified by 16S rDNA sequencing (with 100% identity and 100% coverage) of JD98 stool as significantly labeled by Mal-Fl and potentially affected by amylase inhibitors (Figure 12). To get a clearer picture of the effects of amylase inhibitors on maltodextrin uptake by this bacterium, we performed the Mal-Fl labeling assay on *A. rectalis* ATCC 33656, in which its full 16S sequence matched the 16S V4 region sequence of *A. rectalis* from JD98 stool with 100% identity and 100% coverage. The mean FC of the percentage of Mal-Fl$^+$ cells relative to the non-treated control was significantly lower than 1 with acarbose treatment (0.16-fold; p = 0.0183) but close to 1 with MbA treatment (Figure 18). No significant differences in mean MFI were found in acarbose- nor MbA-treated fluorescent cells compared to the hypothetical mean MFI of 100% (Figure 18). The results of acarbose treatment on Mal-Fl labeling are consistent with those from the JD98 stool labeling; however, this is not the case for MbA, as *A. rectalis* was significantly under-represented in Mal-Fl$^+$ of MbA-treated samples compared to the control (Figure 12).

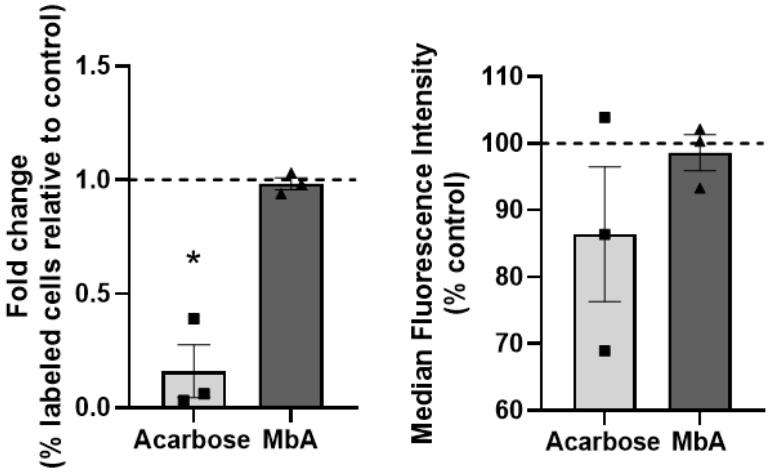

Figure 18. **Labeling of *A. rectalis* ATCC 33656 with Mal-Fl in the absence and presence of amylase inhibitor.** Mean ± SEM (n = 3) of FC of the % labeled cells relative to the non-treated control, and B) MFI as a % of the non-treated control. One sample t-tests with a hypothetical mean of 1 for FC and 100% for MFI were conducted for each treatment group; * p < 0.05.

3.9 Growth of *A. rectalis* on maltodextrin and glucose in the presence of amylase inhibitors

The growth of *A. rectalis* ATCC 33656 in cABB supplemented with 4% NaOAc and 0.2% maltodextrin or glucose, and with or without amylase inhibitor, was evaluated over 72 hours. Curves of a single replicate of the growth assessment of *A. rectalis* on maltodextrin and glucose are shown in Figure 19. Due to the steep growth rate during the exponential phase, along with variation in lag time between replicates, the mean growth curves were not representative of the curves seen in individual experiments. The growth of *A. rectalis* on maltodextrin was affected in a dose-dependent manner by acarbose (Figure 12). At all three concentrations of acarbose, the shape of the curve was altered such that the gradual decrease in OD upon reaching ODmax in the non-treated control was not seen in acarbose-treated groups. Rather, the OD plateaus at the stationary phase. The mean ODmax was significantly decreased in the 100 and 200 µM acarbose groups by 0.3 and 0.5 OD respectively (adjusted $p = 0.0161$ and 0.0089 respectively) but not in the 50 µM group for acarbose (see Appendix B, Figure 28D). There is also a trend of decreasing mean MGR with increasing concentrations of acarbose; however, statistical analyses were not carried out for these groups due to a removed negative value in each group. While the shape of the curves in MbA treatment groups was not altered (Figure 19), the mean ODmax of the 50 µM group was significantly increased by a magnitude of 0.07 OD (adjusted $p = 0.03$; see Appendix B, Figure 28D). The mean MGR of the 100 µM MbA group was also increased by 21.47 mOD/min (adjusted $p = 0.0227$; see Appendix B, Figure 28D). No significant differences were found between mean lag time of the non-treated control and MbA treatment groups (see Appendix B, Figure 28D). Considering all the growth metrics and curve shape, these minor differences in mean ODmax of the 50 µM group and mean MGR of the 100 µM group are not biologically important. Furthermore, the shape of the growth curves on glucose did not change with either treatment (Figure 19)—

however, the mean ODmax of the acarbose group at 200 µM was significantly decreased by 0.07 OD (adjusted p = 0.0180; see Appendix B, Figure 28D). Again, such a minute difference (<0.1 OD) in ODmax is not biologically significant. Overall, growth on glucose was not inhibited by amylase inhibitors. These results, demonstrating the slight inhibition of growth on maltodextrin by acarbose but not MbA, agree with those from the Mal-Fl labeling assays of *A. rectalis* ATCC 33656 isolate (Figure 18).

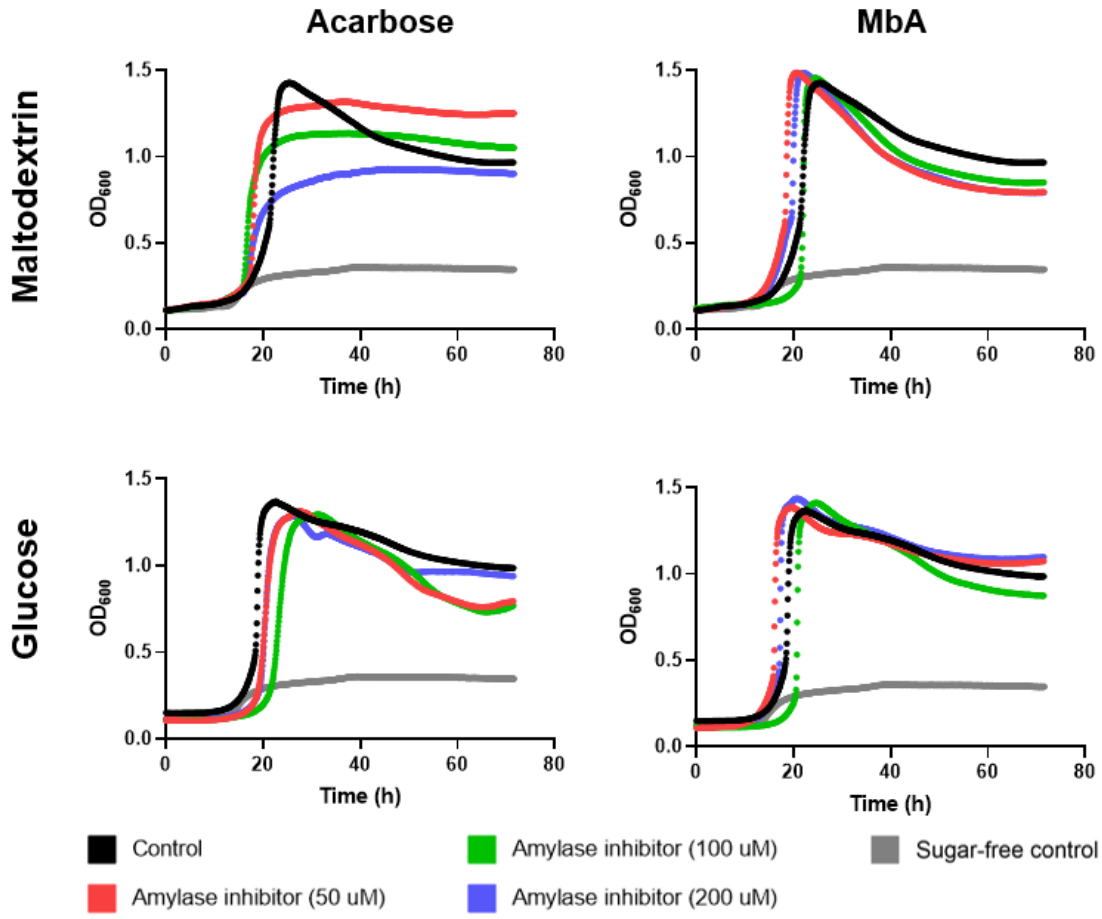

Figure 19. **Growth of *A. rectalis* ATCC 33656 in cABB supplemented with 4% NaOAc and 0.2% maltodextrin (top) or 0.2% glucose (bottom).** Treatment with acarbose (50, 100 and 200 µM) are on the left; treatment with MbA (50, 100 and 200 µM) are on the right. Curves are from one representative replicate of n = 3. Each replicate was performed on a different day.

3.10 Growth of *B. xylanisolvens* on maltodextrin and glucose in the presence of amylase inhibitors

Like *B. vulgatus*, the closely related *B. xylanisolvens* was also identified (with 100% identity and coverage) in JD98 stool to be over-represented in the Mal-Fl$^+$ population in acarbose-treated samples compared to MbA-treated samples (Figure 13). A *B. xylanisolvens* clone, isolated from VF74 stool by another lab member, was grown in MM supplemented with 0.2% maltodextrin or glucose for 72 hours. The full 16S rDNA sequence of this clone matched the 16S V4 region sequence of *B. xylanisolvens* from JD98 stool with 100% identity and coverage. The mean curves of *B. xylanisolvens* grown on maltodextrin show a delayed and slower exponential phase with acarbose treatments, but not complete inhibition of growth (Figure 20). Additionally, the decline in OD upon reaching ODmax in the non-treated control group is stifled in acarbose-treated groups. Though at all concentrations of acarbose, the bacteria can reach the same mean ODmax as that in the control group, with no significant differences in mean MGR (see Appendix B, Figure 28E). Yet, the mean lag time of acarbose at 50 µM was found to be significantly increased by 13 hours (adjusted p = 0.0473; see Appendix B, Figure 28E). In contrast, the mean ODmax of *B. xylanisolvens* grown on glucose in the presence of all concentrations of acarbose is decreased by approximately 0.1 OD compared to the control (adjusted p = 0.0268 for 50 µM; adjusted p = 0.0095 for 100 µM; adjusted p = 0.0008 for 200 µM; see Appendix B, Figure 28E). Despite this, the growth curves plateau at the same mean OD in the stationary phase across the groups (Figure 20). MbA treatment did not affect the shape of the curves for growth on either maltodextrin or glucose. The mean ODmax of the 100 µM group was significantly increased by 0.03 OD compared to the non-treated control for growth on maltodextrin (adjusted p = 0.0251; see Appendix B, Figure 28E), though this is negligible. No other significant differences were found in the mean ODmax, mean MGR, or mean lag time of MbA treatments and non-treated control for growth on maltodextrin or

glucose. The overall results for amylase inhibitor effect on maltodextrin metabolism of *B. xylanisolvens* are similar to what was observed with *B. vulgatus* (Figure 17). Yet, the extent of inhibition by acarbose treatment on maltodextrin metabolism by *B. xylanisolvens* is not as large as is seen in *B. vulgatus*.

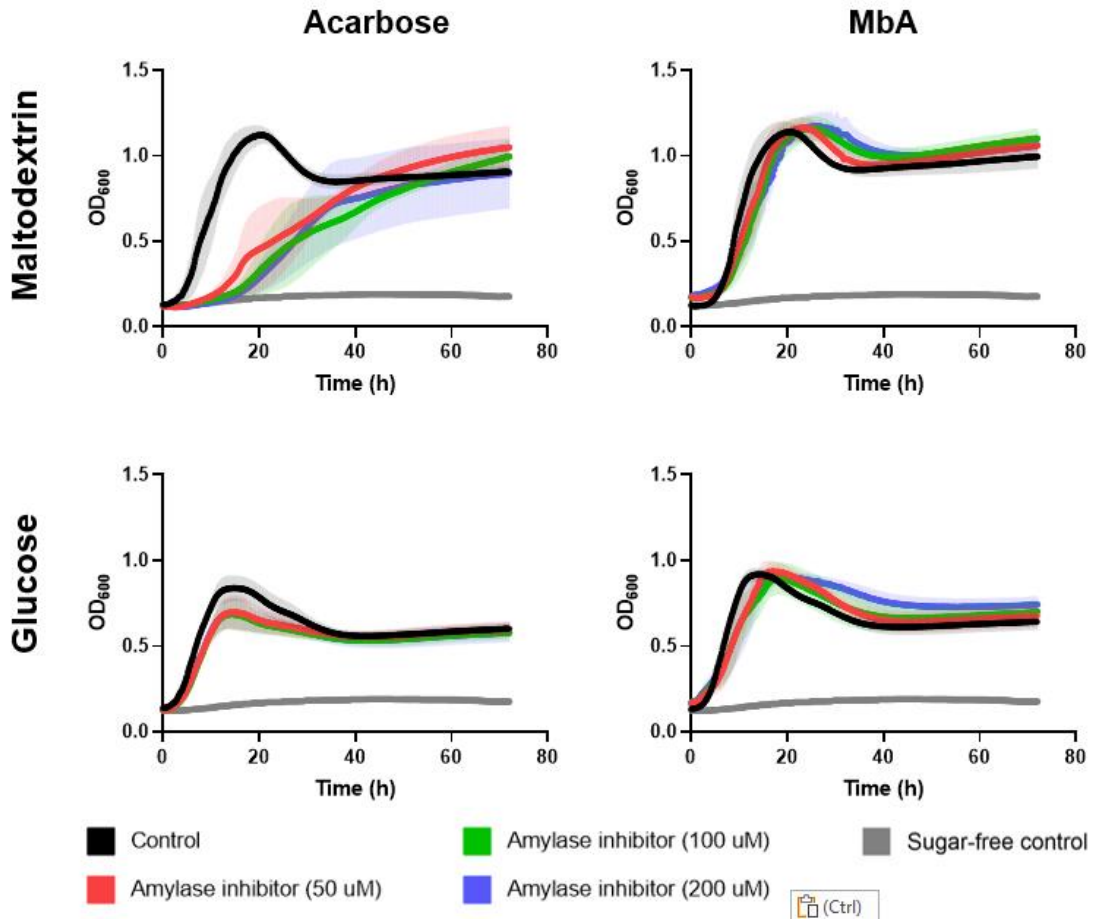

Figure 20. **Growth of *B. xylanisolvens* in MM supplemented with 0.2% maltodextrin (top) or 0.2% glucose (bottom).** Treatment with acarbose (50, 100 and 200 µM) are on the left; treatment with MbA (50, 100 and 200 µM) are on the right. Curves show mean ± SEM (n = 3). Each replicate was performed on a different day.

3.11 Growth of *B. adolescentis* DSM 20083 on maltodextrin and glucose in the presence of amylase inhibitors

Since two *B. adolescentis* ESVs were identified (each with 100% identity and 99.695% coverage) in JD98 stool to be significantly over-represented in the Mal-Fl$^+$ population of non-treated samples compared to acarbose-treated samples (Figure 12), we evaluated the growth of three *B. adolescentis* strains (DSM 20083, C6 and C5) on maltodextrin and glucose with amylase inhibitor treatment. Sequencing of the full 16S rDNA was not carried out in *B. adolescentis* strains due to issues with amplification of the 16S sequence. A gram stain was done in the meantime to verify the morphology and cell wall structure of the bacteria. The gram-stained smears of all three strains confirm gram-positive cell wall structure and irregular rod shape, which are characteristic of *Bifidobacterium* sp.[219] (see Appendix B, Figure 29). All bifidobacteria were grown in ssMRS supplemented with 0.75% maltodextrin for 72 hours before the growth assay, then diluted in fresh ssMRS medium with 0.75% maltodextrin or glucose for the experiment and monitored for another 72 hours. The DSM 20083 strain was partially inhibited by acarbose treatment (Figure 21) with a significant decrease in ODmax by 0.5 with 50 µM acarbose (adjusted $p = 0.0424$; see Appendix B, Figure 28F). The 100 and 200 µM acarbose groups also showed a decrease in ODmax of 0.5 and 0.6 respectively, but were not statistically significant. MbA treatment had a dose-dependent effect on the growth on maltodextrin with ODmax significantly decreased by 0.4, 0.5 and 0.7 with increasing concentration (adjusted $p = 0.0077$ for 50 µM; adjusted $p = 0.0185$ for 100 µM; adjusted $p = 0.0007$ for 200 µM; see Appendix B, Figure 28F). While the ODmax of the 200 µM acarbose group for growth on glucose was significantly increased (adjusted $p = 0.0157$; see Appendix B, Figure 28F), this increase of 0.02 is unimportant. All other treatment groups did not significantly affect the ODmax for growth on glucose. Due to the shape of the curve, which has two exponential phases (Figure 21), calculations of MGR and lag time by BioTek Gen5 software were unreliable

and thus were not analyzed. The first exponential phase is due to growth in media carried over from the previous liquid culture (as shown by the slight growth in the grey control curve where bacteria were inoculated in sugar-free medium) while the second exponential phase is the appropriate growth on the carbon source provided in the assay. Overall, the inhibition by acarbose and MbA on the bacterium's growth on maltodextrin is still apparent.

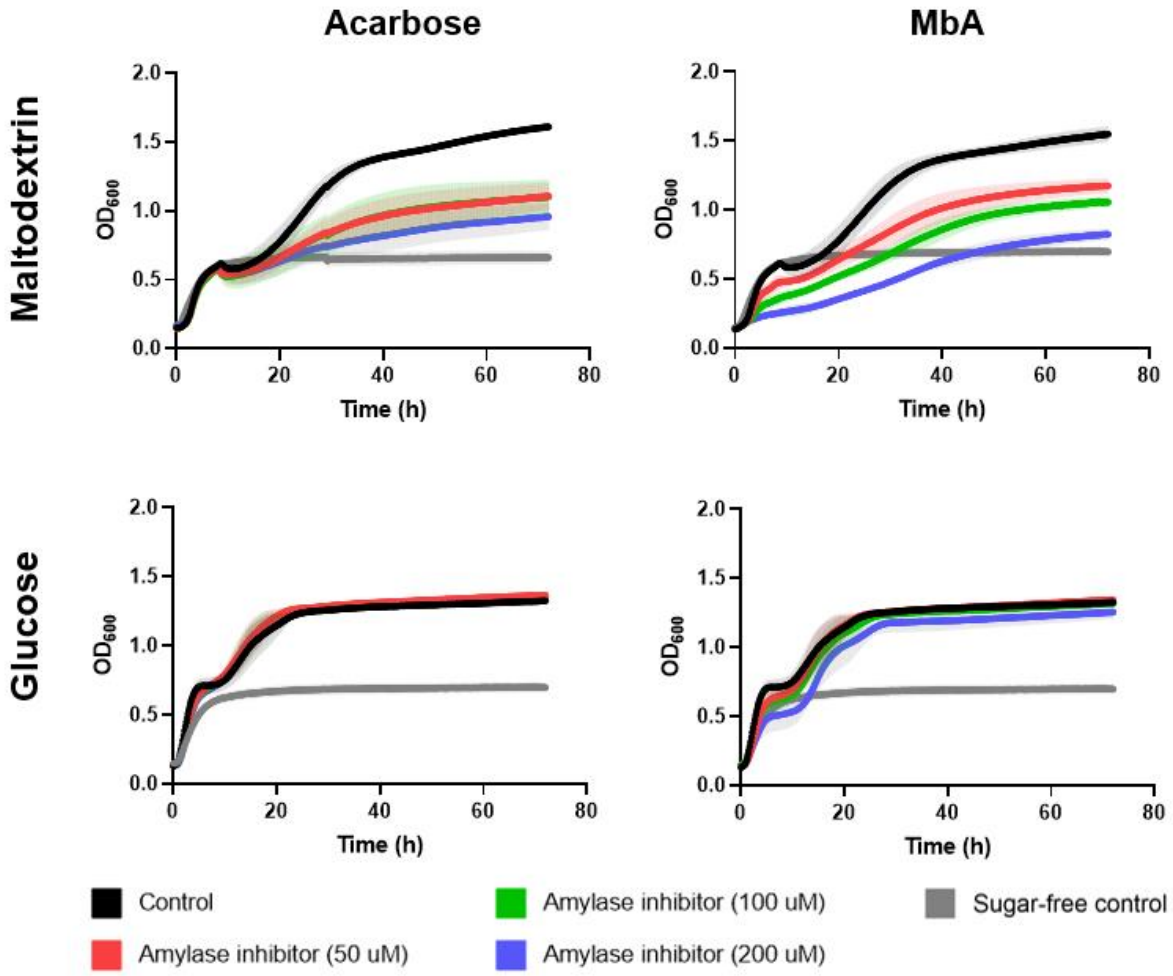

Figure 21. **Growth of *B. adolescentis* DSM 20083 in ssMRS supplemented with 0.75% maltodextrin (top) or 0.75% glucose (bottom).** Treatment with acarbose (50, 100 and 200 µM) are on the left; treatment with MbA (50, 100 and 200 µM) are on the right. Curves show mean ± SEM (n = 3). Each replicate was performed on a different day.

3.12 Growth of *B. adolescentis* C6 on maltodextrin and glucose in the presence of amylase inhibitors

B. adolescentis C6 was another strain that we tested, which was a clone isolated from VF74 stool and identified by MALDI-TOF by another lab member. Unlike the DSM 20083 strain, the growth of the C6 clone in ssMRS with 0.75% maltodextrin was significantly inhibited by all concentrations of acarbose (Figure 22). The mean ODmax was decreased by at least 0.9 in all acarbose groups compared to the non-treated control (adjusted p = 0.0185 for 50 µM; adjusted p = 0.0216 for 100 µM; adjusted p = 0.0096 for 200 µM; see Appendix B, Figure 28G). MbA treatment did not significantly affect the mean ODmax. The mean curves for growth on glucose show that the bacterium's growth is not inhibited by amylase inhibitors (Figure 22), with no significant difference in mean ODmax between control and treatment groups (see Appendix B, Figure 28G). Like *B. adolescentis* DSM 20083, MGR and lag time calculations were inaccurate for *B. adolescentis* C6 due to the double exponential phases in the curves. Particularly for the glucose growth curves, the non-treated control group does not appear to have reached stationary phase. However, since the curves appear sufficiently similar, I would predict that the mean ODmax achieved at stationary phase would be similar across groups, and that growth on glucose is not inhibited by amylase inhibitors. The growth of this strain on maltodextrin was inhibited by acarbose but not MbA, showing a different phenotype than the *B. adolescentis* DSM 20083 strain.

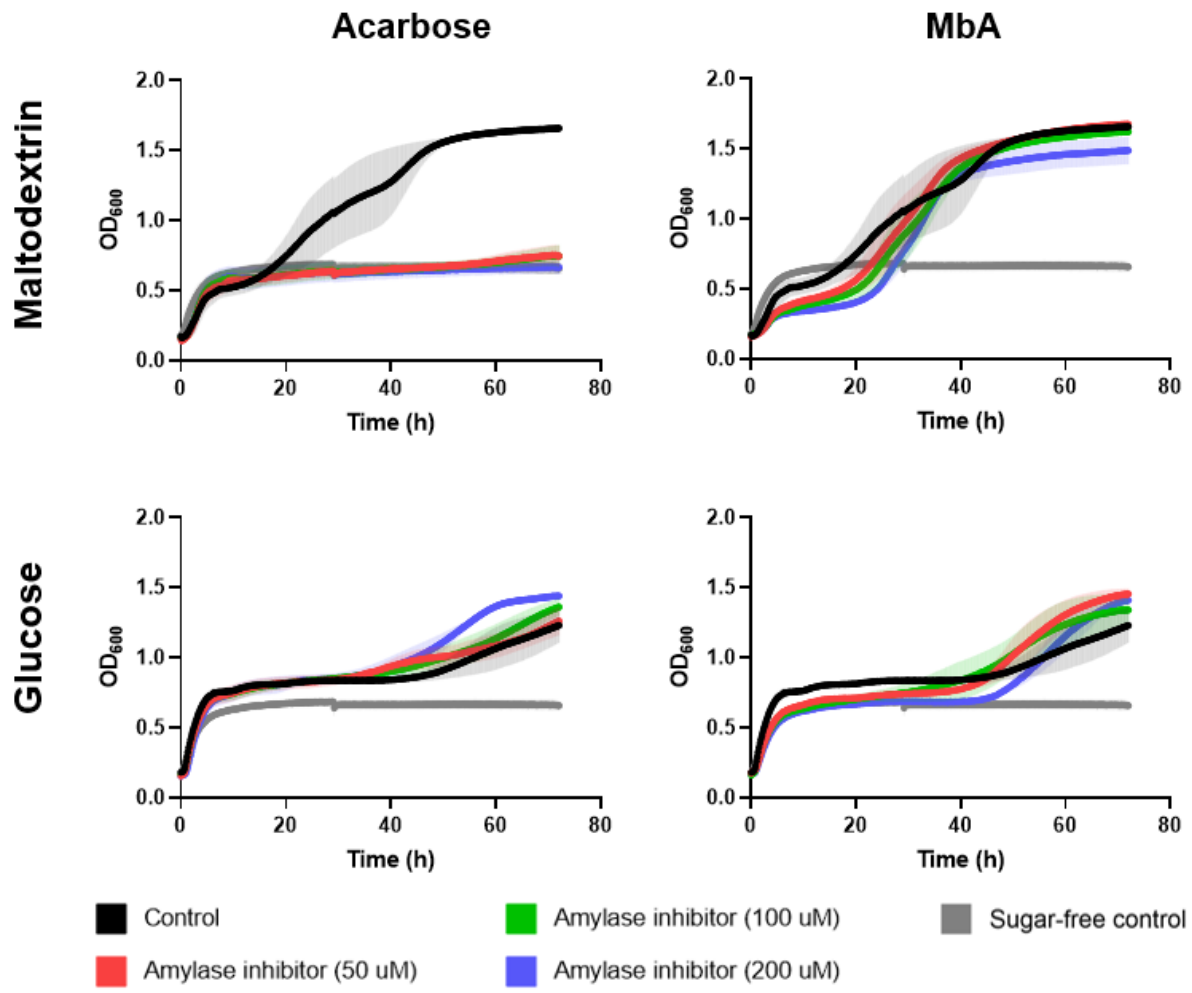

Figure 22. **Growth of *B. adolescentis* C6 in ssMRS supplemented with 0.75% maltodextrin (top) or 0.75% glucose (bottom).** Treatment with acarbose (50, 100 and 200 µM) are on the left; treatment with MbA (50, 100 and 200 µM) are on the right. Curves show mean ± SEM (n = 3). Each replicate was performed on a different day.

3.13 Growth of *B. adolescentis* C5 on maltodextrin and glucose in the presence of amylase inhibitors

The last strain of *B. adolescentis* that we tested, C5, was another clone isolated from VF74 stool and identified by MALDI-TOF by another member of the Castagner lab. Although only two replicates of the experiment have been conducted for growth in ssMRS supplemented with 0.75% maltodextrin, the mean curves of the data show inhibition by acarbose treatments and slight dose-dependent inhibition by MbA (Figure 23). The curves for growth on glucose in the presence of acarbose also exhibit a slight dose-dependent effect on the MGR by acarbose but only one independent experiment has been carried out for these conditions. Moreover, the OD measured at stationary phase are relatively similar across all treated groups and the non-treated control. It seems that this strain of *B. adolescentis* presents a phenotype that is slightly different than the two other strains, but this needs to be confirmed with more replicates.

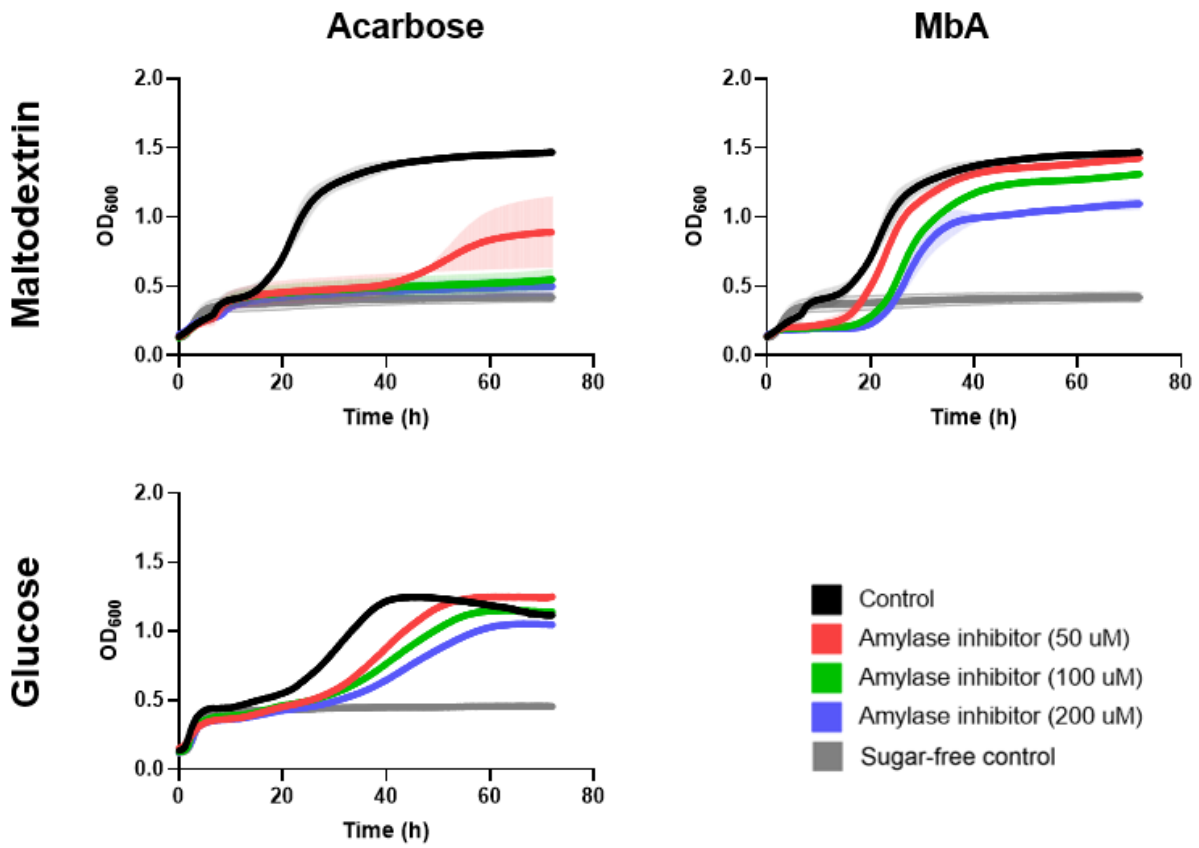

Figure 23. **Growth of *B. adolescentis* C5 in ssMRS supplemented with 0.75% maltodextrin (top) or 0.75% glucose (bottom).** Treatment with acarbose (50, 100 and 200 µM) are on the left; treatment with MbA (50, 100 and 200 µM) are on the right. Curves show mean ± SEM (n = 2 for maltodextrin ± acarbose and maltodextrin ± MbA; n = 1 for glucose ± acarbose). Each replicate was performed on a different day.

3.14 Growth of *B. longum* subsp. *infantis* on maltodextrin in the presence of amylase inhibitors

The last bacterium that we investigated was *B. longum* subsp. *infantis* ATCC 15697 since multiple ESVs of *Bifidobacterium* spp. had been identified in our 16S sequencing data of JD98 stool as potentially affected by amylase inhibitors, and because *B. longum* was found to be increased in diabetic patients treated with acarbose[180,183]. The mean growth curves from two replicates shows that growth in ssMRS with 0.75% maltodextrin was not inhibited by acarbose (Figure 24). Treatment with MbA may have a slight inhibitory effect on maltodextrin growth; however, only one independent experiment with these conditions has been conducted so far. Completion of these experiments in triplicate, as well as assessing the growth on glucose, are needed to confirm these results and make conclusions on the effect of amylase inhibitors on the growth of *B. longum* subsp. *infantis* and *B. adolescentis* C5 on maltodextrin.

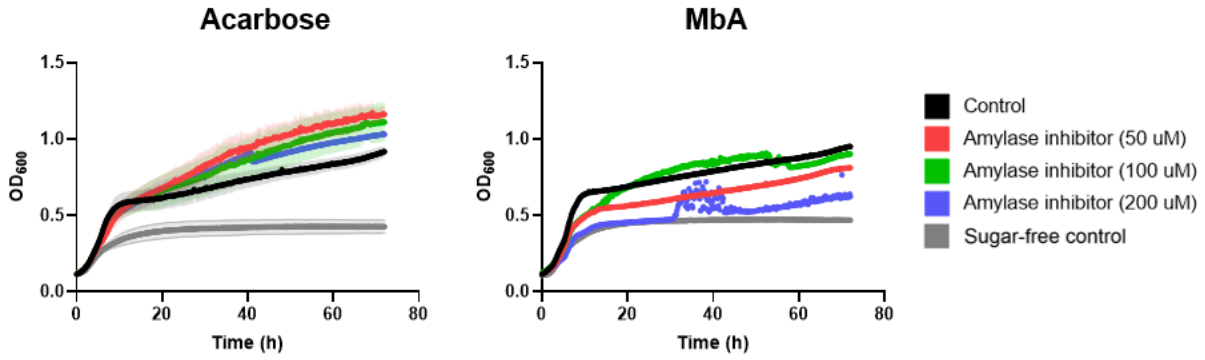

Figure 24. **Growth of *B. longum* subsp. *infantis* ATCC 15697 in ssMRS supplemented with 0.75% maltodextrin.** Treatment with acarbose (50, 100 and 200 µM) are on the left; treatment with MbA (50, 100 and 200 µM) are on the right. Curves show mean ± SEM (n = 2 for maltodextrin ± acarbose; n = 1 for maltodextrin ± MbA). Each replicate was performed on a different day.

4 Discussion

This thesis demonstrates the application of an unbiased functional method involving fluorescently-labeled glycans, FACS and amplicon sequencing to probe and identify bacteria from stool samples that are affected by amylase inhibitors. Subsequent culture-based experiments were used to validate the findings.

The Mal-Fl probe was synthesized via a transesterification between maltodextrin (DP 14-25) and fluorescein-NHS carried out in basic conditions. Size exclusion chromatography with Sephadex LH-20, which has an exclusion limit of 4000-5000 (depending on the solvent), was used to purify the crude reaction to remove unreacted dye (376.06 Da) and other impurities. LC-MS was used to assess purity of purified fractions based on peak integrations at 280 nm absorbance. Only fractions with at least 85% purity were pooled and used for subsequent labeling assays. The purified probe was then characterized by MALDI-TOF MS which recorded the masses of monofunctionalized maltodextrins (Figure 8) and some non-functionalized sugars. Since we quantified the probe concentration based on fluorescence signal, the presence of non-functionalized maltodextrins was not critical.

Purified Mal-Fl was used to metabolically label bacteria from stool samples of healthy volunteers. Here, we used stool samples as a proxy for the GM. The stools were aliquoted in an anerobic chamber immediately after collection, and then stored frozen at -80º C. In these conditions, most cells from the stool remain intact and metabolically active, and the composition does not significantly differ from that of a fresh stool sample[207,220,221]. Human faecal samples are often used due to the non-invasive and practical method of collection[222]. However, it is important to note that gut mucosal communities are distinct from gut lumen microbiota[223]. Fecal samples are most representative of the gut lumen and thus lack representation of the mucosal-associated

microbiota[222,224]. The stool consistency, which reflects transit time, can further affect the diversity, enterotype and community composition[225]. Other types of samples of the GM, including mucosal biopsies and intestinal fluid, can be used in place of fecal samples to study bacteria from a different niche.

The short incubation of one hour with our fluorescent probe ensured that our method did not bias the growth of certain bacteria but would be enough time for necessary transport and GH genes to be upregulated. Flow cytometry then allowed us to distinguish and quantify bacteria based on their ability to take up the fluorescently-labeled glycan. Comparisons of the percentage of Mal-Fl$^+$ cells between samples with and without amylase inhibitor treatment reflects a crude analysis of the amylase inhibitors' effect on maltodextrin uptake by gut bacteria (Figure 9). Indeed, even if no significant differences in the level of labeling was observed, the amylase inhibitors could nonetheless be affecting certain bacteria one way and other bacteria a different way, resulting in a null net effect in the percentage of labeled cells. Both acarbose and MbA had an effect on maltodextrin uptake that manifested in either the positive or negative direction in different stools. With acarbose, the proportion of Mal-Fl$^+$ cells decreased in YM54 stool, increased in VF74 stool, and was unchanged in JD98 stool. As for MbA, an increase in Mal-Fl$^+$ cells was observed in JD98 while a decrease was seen in YM54. Such variation in responses across stools highlights the importance of interindividual differences in GM.

This preliminary labeling assay highlighted stools in which we prioritized for further investigation through FACS and amplicon sequencing. The increased proportion of labeled cells in VF74 and JD98 stools treated with acarbose or MbA was most intriguing as it contrasted our expectation that inhibition of GHs by the amylase inhibitors would lead to a decrease in the level of labeling by Mal-Fl. We hypothesized that the amylase inhibitors were stimulating uptake in specific bacteria,

thus increasing the proportion of labeled cells. After sorting Mal-Fl$^+$ from Mal-Fl$^-$ cells in labeled samples and sequencing the 16S rDNA, we identified the bacteria from these populations. By comparing the abundances of identified bacteria in the Mal-Fl$^+$ population from amylase inhibitor treated vs. non-treated samples, we pinpointed bacteria that were presumably affected by the amylase inhibitors (Figure 12, Figure 13, and Figure 14).

In JD98 stool, although the percentage of labeled cells was significantly increased by MbA (Figure 9), the composition of these labeled cells remained similar to the composition of non-treated Mal-Fl$^+$ cells as shown by the RDA plot (Figure 10). Interestingly, while the percentage of labeled cells in acarbose-treated samples did not differ from the control (Figure 9), the composition of Mal-Fl$^+$ cells of acarbose-treated samples was distinct from that of both MbA-treated and untreated samples (Figure 10). This suggested that acarbose treatment had a greater impact in altering the function of the community such that the composition of maltodextrin-labeled cells shifted.

Previous work to validate this method of metabolic labeling coupled with FACS and 16S sequencing in stool samples was done by other lab members and has been submitted for publication[217]. With the goal of revealing "who eats what?" in the GM, three different fluorescent glycan probes (CD-F, NYST-F and GMP-F) were used in three stool samples in a proof-of-principle study. Subsequent, unpublished work expanded to ten stool samples with an array of fluorescently-labeled glycans including xylotetraose, mannotetraose, cyclodextrin, fructooligosaccharide, arabinoxylotetraose, maltodextrin, galactomannopentaose, and nystose. While these preliminary experiments demonstrated the use of this method in identifying glycan consumers of the GM, an important limitation was that only one replicate per probe and stool sample were conducted. Here, I've performed the labeling, sorting and sequencing experiments on JD98 stool in quadruplicate and so we can compare the abundances of specific bacteria between

amylase inhibitor-treated and non-treated groups. We can also conclude from our DAA of non-labeled vs Mal-Fl$^+$ samples that bacteria statistically overrepresented in the Mal-Fl$^+$ samples are truly labeled and take up our Mal-Fl probe in JD98 stool. These bacteria include *Agathobacter rectalis*, *Bifidobacterium adolescentis*, *Bifidobacterium bifidum*, *Blautia massiliensis*, *Dialister invisus*, and *Faecalibacterium prausnitzii* (Figure 11). Indeed, starch metabolism has been characterized in *A. rectalis*[41,69-71] and in bifidobacteria[41,62,226]. Starch metabolism in *F. prausnitzii* is not as well-understood. Incubation of high amylose starch in fresh human faecal samples led to an increase in the bacterium[227], though monocultures of *F. prausnitzii* strains exhibited little to no growth on starch[228,229]. It has also been shown that strains of *F. prausnitzii* can be phylogenetically and genomically diverse[230], which may explain the functional diversity of this species. Furthermore, while GHs involved in starch metabolism have been detected in the genome of *F. prausnitzii*, the activity of these genes remains to be characterized in culture[231]. No data on the ability to metabolize starch have been reported in *Dialister invisus* nor *Blautia massiliensis*. We have thus shed light on potentially novel starch-utilizers in the GM.

E. eligens and *R. bromii* were identified as Mal-Fl$^+$ from DAA of the ten stool samples tested in previous work. In the present work, these bacteria were not identified to be significantly labeled by Mal-Fl in JD98 stool because of a low number of reads in all the samples, even in the non-labeled negative control. Presumably, the negative control sample reflects the composition of the JD98 GM and so we can conclude that these bacteria are not prominent members of the JD98 community. In this regard, it was valuable to have information across multiple stool samples despite the small number of replicates per stool. We demonstrated through *in vitro* growth assays that both do indeed metabolize starch, although growth of *E. eligens* was to a much smaller extent (Figure 15). Both bacteria are further not affected by amylase inhibitors. These findings are in

accordance with those from the study done by Santilli *et al*.[174] where they also did not observe inhibition of growth on starch in *R. bromii* by acarbose. Zhang *et al*.[164] showed that the relative abundance of the genus *Ruminococcus* 2 was increased by acarbose in diabetic rats. This enrichment could be a result of a lack of GH inhibition by acarbose in some *Ruminococcus* species, such as *R. bromii*, which gives these bacteria a competitive advantage for the ensuing influx of carbohydrates into the large intestine.

The labeling of *B. vulgatus* isolate with Mal-Fl was dramatically increased in proportion of labeled cells by acarbose (Figure 16). Though, due to the large variation between experiments, the increase was not statistically significant. Hehemann *et al*. showed that the extent of labeling by fluorescent glycans (i.e., the uptake efficiency) in pure culture of *B. theta* was heterogeneous[211]. Indeed, the proportion of Mal-Fl$^+$ cells was never greater than 30% in *B. vulgatus* (Appendix B, see Figure 30). It is possible that the slightest variation in growth conditions on different days led to a fluctuation in the heterogeneity of uptake efficiency, particularly since the magnitude of the fold change was extreme in acarbose-treated samples (148-, 15- and 167- fold). Overall, the labeling of the isolate was consistent with the findings from labeled and sequenced VF74 and JD98 stools, where *B. vulgatus* was over-represented in the Mal-Fl$^+$ acarbose-treated population compared to Mal-Fl$^+$ MbA-treated samples (Figure 13 and Figure 14). However, these labeling results seemed to contradict the growth inhibition on maltodextrin seen in *B. vulgatus* treated with acarbose (Figure 17). Indeed, a depletion of *B. vulgatus* in T2D patients has also been observed[180]. In our growth assays, acarbose treatment seems to cause complete inhibition of maltodextrin metabolism such that the ODmax of acarbose-treated groups is lower than that of the sugar-free control (which causes slight growth due to minute amounts of sugar carried over from the overnight media). We showed that this inhibition is specific for maltodextrin metabolism and was not due to microbicidal

activity as the bacterium's growth on glucose was not affected by acarbose. Considering these results, the increased Mal-Fl labeling seen in VF74 and JD98 stools seems to be a result of mechanisms that are more complex than we originally hypothesized. Given the tetrasaccharide-mimicking structure of acarbose, we postulate that the increased uptake efficiency of Mal-Fl can be due to inhibition of periplasmic GHs (i.e., SusA and/or SusB) by acarbose, leading to trapped fluorescent maltooligosaccharides in the periplasm. Even if SusG is inhibited by acarbose, it has been shown that only SusC and D are needed to import maltoheptaose, a maltooligosaccharide with seven glucose units[232]. The trapped maltooligosaccharides could in turn stimulate SusR to upregulate transcription of Sus genes and take up more fluorescent maltooligosaccharides, which may explain the slight increase in fluorescence intensity of labeled cells. To elucidate the mechanisms of inhibition by acarbose in *B. vulgatus*, kinetic studies on purified Sus proteins and quantitative PCR should be carried out in future investigations. Importantly, *B. vulgatus* has been implicated in the development of metabolic disorders like T2D due to its ability to synthesize branched-chain amino acids and secondary BAs[141,180,233]. Thus, inhibition of this organism's growth by acarbose may be one of the mechanisms of the medication's anti-diabetic effects.

A. rectalis was identified to be over-represented in Mal-Fl$^+$ non-treated samples compared to either acarbose- or MbA-treated samples of JD98 stool (Figure 12). Labeling with Mal-Fl in pure culture of *A. rectalis* demonstrated a decrease in the proportion of labeled cells by acarbose but no change by MbA (Figure 18). The discrepancy in MbA's effect on Mal-Fl labeling of *A. rectalis* in JD98 stool vs. in pure culture may be due to strain differences, which would not be accurately discernible without the complete 16S rDNA sequence. The growth pattern of *A. rectalis* on maltodextrin is further modified by acarbose but not MbA (Figure 19). In the non-treated control, *A. rectalis* abruptly reaches ODmax which leads to a decline in OD until a plateau is reached. Usually, this

decline is associated with a death phase where cells lose viability from deteriorated culture conditions and consequently lyse. Lysis of these cells can benefit the small population of cells that are viable as nutrients are released into the culture[234]. In acarbose-treated groups, the decline phase is abolished. Since the decrease in ODmax in *A. rectalis* was only significant at the two higher doses of acarbose, acarbose could be restricting maltodextrin metabolism in a way that preserves culture conditions and viability of cells at lower concentrations (i.e., less toxic metabolites produced, or slower utilization of available nutrients). At higher concentrations, the inhibition of maltodextrin metabolism may solely restrict growth. Unlike *B. vulgatus*, the labelings of *A. rectalis* isolate with Mal-Fl agree with results of the growth assay such that a decrease in the proportion of labeled cells is accompanied with inhibition of growth on maltodextrin by acarbose (Figure 18 and Figure 19). This further supports our hypothesis that the increase in the level of labeling seen in *B. vulgatus* may be from trapped fluorescent maltooligosaccharides in the periplasm since this does not occur in *A. rectalis*, a gram-positive bacterium lacking an outer membrane. In fact, the entire starch uptake system in *A. rectalis* is different from the Sus in Bacteroidetes, and so acarbose may simply inhibit the extracellular GH13s of *A. rectalis*, thus inhibiting uptake of maltodextrin. Even the extent of growth inhibition at the two higher doses of acarbose in *A. rectalis* was much less than in *B. vulgatus* (Figure 17, Figure 19), further highlighting the differences in their starch-utilizing systems and how that dictates how they respond to amylase inhibitors.

B. xylanisolvens was identified to be enriched in acarbose-treated samples compared to MbA-treated JD98 stool samples, like *B. vulgatus* (Figure 13). Interestingly, the growth of *B. xylanisolvens* on maltodextrin was not as inhibited by acarbose as it was in *B. vulgatus*, even though these two Bacteroidetes likely have similar Sus-like systems (Figure 17, Figure 20). From the growth curves, it appears that acarbose slows exponential growth in *B. xylanisolvens*, but the

bacterium is nevertheless able to reach the same OD as the non-treated control group in stationary phase (Figure 20). *In vivo*, this might give a competitive advantage to *B. xylanisolvens* over other fully inhibited *Bacteroides* species. Ultimately, we've demonstrated the selective effects of acarbose in two closely related species. Future experiments involving the labeling of *B. xylanisolvens* isolate with Mal-Fl could reveal more information on whether inhibition of maltodextrin metabolism by acarbose leads to an increase in Mal-Fl labeling in *Bacteroides* species.

The genus *Bifidobacterium* is consistently observed to be increased by acarbose across many studies. Moreover, *B. adolescentis* was found to be increased in relative abundance by acarbose in T2D patients[180]. Interestingly, our amplicon sequencing data from labeled and sorted JD98 stool identified two *B. adolescentis* ESVs significantly over-represented in the Mal-Fl$^+$ population of non-treated samples vs. acarbose-treated samples (Figure 12). In accordance, the growth on maltodextrin of all three strains of *B. adolescentis* that we tested were inhibited by acarbose to varying extents, with *B. adolescentis* DSM 20083 being the least inhibited of the three strains (Figure 21, Figure 22, and Figure 23). These results show that the effects of acarbose are even selective for strains of a particular species, and that strains that are less or not inhibited by acarbose could become enriched as a result. We furthermore assessed the growth of *B. longum* subsp. *infantis* on maltodextrin, which did not seem to be inhibited by acarbose (Figure 24), although this must be replicated since we have only performed 2 replicates at this time. This species was found to be enriched in diabetic patients treated with acarbose, and inversely correlated with changes in body weight and HbA1c[180,183]. So far, our findings suggest that this bacterium can thrive in the GM from a lack of inhibition on maltodextrin metabolism by acarbose, which may ultimately benefit the host.

Out of all the tested bacterial isolates, the growth on maltodextrin of only *B. adolescentis* DSM 20083, and potentially *B. adolescentis* C5 and *B. longum* subsp. *infantis*, is inhibited by MbA (Figure 21, Figure 23, and Figure 24). However, the effect is small so more replicates would need to be performed to thoroughly validate this finding. Combining the results from *B. vulgatus* and *A. rectalis* isolate labeling assays with Mal-Fl, where MbA treatment did not affect Mal-Fl uptake in either bacterium (Figure 16 and Figure 18), and the RDA of the composition of labeled JD98 stool samples, where Mal-Fl^+ samples from the non-treated control and MbA-treated groups clustered together (Figure 10), we can conclude that MbA had less impact on maltodextrin metabolism by gut bacteria compared to acarbose.

Ultimately, the work in this thesis sheds light on how antidiabetics, specifically amylase inhibitors, have an impact on distinct members of the GM. Starting from a complex and diverse community, we narrowed it down to a few individual microbial taxa and examined them closely as isolates. By identifying those that are affected by amylase inhibitors, future work can involve unveiling the molecular mechanisms of inhibition by these compounds on metabolic machinery, such as in the intriguing case of *B. vulgatus*.

5 Conclusion

As the importance of translating "who is there" to "what are they doing" has driven the innovation of function-driven genomics to study the GM, we applied a method that incorporates metabolic labeling with fluorescent glycan probes with FACS and 16S rDNA sequencing to pinpoint members of the GM that are affected by amylase inhibitors in their ability to take up glycans. While this method has the advantage of being culture-independent, validation of our method through growth assays of cultured isolates were essential for understanding how metabolism, and not just uptake, of maltodextrin was affected by amylase inhibitors.

Here, we used the stool samples of healthy volunteers. Indeed, it would be more relevant to test stool samples from diabetic individuals since their GMs are typically characterized by dysbiosis. However, the significance of interindividual differences in GM complicates the ability to generalize findings from a sample to a population. This method is not high-throughput enough to test a sufficiently large sample size to be able to generalize. Even so, we uncovered a few key members of the GM that are affected by amylase inhibitor. In doing so, we can begin to predict how the effect on a bacterium's metabolism and growth on starch affects the host by integrating information on outcomes of host health and specific functions carried out by these bacteria. We can further expand our sample type to mucosal biopsies to probe mucosa-associated microbes. Importantly, this work demonstrates that different strains of a species can be affected differently *in vitro* by acarbose. This highlights the importance of going beyond the genus or even species level when looking at the impact of acarbose or other amylase inhibitors on the GM.

Patnode *et al.*[216] emphasized the importance of considering an organism's response in the context of a community of interacting microbes. While our method evaluates the effect in a community-context, we lack the ability to interpret cross-feeding behavior and other interactions between

members of the GM. Co-culture methods could be used to further study the interactions between bacteria identified by this culture-independent method. The pipeline can be further adapted to include culturomics, to isolate potential amylase inhibitor-affected bacteria; metatranscriptomics, to examine and compare gene expression; metabolomics, to measure the levels of important metabolites such as SCFAs; and single-cell genomics, to scrutinize the genetic potential of an individual cell.

To conclude, we investigated the effects of amylase inhibitors on maltodextrin metabolism by gut bacteria using a functional pipeline. Our work identifies several gut bacteria in which maltodextrin metabolism is inhibited by acarbose. We also provide more evidence that MbA has less of an impact on metabolic activity of gut bacteria. This work contributes to our better understanding of the consequences of these oral medications on the GM and its host.

References

1 Rinninella, E. *et al.* What is the Healthy Gut Microbiota Composition? A Changing Ecosystem across Age, Environment, Diet, and Diseases. *Microorganisms* **7**, 14, doi:10.3390/microorganisms7010014 (2019).

2 Thursby, E. & Juge, N. Introduction to the human gut microbiota. *Biochemical Journal* **474**, 1823-1836, doi:10.1042/bcj20160510 (2017).

3 Gill, S. R. *et al.* Metagenomic Analysis of the Human Distal Gut Microbiome. *Science* **312**, 1355-1359, doi:doi:10.1126/science.1124234 (2006).

4 Ley, R. E., Peterson, D. A. & Gordon, J. I. Ecological and evolutionary forces shaping microbial diversity in the human intestine. *Cell* **124**, 837-848, doi:10.1016/j.cell.2006.02.017 (2006).

5 Claesson, M. J. *et al.* Comparative Analysis of Pyrosequencing and a Phylogenetic Microarray for Exploring Microbial Community Structures in the Human Distal Intestine. *PLoS ONE* **4**, e6669, doi:10.1371/journal.pone.0006669 (2009).

6 Woting, A. & Blaut, M. The Intestinal Microbiota in Metabolic Disease. *Nutrients* **8**, 202, doi:10.3390/nu8040202 (2016).

7 Kaoutari, A. E., Armougom, F., Gordon, J. I., Raoult, D. & Henrissat, B. The abundance and variety of carbohydrate-active enzymes in the human gut microbiota. *Nature Reviews Microbiology* **11**, 497-504, doi:10.1038/nrmicro3050 (2013).

8 Arumugam, M. *et al.* Enterotypes of the human gut microbiome. *Nature* **473**, 174-180, doi:10.1038/nature09944 (2011).

9 Costea, P. I. *et al.* Enterotypes in the landscape of gut microbial community composition. *Nature Microbiology* **3**, 8-16, doi:10.1038/s41564-017-0072-8 (2018).

10 Mazmanian, S. K., Liu, C. H., Tzianabos, A. O. & Kasper, D. L. An immunomodulatory molecule of symbiotic bacteria directs maturation of the host immune system. *Cell* **122**, 107-118, doi:10.1016/j.cell.2005.05.007 (2005).

11 Smith, K., McCoy, K. D. & Macpherson, A. J. Use of axenic animals in studying the adaptation of mammals to their commensal intestinal microbiota. *Semin Immunol* **19**, 59-69, doi:10.1016/j.smim.2006.10.002 (2007).

12 Petersson, J. *et al.* Importance and regulation of the colonic mucus barrier in a mouse model of colitis. *Am J Physiol Gastrointest Liver Physiol* **300**, G327-333, doi:10.1152/ajpgi.00422.2010 (2011).

13 Sano, T. *et al.* An IL-23R/IL-22 Circuit Regulates Epithelial Serum Amyloid A to Promote Local Effector Th17 Responses. *Cell* **163**, 381-393, doi:10.1016/j.cell.2015.08.061 (2015).

14 Nagai, M., Obata, Y., Takahashi, D. & Hase, K. Fine-tuning of the mucosal barrier and metabolic systems using the diet-microbial metabolite axis. *Int Immunopharmacol* **37**, 79-86, doi:10.1016/j.intimp.2016.04.001 (2016).

15 LeBlanc, J. G. *et al.* Bacteria as vitamin suppliers to their host: a gut microbiota perspective. *Curr Opin Biotechnol* **24**, 160-168, doi:10.1016/j.copbio.2012.08.005 (2013).

16 Martens, J. H., Barg, H., Warren, M. J. & Jahn, D. Microbial production of vitamin B12. *Appl Microbiol Biotechnol* **58**, 275-285, doi:10.1007/s00253-001-0902-7 (2002).

17 Pompei, A. *et al.* Folate production by bifidobacteria as a potential probiotic property. *Appl Environ Microbiol* **73**, 179-185, doi:10.1128/aem.01763-06 (2007).

18 Staley, C., Weingarden, A. R., Khoruts, A. & Sadowsky, M. J. Interaction of gut microbiota with bile acid metabolism and its influence on disease states. *Applied Microbiology and Biotechnology* **101**, 47-64, doi:10.1007/s00253-016-8006-6 (2017).
19 Sorg, J. A. & Sonenshein, A. L. Chenodeoxycholate is an inhibitor of Clostridium difficile spore germination. *J Bacteriol* **191**, 1115-1117, doi:10.1128/jb.01260-08 (2009).
20 Rowland, I. *et al.* Gut microbiota functions: metabolism of nutrients and other food components. *Eur J Nutr* **57**, 1-24, doi:10.1007/s00394-017-1445-8 (2018).
21 Rothschild, D. *et al.* Environment dominates over host genetics in shaping human gut microbiota. *Nature* **555**, 210-215, doi:10.1038/nature25973 (2018).
22 Wu, G. D. *et al.* Linking long-term dietary patterns with gut microbial enterotypes. *Science* **334**, 105-108, doi:10.1126/science.1208344 (2011).
23 Caporaso, J. G. *et al.* Moving pictures of the human microbiome. *Genome Biology* **12**, R50, doi:10.1186/gb-2011-12-5-r50 (2011).
24 Lozupone, C. A., Stombaugh, J. I., Gordon, J. I., Jansson, J. K. & Knight, R. Diversity, stability and resilience of the human gut microbiota. *Nature* **489**, 220-230, doi:10.1038/nature11550 (2012).
25 David, L. A. *et al.* Diet rapidly and reproducibly alters the human gut microbiome. *Nature* **505**, 559-563, doi:10.1038/nature12820 (2014).
26 Wu, M. *et al.* Genetic determinants of in vivo fitness and diet responsiveness in multiple human gut Bacteroides. *Science* **350**, aac5992, doi:10.1126/science.aac5992 (2015).
27 Desai, M. S. *et al.* A Dietary Fiber-Deprived Gut Microbiota Degrades the Colonic Mucus Barrier and Enhances Pathogen Susceptibility. *Cell* **167**, 1339-1353.e1321, doi:10.1016/j.cell.2016.10.043 (2016).
28 Rachel *et al.* Diet Dominates Host Genotype in Shaping the Murine Gut Microbiota. *Cell Host & Microbe* **17**, 72-84, doi:10.1016/j.chom.2014.11.010 (2015).
29 Deehan, E. C. *et al.* Precision Microbiome Modulation with Discrete Dietary Fiber Structures Directs Short-Chain Fatty Acid Production. *Cell Host Microbe* **27**, 389-404.e386, doi:10.1016/j.chom.2020.01.006 (2020).
30 Bertozzi, C. R. & Rabuka, D. in *Essentials of Glycobiology* (eds A. Varki *et al.*) (Cold Spring Harbor Laboratory Press Copyright © 2009, The Consortium of Glycobiology Editors, La Jolla, California., 2009).
31 Porter, N. T. & Martens, E. C. The Critical Roles of Polysaccharides in Gut Microbial Ecology and Physiology. *Annual Review of Microbiology* **71**, 349-369, doi:10.1146/annurev-micro-102215-095316 (2017).
32 Brayer, G. D., Luo, Y. & Withers, S. G. The structure of human pancreatic alpha-amylase at 1.8 A resolution and comparisons with related enzymes. *Protein Sci* **4**, 1730-1742, doi:10.1002/pro.5560040908 (1995).
33 Gropper, S. S., Smith, J.L., Groff, J.L. *Advanced nutrition and human metabolism*. (Wadsworth Publishing, 2008).
34 Stephen, A., Haddad, A. & Phillips, S. Passage of carbohydrate into the colon. *Gastroenterology.* **85**, 589 (1983).
35 Tan, J. *et al.* The role of short-chain fatty acids in health and disease. *Adv Immunol* **121**, 91-119, doi:10.1016/b978-0-12-800100-4.00003-9 (2014).
36 Englyst, H. N., Kingman, S. M. & Cummings, J. H. Classification and measurement of nutritionally important starch fractions. *Eur J Clin Nutr* **46 Suppl 2**, S33-50 (1992).

37 Henrissat, B. A classification of glycosyl hydrolases based on amino acid sequence similarities. *Biochem J* **280 (Pt 2)**, 309-316, doi:10.1042/bj2800309 (1991).
38 Lombard, V. *et al.* A hierarchical classification of polysaccharide lyases for glycogenomics. *Biochem J* **432**, 437-444, doi:10.1042/bj20101185 (2010).
39 Drula, E. *et al.* The carbohydrate-active enzyme database: functions and literature. *Nucleic Acids Res* **50**, D571-d577, doi:10.1093/nar/gkab1045 (2022).
40 Cordain, L. *et al.* Origins and evolution of the Western diet: health implications for the 21st century. *The American Journal of Clinical Nutrition* **81**, 341-354, doi:10.1093/ajcn.81.2.341 (2005).
41 Cerqueira, F. M., Photenhauer, A. L., Pollet, R. M., Brown, H. A. & Koropatkin, N. M. Starch Digestion by Gut Bacteria: Crowdsourcing for Carbs. *Trends in Microbiology* **28**, 95-108, doi:10.1016/j.tim.2019.09.004 (2020).
42 Møller, M. S. & Svensson, B. Structural biology of starch-degrading enzymes and their regulation. *Current Opinion in Structural Biology* **40**, 33-42, doi:https://doi.org/10.1016/j.sbi.2016.07.006 (2016).
43 Stam, M. R., Danchin, E. G. J., Rancurel, C., Coutinho, P. M. & Henrissat, B. Dividing the large glycoside hydrolase family 13 into subfamilies: towards improved functional annotations of α-amylase-related proteins. *Protein Engineering, Design and Selection* **19**, 555-562, doi:10.1093/protein/gzl044 (2006).
44 Martens, E. C., Koropatkin, N. M., Smith, T. J. & Gordon, J. I. Complex Glycan Catabolism by the Human Gut Microbiota: The Bacteroidetes Sus-like Paradigm. *Journal of Biological Chemistry* **284**, 24673-24677, doi:10.1074/jbc.r109.022848 (2009).
45 Shipman, J. A., Berleman, J. E. & Salyers, A. A. Characterization of four outer membrane proteins involved in binding starch to the cell surface of Bacteroides thetaiotaomicron. *J Bacteriol* **182**, 5365-5372, doi:10.1128/jb.182.19.5365-5372.2000 (2000).
46 Tancula, E., Feldhaus, M. J., Bedzyk, L. A. & Salyers, A. A. Location and characterization of genes involved in binding of starch to the surface of Bacteroides thetaiotaomicron. *J Bacteriol* **174**, 5609-5616, doi:10.1128/jb.174.17.5609-5616.1992 (1992).
47 Shipman, J. A., Cho, K. H., Siegel, H. A. & Salyers, A. A. Physiological characterization of SusG, an outer membrane protein essential for starch utilization by Bacteroides thetaiotaomicron. *J Bacteriol* **181**, 7206-7211, doi:10.1128/jb.181.23.7206-7211.1999 (1999).
48 Koropatkin, N. M. & Smith, T. J. SusG: A Unique Cell-Membrane-Associated α-Amylase from a Prominent Human Gut Symbiont Targets Complex Starch Molecules. *Structure* **18**, 200-215, doi:https://doi.org/10.1016/j.str.2009.12.010 (2010).
49 Arnal, G., Cockburn, D. W., Brumer, H. & Koropatkin, N. M. Structural basis for the flexible recognition of α-glucan substrates by Bacteroides thetaiotaomicron SusG. *Protein Science* **27**, 1093-1101, doi:https://doi.org/10.1002/pro.3410 (2018).
50 Reeves, A. R., D'Elia, J. N., Frias, J. & Salyers, A. A. A Bacteroides thetaiotaomicron outer membrane protein that is essential for utilization of maltooligosaccharides and starch. *J Bacteriol* **178**, 823-830, doi:10.1128/jb.178.3.823-830.1996 (1996).
51 D'Elia, J. N. & Salyers, A. A. Effect of regulatory protein levels on utilization of starch by Bacteroides thetaiotaomicron. *J Bacteriol* **178**, 7180-7186, doi:10.1128/jb.178.24.7180-7186.1996 (1996).

52 Rogowski, A. *et al.* Glycan complexity dictates microbial resource allocation in the large intestine. *Nature Communications* **6**, 7481, doi:10.1038/ncomms8481 (2015).
53 Martens, E. C. *et al.* Recognition and Degradation of Plant Cell Wall Polysaccharides by Two Human Gut Symbionts. *PLoS Biology* **9**, e1001221, doi:10.1371/journal.pbio.1001221 (2011).
54 Sonnenburg, E. D. *et al.* Specificity of polysaccharide use in intestinal bacteroides species determines diet-induced microbiota alterations. *Cell* **141**, 1241-1252, doi:10.1016/j.cell.2010.05.005 (2010).
55 Cuskin, F. *et al.* Human gut Bacteroidetes can utilize yeast mannan through a selfish mechanism. *Nature* **517**, 165-169, doi:10.1038/nature13995 (2015).
56 Hehemann, J.-H., Kelly, A. G., Pudlo, N. A., Martens, E. C. & Boraston, A. B. Bacteria of the human gut microbiome catabolize red seaweed glycans with carbohydrate-active enzyme updates from extrinsic microbes. *Proceedings of the National Academy of Sciences* **109**, 19786, doi:10.1073/pnas.1211002109 (2012).
57 Foley, M. H., Cockburn, D. W. & Koropatkin, N. M. The Sus operon: a model system for starch uptake by the human gut Bacteroidetes. *Cellular and Molecular Life Sciences* **73**, 2603-2617, doi:10.1007/s00018-016-2242-x (2016).
58 Leitch, E. C. M., Walker, A. W., Duncan, S. H., Holtrop, G. & Flint, H. J. Selective colonization of insoluble substrates by human faecal bacteria. *Environmental microbiology* **9**, 667-679 (2007).
59 Kovatcheva-Datchary, P. *et al.* Linking phylogenetic identities of bacteria to starch fermentation in an in vitro model of the large intestine by RNA-based stable isotope probing. *Environmental microbiology* **11**, 914-926 (2009).
60 Underwood, M. A., German, J. B., Lebrilla, C. B. & Mills, D. A. Bifidobacterium longum subspecies infantis: champion colonizer of the infant gut. *Pediatric Research* **77**, 229-235, doi:10.1038/pr.2014.156 (2015).
61 Zúñiga, M., Monedero, V. & Yebra, M. J. Utilization of Host-Derived Glycans by Intestinal Lactobacillus and Bifidobacterium Species. *Frontiers in Microbiology* **9**, doi:10.3389/fmicb.2018.01917 (2018).
62 Crittenden, R. G. *et al.* Selection of a Bifidobacterium strain to complement resistant starch in a synbiotic yoghurt. *J Appl Microbiol* **90**, 268-278, doi:10.1046/j.1365-2672.2001.01240.x (2001).
63 Duranti, S. *et al.* Genomic characterization and transcriptional studies of the starch-utilizing strain Bifidobacterium adolescentis 22L. *Appl Environ Microbiol* **80**, 6080-6090, doi:10.1128/aem.01993-14 (2014).
64 Ze, X., Duncan, S. H., Louis, P. & Flint, H. J. Ruminococcus bromii is a keystone species for the degradation of resistant starch in the human colon. *Isme j* **6**, 1535-1543, doi:10.1038/ismej.2012.4 (2012).
65 Mukhopadhya, I. *et al.* Sporulation capability and amylosome conservation among diverse human colonic and rumen isolates of the keystone starch-degrader Ruminococcus bromii. *Environmental Microbiology* **20**, 324-336, doi:https://doi.org/10.1111/1462-2920.14000 (2018).
66 Ze, X. *et al.* Unique organization of extracellular amylases into amylosomes in the resistant starch-utilizing human colonic Firmicutes bacterium Ruminococcus bromii. *MBio* **6**, e01058-01015 (2015).

67 Bayer, E. A., Belaich, J.-P., Shoham, Y. & Lamed, R. The Cellulosomes: Multienzyme Machines for Degradation of Plant Cell Wall Polysaccharides. *Annual Review of Microbiology* **58**, 521-554, doi:10.1146/annurev.micro.57.030502.091022 (2004).
68 Stahl, S. W. *et al.* Single-molecule dissection of the high-affinity cohesin-dockerin complex. *Proceedings of the National Academy of Sciences* **109**, 20431-20436, doi:10.1073/pnas.1211929109 (2012).
69 Cockburn, D. W. *et al.* Molecular details of a starch utilization pathway in the human gut symbiont Eubacterium rectale. *Molecular Microbiology* **95**, 209-230, doi:https://doi.org/10.1111/mmi.12859 (2015).
70 Scott, K. P. *et al.* Substrate-driven gene expression in Roseburia inulinivorans: Importance of inducible enzymes in the utilization of inulin and starch. *Proceedings of the National Academy of Sciences* **108**, 4672-4679, doi:10.1073/pnas.1000091107 (2011).
71 Ramsay, A. G., Scott, K. P., Martin, J. C., Rincon, M. T. & Flint, H. J. Cell-associated α-amylases of butyrate-producing Firmicute bacteria from the human colon. *Microbiology* **152**, 3281-3290, doi:https://doi.org/10.1099/mic.0.29233-0 (2006).
72 Gänzle, M. G. & Follador, R. Metabolism of Oligosaccharides and Starch in Lactobacilli: A Review. *Frontiers in Microbiology* **3**, doi:10.3389/fmicb.2012.00340 (2012).
73 Neubauer, H., Glaasker, E., Hammes, W. P., Poolman, B. & Konings, W. N. Mechanism of maltose uptake and glucose excretion in Lactobacillus sanfrancisco. *Journal of bacteriology* **176**, 3007-3012, doi:10.1128/jb.176.10.3007-3012.1994 (1994).
74 Cockburn, D. W. & Koropatkin, N. M. Polysaccharide Degradation by the Intestinal Microbiota and Its Influence on Human Health and Disease. *Journal of Molecular Biology* **428**, 3230-3252, doi:10.1016/j.jmb.2016.06.021 (2016).
75 Bergman, E. N. Energy contributions of volatile fatty acids from the gastrointestinal tract in various species. *Physiological Reviews* **70**, 567-590, doi:10.1152/physrev.1990.70.2.567 (1990).
76 Wong, J. M. W., de Souza, R., Kendall, C. W. C., Emam, A. & Jenkins, D. J. A. Colonic Health: Fermentation and Short Chain Fatty Acids. *Journal of Clinical Gastroenterology* **40** (2006).
77 Suzuki, T., Yoshida, S. & Hara, H. Physiological concentrations of short-chain fatty acids immediately suppress colonic epithelial permeability. *British Journal of Nutrition* **100**, 297-305, doi:10.1017/S0007114508888733 (2008).
78 Pomare, E. W., Branch, W. J. & Cummings, J. H. Carbohydrate fermentation in the human colon and its relation to acetate concentrations in venous blood. *The Journal of Clinical Investigation* **75**, 1448-1454, doi:10.1172/JCI111847 (1985).
79 Corrêa-Oliveira, R., Fachi, J. L., Vieira, A., Sato, F. T. & Vinolo, M. A. R. Regulation of immune cell function by short-chain fatty acids. *Clinical & Translational Immunology* **5**, e73, doi:https://doi.org/10.1038/cti.2016.17 (2016).
80 Koh, A., De Vadder, F., Kovatcheva-Datchary, P. & Bäckhed, F. From Dietary Fiber to Host Physiology: Short-Chain Fatty Acids as Key Bacterial Metabolites. *Cell* **165**, 1332-1345, doi:10.1016/j.cell.2016.05.041 (2016).
81 MacDonald, V. E. & Howe, L. J. Histone acetylation: Where to go and how to get there. *Epigenetics* **4**, 139-143, doi:10.4161/epi.4.3.8484 (2009).

82 Boffa, L. C., Vidali, G., Mann, R. S. & Allfrey, V. G. Suppression of histone deacetylation in vivo and in vitro by sodium butyrate. *Journal of Biological Chemistry* **253**, 3364-3366, doi:https://doi.org/10.1016/S0021-9258(17)34804-4 (1978).
83 Kiefer, J., Beyer-Sehlmeyer, G. & Pool-Zobel, B. L. Mixtures of SCFA, composed according to physiologically available concentrations in the gut lumen, modulate histone acetylation in human HT29 colon cancer cells. *British Journal of Nutrition* **96**, 803-810, doi:10.1017/BJN20061948 (2006).
84 Waldecker, M., Kautenburger, T., Daumann, H., Busch, C. & Schrenk, D. Inhibition of histone-deacetylase activity by short-chain fatty acids and some polyphenol metabolites formed in the colon. *The Journal of Nutritional Biochemistry* **19**, 587-593, doi:https://doi.org/10.1016/j.jnutbio.2007.08.002 (2008).
85 Hayden, M. S., West, A. P. & Ghosh, S. NF-κB and the immune response. *Oncogene* **25**, 6758-6780, doi:10.1038/sj.onc.1209943 (2006).
86 Usami, M. *et al.* Butyrate and trichostatin A attenuate nuclear factor κB activation and tumor necrosis factor α secretion and increase prostaglandin E2 secretion in human peripheral blood mononuclear cells. *Nutrition Research* **28**, 321-328, doi:https://doi.org/10.1016/j.nutres.2008.02.012 (2008).
87 Kendrick, S. F. W. *et al.* Acetate, the key modulator of inflammatory responses in acute alcoholic hepatitis. *Hepatology* **51**, 1988-1997, doi:https://doi.org/10.1002/hep.23572 (2010).
88 Lucas, J. L. *et al.* Induction of Foxp3+ regulatory T cells with histone deacetylase inhibitors. *Cellular Immunology* **257**, 97-104, doi:https://doi.org/10.1016/j.cellimm.2009.03.004 (2009).
89 Tao, R. *et al.* Deacetylase inhibition promotes the generation and function of regulatory T cells. *Nature Medicine* **13**, 1299-1307, doi:10.1038/nm1652 (2007).
90 Le Poul, E. *et al.* Functional Characterization of Human Receptors for Short Chain Fatty Acids and Their Role in Polymorphonuclear Cell Activation*. *Journal of Biological Chemistry* **278**, 25481-25489, doi:https://doi.org/10.1074/jbc.M301403200 (2003).
91 Tolhurst, G. *et al.* Short-Chain Fatty Acids Stimulate Glucagon-Like Peptide-1 Secretion via the G-Protein–Coupled Receptor FFAR2. *Diabetes* **61**, 364-371, doi:10.2337/db11-1019 (2012).
92 Lee Kennedy, R. *et al.* Free fatty acid receptors: emerging targets for treatment of diabetes and its complications. *Therapeutic advances in endocrinology and metabolism* **1**, 165-175 (2010).
93 Roelofsen, H., Priebe, M. G. & Vonk, R. J. The interaction of short-chain fatty acids with adipose tissue: relevance for prevention of type 2 diabetes. *Benef Microbes* **1**, 433-437, doi:10.3920/bm2010.0028 (2010).
94 Ge, H. *et al.* Activation of G protein-coupled receptor 43 in adipocytes leads to inhibition of lipolysis and suppression of plasma free fatty acids. *Endocrinology* **149**, 4519-4526, doi:10.1210/en.2008-0059 (2008).
95 Hong, Y. H. *et al.* Acetate and propionate short chain fatty acids stimulate adipogenesis via GPCR43. *Endocrinology* **146**, 5092-5099, doi:10.1210/en.2005-0545 (2005).
96 Cox, M. A. *et al.* Short-chain fatty acids act as antiinflammatory mediatorsby regulating prostaglandin E2 and cytokines. *World Journal of Gastroenterology* **15**, 5549, doi:10.3748/wjg.15.5549 (2009).

97 Karaki, S.-i. *et al.* Expression of the short-chain fatty acid receptor, GPR43, in the human colon. *Journal of Molecular Histology* **39**, 135-142, doi:10.1007/s10735-007-9145-y (2008).
98 Tazoe, H. *et al.* Expression of short-chain fatty acid receptor GPR41 in the human colon. *Biomedical Research* **30**, 149-156, doi:10.2220/biomedres.30.149 (2009).
99 Kimura, I. *et al.* Short-chain fatty acids and ketones directly regulate sympathetic nervous system via G protein-coupled receptor 41 (GPR41). *Proceedings of the National Academy of Sciences* **108**, 8030-8035, doi:10.1073/pnas.1016088108 (2011).
100 De Vadder, F. *et al.* Microbiota-Generated Metabolites Promote Metabolic Benefits via Gut-Brain Neural Circuits. *Cell* **156**, 84-96, doi:https://doi.org/10.1016/j.cell.2013.12.016 (2014).
101 Thangaraju, M. *et al.* GPR109A is a G-protein-coupled receptor for the bacterial fermentation product butyrate and functions as a tumor suppressor in colon. *Cancer Res* **69**, 2826-2832, doi:10.1158/0008-5472.Can-08-4466 (2009).
102 Wanders, D., Graff, E. C. & Judd, R. L. Effects of high fat diet on GPR109A and GPR81 gene expression. *Biochemical and Biophysical Research Communications* **425**, 278-283, doi:https://doi.org/10.1016/j.bbrc.2012.07.082 (2012).
103 Kang, I., Kim, S.-W. & Youn, J. H. Effects of Nicotinic Acid on Gene Expression: Potential Mechanisms and Implications for Wanted and Unwanted Effects of the Lipid-Lowering Drug. *The Journal of Clinical Endocrinology & Metabolism* **96**, 3048-3055, doi:10.1210/jc.2011-1104 (2011).
104 Singh, N. *et al.* Activation of Gpr109a, receptor for niacin and the commensal metabolite butyrate, suppresses colonic inflammation and carcinogenesis. *Immunity* **40**, 128-139, doi:10.1016/j.immuni.2013.12.007 (2014).
105 Gómez de Cedrón, M. & Ramírez de Molina, A. in *Precision Medicine for Investigators, Practitioners and Providers* (eds Joel Faintuch & Salomao Faintuch) 291-299 (Academic Press, 2020).
106 Fragiadakis, G. K. *et al.* Links between environment, diet, and the hunter-gatherer microbiome. *Gut Microbes* **10**, 216-227, doi:10.1080/19490976.2018.1494103 (2019).
107 Sonnenburg, E. D. *et al.* Diet-induced extinctions in the gut microbiota compound over generations. *Nature* **529**, 212-215, doi:10.1038/nature16504 (2016).
108 Brown, K., DeCoffe, D., Molcan, E. & Gibson, D. L. Diet-induced dysbiosis of the intestinal microbiota and the effects on immunity and disease. *Nutrients* **4**, 1095-1119, doi:10.3390/nu4081095 (2012).
109 De Filippo, C. *et al.* Impact of diet in shaping gut microbiota revealed by a comparative study in children from Europe and rural Africa. *Proceedings of the National Academy of Sciences* **107**, 14691-14696, doi:10.1073/pnas.1005963107 (2010).
110 Park, Y., Subar, A. F., Hollenbeck, A. & Schatzkin, A. Dietary fiber intake and mortality in the NIH-AARP diet and health study. *Arch Intern Med* **171**, 1061-1068, doi:10.1001/archinternmed.2011.18 (2011).
111 Khor, B., Gardet, A. & Xavier, R. J. Genetics and pathogenesis of inflammatory bowel disease. *Nature* **474**, 307-317, doi:10.1038/nature10209 (2011).
112 Nishida, A. *et al.* Gut microbiota in the pathogenesis of inflammatory bowel disease. *Clinical Journal of Gastroenterology* **11**, 1-10, doi:10.1007/s12328-017-0813-5 (2018).

113 Liu, J. Z. *et al.* Association analyses identify 38 susceptibility loci for inflammatory bowel disease and highlight shared genetic risk across populations. *Nat Genet* **47**, 979-986, doi:10.1038/ng.3359 (2015).
114 Sheehan, D., Moran, C. & Shanahan, F. The microbiota in inflammatory bowel disease. *J Gastroenterol* **50**, 495-507, doi:10.1007/s00535-015-1064-1 (2015).
115 Fujimoto, T. *et al.* Decreased abundance of Faecalibacterium prausnitzii in the gut microbiota of Crohn's disease. *J Gastroenterol Hepatol* **28**, 613-619, doi:10.1111/jgh.12073 (2013).
116 Nishino, K. *et al.* Analysis of endoscopic brush samples identified mucosa-associated dysbiosis in inflammatory bowel disease. *Journal of Gastroenterology* **53**, 95-106, doi:10.1007/s00535-017-1384-4 (2018).
117 Takahashi, K. *et al.* Reduced Abundance of Butyrate-Producing Bacteria Species in the Fecal Microbial Community in Crohn's Disease. *Digestion* **93**, 59-65, doi:10.1159/000441768 (2016).
118 Machiels, K. *et al.* A decrease of the butyrate-producing species Roseburia hominis and Faecalibacterium prausnitzii defines dysbiosis in patients with ulcerative colitis. *Gut* **63**, 1275-1283, doi:10.1136/gutjnl-2013-304833 (2014).
119 Sun, M., Wu, W., Liu, Z. & Cong, Y. Microbiota metabolite short chain fatty acids, GPCR, and inflammatory bowel diseases. *J Gastroenterol* **52**, 1-8, doi:10.1007/s00535-016-1242-9 (2017).
120 Hu, F. *Obesity epidemiology*. (Oxford University Press, 2008).
121 Hruby, A. & Hu, F. B. The Epidemiology of Obesity: A Big Picture. *Pharmacoeconomics* **33**, 673-689, doi:10.1007/s40273-014-0243-x (2015).
122 Murphy, E. F. *et al.* Composition and energy harvesting capacity of the gut microbiota: relationship to diet, obesity and time in mouse models. *Gut* **59**, 1635-1642, doi:10.1136/gut.2010.215665 (2010).
123 Turnbaugh, P. J. *et al.* An obesity-associated gut microbiome with increased capacity for energy harvest. *Nature* **444**, 1027-1031, doi:10.1038/nature05414 (2006).
124 Schwiertz, A. *et al.* Microbiota and SCFA in Lean and Overweight Healthy Subjects. *Obesity* **18**, 190-195, doi:10.1038/oby.2009.167 (2010).
125 Duncan, S. H. *et al.* Human colonic microbiota associated with diet, obesity and weight loss. *Int J Obes (Lond)* **32**, 1720-1724, doi:10.1038/ijo.2008.155 (2008).
126 Karlsson, C. L. *et al.* The microbiota of the gut in preschool children with normal and excessive body weight. *Obesity (Silver Spring)* **20**, 2257-2261, doi:10.1038/oby.2012.110 (2012).
127 Whang, A., Nagpal, R. & Yadav, H. Bi-directional drug-microbiome interactions of anti-diabetics. *EBioMedicine* **39**, 591-602, doi:10.1016/j.ebiom.2018.11.046 (2019).
128 Cani, P. D. *et al.* Metabolic Endotoxemia Initiates Obesity and Insulin Resistance. *Diabetes* **56**, 1761-1772, doi:10.2337/db06-1491 (2007).
129 Shi, H. *et al.* TLR4 links innate immunity and fatty acid-induced insulin resistance. *J Clin Invest* **116**, 3015-3025, doi:10.1172/jci28898 (2006).
130 Anderson, P. D. *et al.* Innate Immunity Modulates Adipokines in Humans. *The Journal of Clinical Endocrinology & Metabolism* **92**, 2272-2279, doi:10.1210/jc.2006-2545 (2007).
131 Ridaura, V. K. *et al.* Gut microbiota from twins discordant for obesity modulate metabolism in mice. *Science* **341**, 1241214, doi:10.1126/science.1241214 (2013).

132 Liu, R. *et al.* Gut microbiome and serum metabolome alterations in obesity and after weight-loss intervention. *Nature Medicine* **23**, 859-868, doi:10.1038/nm.4358 (2017).
133 Organization, W. H. *Diabetes*, <https://www.who.int/news-room/fact-sheets/detail/diabetes> (2021).
134 Organization, W. H. *The top 10 causes of death*, <https://www.who.int/news-room/fact-sheets/detail/the-top-10-causes-of-death> (2020).
135 Atlas, D. International diabetes federation. *IDF Diabetes Atlas, 7th edn. Brussels, Belgium: International Diabetes Federation* (2015).
136 Esser, N., Legrand-Poels, S., Piette, J., Scheen, A. J. & Paquot, N. Inflammation as a link between obesity, metabolic syndrome and type 2 diabetes. *Diabetes Res Clin Pract* **105**, 141-150, doi:10.1016/j.diabres.2014.04.006 (2014).
137 Wang, X. *et al.* Inflammatory markers and risk of type 2 diabetes: a systematic review and meta-analysis. *Diabetes Care* **36**, 166-175, doi:10.2337/dc12-0702 (2013).
138 Al-Shukaili, A. *et al.* Analysis of inflammatory mediators in type 2 diabetes patients. *Int J Endocrinol* **2013**, 976810, doi:10.1155/2013/976810 (2013).
139 Qin, J. *et al.* A metagenome-wide association study of gut microbiota in type 2 diabetes. *Nature* **490**, 55-60, doi:10.1038/nature11450 (2012).
140 Karlsson, F. H. *et al.* Gut metagenome in European women with normal, impaired and diabetic glucose control. *Nature* **498**, 99-103, doi:10.1038/nature12198 (2013).
141 Pedersen, H. K. *et al.* Human gut microbes impact host serum metabolome and insulin sensitivity. *Nature* **535**, 376-381, doi:10.1038/nature18646 (2016).
142 Velagapudi, V. R. *et al.* The gut microbiota modulates host energy and lipid metabolism in mice. *J Lipid Res* **51**, 1101-1112, doi:10.1194/jlr.M002774 (2010).
143 Gao, Z. *et al.* Butyrate Improves Insulin Sensitivity and Increases Energy Expenditure in Mice. *Diabetes* **58**, 1509-1517, doi:10.2337/db08-1637 (2009).
144 Wewalka, M., Patti, M. E., Barbato, C., Houten, S. M. & Goldfine, A. B. Fasting serum taurine-conjugated bile acids are elevated in type 2 diabetes and do not change with intensification of insulin. *J Clin Endocrinol Metab* **99**, 1442-1451, doi:10.1210/jc.2013-3367 (2014).
145 Tomkin, G. H. & Owens, D. Obesity diabetes and the role of bile acids in metabolism. *J Transl Int Med* **4**, 73-80, doi:10.1515/jtim-2016-0018 (2016).
146 Spanogiannopoulos, P., Bess, E. N., Carmody, R. N. & Turnbaugh, P. J. The microbial pharmacists within us: a metagenomic view of xenobiotic metabolism. *Nature Reviews Microbiology* **14**, 273-287, doi:10.1038/nrmicro.2016.17 (2016).
147 Vich Vila, A. *et al.* Impact of commonly used drugs on the composition and metabolic function of the gut microbiota. *Nature Communications* **11**, 362, doi:10.1038/s41467-019-14177-z (2020).
148 Weersma, R. K., Zhernakova, A. & Fu, J. Interaction between drugs and the gut microbiome. *Gut* **69**, 1510-1519, doi:10.1136/gutjnl-2019-320204 (2020).
149 Takagi, T. *et al.* The influence of long-term use of proton pump inhibitors on the gut microbiota: an age-sex-matched case-control study. *Journal of Clinical Biochemistry and Nutrition* **62**, 100-105, doi:10.3164/jcbn.17-78 (2018).
150 Tsuda, A. *et al.* Influence of Proton-Pump Inhibitors on the Luminal Microbiota in the Gastrointestinal Tract. *Clinical and Translational Gastroenterology* **6** (2015).
151 Haiser, H. J. & Turnbaugh, P. J. Developing a metagenomic view of xenobiotic metabolism. *Pharmacol Res* **69**, 21-31, doi:10.1016/j.phrs.2012.07.009 (2013).

152 Bachrach, W. H. Sulfasalazine: I. An historical perspective. *Am J Gastroenterol* **83**, 487-496 (1988).
153 Chaudhury, A. *et al.* Clinical Review of Antidiabetic Drugs: Implications for Type 2 Diabetes Mellitus Management. *Frontiers in endocrinology* **8**, 6-6, doi:10.3389/fendo.2017.00006 (2017).
154 Rena, G., Hardie, D. G. & Pearson, E. R. The mechanisms of action of metformin. *Diabetologia* **60**, 1577-1585, doi:10.1007/s00125-017-4342-z (2017).
155 McCreight, L. J., Bailey, C. J. & Pearson, E. R. Metformin and the gastrointestinal tract. *Diabetologia* **59**, 426-435, doi:10.1007/s00125-015-3844-9 (2016).
156 Bauer, P. V. *et al.* Metformin Alters Upper Small Intestinal Microbiota that Impact a Glucose-SGLT1-Sensing Glucoregulatory Pathway. *Cell Metabolism* **27**, 101-117.e105, doi:10.1016/j.cmet.2017.09.019 (2018).
157 Wu, H. *et al.* Metformin alters the gut microbiome of individuals with treatment-naive type 2 diabetes, contributing to the therapeutic effects of the drug. *Nat Med* **23**, 850-858, doi:10.1038/nm.4345 (2017).
158 Forslund, K. *et al.* Disentangling type 2 diabetes and metformin treatment signatures in the human gut microbiota. *Nature* **528**, 262-266, doi:10.1038/nature15766 (2015).
159 Shin, N.-R. *et al.* An increase in the Akkermansia spp. population induced by metformin treatment improves glucose homeostasis in diet-induced obese mice. *Gut* **63**, 727-735, doi:10.1136/gutjnl-2012-303839 (2014).
160 Sun, L. *et al.* Gut microbiota and intestinal FXR mediate the clinical benefits of metformin. *Nature medicine* **24**, 1919-1929, doi:10.1038/s41591-018-0222-4 (2018).
161 Lee, H., Ko, G. & Griffiths, M. W. Effect of Metformin on Metabolic Improvement and Gut Microbiota. *Applied and Environmental Microbiology* **80**, 5935-5943, doi:doi:10.1128/AEM.01357-14 (2014).
162 de la Cuesta-Zuluaga, J. *et al.* Metformin Is Associated With Higher Relative Abundance of Mucin-Degrading Akkermansia muciniphila and Several Short-Chain Fatty Acid–Producing Microbiota in the Gut. *Diabetes Care* **40**, 54-62, doi:10.2337/dc16-1324 (2016).
163 Plovier, H. *et al.* A purified membrane protein from Akkermansia muciniphila or the pasteurized bacterium improves metabolism in obese and diabetic mice. *Nature Medicine* **23**, 107-113, doi:10.1038/nm.4236 (2017).
164 Zhang, M. *et al.* Effects of metformin, acarbose, and sitagliptin monotherapy on gut microbiota in Zucker diabetic fatty rats. *BMJ Open Diabetes Research & Care* **7**, e000717, doi:10.1136/bmjdrc-2019-000717 (2019).
165 Chen, J., Wang, R., Li, X. F. & Wang, R. L. Bifidobacterium adolescentis supplementation ameliorates visceral fat accumulation and insulin sensitivity in an experimental model of the metabolic syndrome. *Br J Nutr* **107**, 1429-1434, doi:10.1017/s0007114511004491 (2012).
166 Cani, P. D. *et al.* Changes in Gut Microbiota Control Metabolic Endotoxemia-Induced Inflammation in High-Fat Diet–Induced Obesity and Diabetes in Mice. *Diabetes* **57**, 1470-1481, doi:10.2337/db07-1403 (2008).
167 Tong, X. *et al.* Structural Alteration of Gut Microbiota during the Amelioration of Human Type 2 Diabetes with Hyperlipidemia by Metformin and a Traditional Chinese Herbal Formula: a Multicenter, Randomized, Open Label Clinical Trial. *mBio* **9**, e02392-02317, doi:10.1128/mBio.02392-17.

168 Derosa, G. & Maffioli, P. α-Glucosidase inhibitors and their use in clinical practice. *Arch Med Sci* **8**, 899-906, doi:10.5114/aoms.2012.31621 (2012).
169 Baron, A. D. Postprandial hyperglycaemia and alpha-glucosidase inhibitors. *Diabetes Res Clin Pract* **40 Suppl**, S51-55, doi:10.1016/s0168-8227(98)00043-6 (1998).
170 Derosa, G. *et al.* Acarbose actions on insulin resistance and inflammatory parameters during an oral fat load. *Eur J Pharmacol* **651**, 240-250, doi:10.1016/j.ejphar.2010.11.015 (2011).
171 Hirano, M. *et al.* Early improvement in carotid plaque echogenicity by acarbose in patients with acute coronary syndromes. *Circ J* **76**, 1452-1460, doi:10.1253/circj.cj-11-1524 (2012).
172 Li, C. *et al.* Acarbose rearrangement mechanism implied by the kinetic and structural analysis of human pancreatic alpha-amylase in complex with analogues and their elongated counterparts. *Biochemistry* **44**, 3347-3357, doi:10.1021/bi048334e (2005).
173 Williams, L. K. *et al.* The amylase inhibitor montbretin A reveals a new glycosidase inhibition motif. *Nature Chemical Biology* **11**, 691-696, doi:10.1038/nchembio.1865 (2015).
174 Santilli, A. D., Dawson, E. M., Whitehead, K. J. & Whitehead, D. C. Nonmicrobicidal Small Molecule Inhibition of Polysaccharide Metabolism in Human Gut Microbes: A Potential Therapeutic Avenue. *ACS Chem Biol* **13**, 1165-1172, doi:10.1021/acschembio.8b00309 (2018).
175 Lebovitz, H. E. alpha-Glucosidase inhibitors. *Endocrinol Metab Clin North Am* **26**, 539-551, doi:10.1016/s0889-8529(05)70266-8 (1997).
176 *ACARBOSE-acarbose tablet*, <https://dailymed.nlm.nih.gov/dailymed/drugInfo.cfm?setid=6c2db888-775c-4baf-a1b4-1cfa63b83357>
177 McIver L.A., T. J. *Acarbose*, <https://www.ncbi.nlm.nih.gov/books/NBK493214/>
178 Strokopytov, B. *et al.* X-ray structure of cyclodextrin glycosyltransferase complexed with acarbose. Implications for the catalytic mechanism of glycosidases. *Biochemistry* **34**, 2234-2240, doi:10.1021/bi00007a018 (1995).
179 Hemker, M. *et al.* Identification, Cloning, Expression, and Characterization of the Extracellular Acarbose-Modifying Glycosyltransferase, AcbD, from Actinoplanes sp. Strain SE50. *Journal of Bacteriology* **183**, 4484-4492, doi:doi:10.1128/JB.183.15.4484-4492.2001 (2001).
180 Gu, Y. *et al.* Analyses of gut microbiota and plasma bile acids enable stratification of patients for antidiabetic treatment. *Nature Communications* **8**, doi:10.1038/s41467-017-01682-2 (2017).
181 Zhang, X. *et al.* Effects of Acarbose on the Gut Microbiota of Prediabetic Patients: A Randomized, Double-blind, Controlled Crossover Trial. *Diabetes Therapy* **8**, 293-307, doi:10.1007/s13300-017-0226-y (2017).
182 Baxter, N. T., Lesniak, N. A., Sinani, H., Schloss, P. D., Koropatkin, N. M. The glucoamylase inhibitor acarbose has a diet-dependent and reversible effect on the murine gut microbiome. *mSphere* **4**, doi:https://doi.org/10.1128/mSphere.00528-18 (2019).
183 Su, B. *et al.* Acarbose treatment affects the serum levels of inflammatory cytokines and the gut content of bifidobacteria in Chinese patients with type 2 diabetes mellitus. *J Diabetes* **7**, 729-739, doi:10.1111/1753-0407.12232 (2015).

184 Maruhama, Y. *et al.* Effects of a glucoside-hydrolase inhibitor (Bay g 5421) on serum lipids, lipoproteins and bile acids, fecal fat and bacterial flora, and intestinal gas production in hyperlipidemic patients. *The Tohoku Journal of Experimental Medicine* **132**, 453-462, doi:10.1620/tjem.132.453 (1980).
185 Wolever, T. M. S. & Chiasson, J.-L. Acarbose raises serum butyrate in human subjects withimpaired glucose tolerance. *British Journal of Nutrition* **84**, 57-61, doi:10.1017/S0007114500001239 (2000).
186 Dehghan-Kooshkghazi, M. & Mathers, J. C. Starch digestion, large-bowel fermentation and intestinal mucosal cell proliferation in rats treated with the α-glucosidase inhibitor acarbose. *British Journal of Nutrition* **91**, 357-365, doi:10.1079/BJN20031063 (2004).
187 Weaver, G. A. *et al.* Biomarkers of Human Colonic Cell Growth Are Influenced Differently by a History of Colonic Neoplasia and the Consumption of Acarbose. *The Journal of Nutrition* **130**, 2718-2725, doi:10.1093/jn/130.11.2718 (2000).
188 Holt, P. R. *et al.* Effects of acarbose on fecal nutrients, colonic pH, and short-chain fatty acids and rectal proliferative indices. *Metabolism - Clinical and Experimental* **45**, 1179-1187, doi:10.1016/S0026-0495(96)90020-7 (1996).
189 Wolin, M. J. *et al.* Changes of fermentation pathways of fecal microbial communities associated with a drug treatment that increases dietary starch in the human colon. *Appl Environ Microbiol* **65**, 2807-2812, doi:10.1128/aem.65.7.2807-2812.1999 (1999).
190 Smith, B. J. *et al.* Changes in the gut microbiome and fermentation products concurrent with enhanced longevity in acarbose-treated mice. *BMC Microbiology* **19**, doi:10.1186/s12866-019-1494-7 (2019).
191 Weaver, G. A. *et al.* Acarbose Enhances Human Colonic Butyrate Production. *The Journal of Nutrition* **127**, 717-723, doi:10.1093/jn/127.5.717 (1997).
192 De Vuyst, L. & Leroy, F. Cross-feeding between bifidobacteria and butyrate-producing colon bacteria explains bifdobacterial competitiveness, butyrate production, and gas production. *Int J Food Microbiol* **149**, 73-80, doi:10.1016/j.ijfoodmicro.2011.03.003 (2011).
193 Fernandes, J., Su, W., Rahat-Rozenbloom, S., Wolever, T. M. S. & Comelli, E. M. Adiposity, gut microbiota and faecal short chain fatty acids are linked in adult humans. *Nutr Diabetes* **4**, e121-e121, doi:10.1038/nutd.2014.23 (2014).
194 Watanabe, Y., Nagai, F. & Morotomi, M. Characterization of Phascolarctobacterium succinatutens sp. nov., an asaccharolytic, succinate-utilizing bacterium isolated from human feces. *Applied and environmental microbiology* **78**, 511-518, doi:10.1128/AEM.06035-11 (2012).
195 Jumas-Bilak, E. *et al.* Dialister micraerophilus sp. nov. and Dialister propionicifaciens sp. nov., isolated from human clinical samples. *Int J Syst Evol Microbiol* **55**, 2471-2478, doi:10.1099/ijs.0.63715-0 (2005).
196 Chiasson, J. L. *et al.* Acarbose treatment and the risk of cardiovascular disease and hypertension in patients with impaired glucose tolerance: the STOP-NIDDM trial. *Jama* **290**, 486-494, doi:10.1001/jama.290.4.486 (2003).
197 Hanefeld, M. *et al.* Acarbose reduces the risk for myocardial infarction in type 2 diabetic patients: meta-analysis of seven long-term studies. *Eur Heart J* **25**, 10-16, doi:10.1016/s0195-668x(03)00468-8 (2004).

198 Zhang, L. *et al.* Alpha-Glucosidase Inhibitors Alter Gut Microbiota and Ameliorate Collagen-Induced Arthritis. *Frontiers in Pharmacology* **10**, doi:10.3389/fphar.2019.01684 (2020).
199 Chen, H.-H. *et al.* Acarbose Decreases the Rheumatoid Arthritis Risk of Diabetic Patients and Attenuates the Incidence and Severity of Collagen-induced Arthritis in Mice. *Scientific Reports* **5**, 18288, doi:10.1038/srep18288 (2016).
200 Chen, H. H. *et al.* Oral administration of acarbose ameliorates imiquimod-induced psoriasis-like dermatitis in a mouse model. *Int Immunopharmacol* **33**, 70-82, doi:10.1016/j.intimp.2016.02.001 (2016).
201 Harrison, D. E. *et al.* Acarbose, 17-α-estradiol, and nordihydroguaiaretic acid extend mouse lifespan preferentially in males. *Aging Cell* **13**, 273-282, doi:https://doi.org/10.1111/acel.12170 (2014).
202 Harrison, D. E. *et al.* Acarbose improves health and lifespan in aging HET3 mice. *Aging Cell* **18**, e12898, doi:https://doi.org/10.1111/acel.12898 (2019).
203 Tarling, C. A. *et al.* The search for novel human pancreatic alpha-amylase inhibitors: high-throughput screening of terrestrial and marine natural product extracts. *Chembiochem* **9**, 433-438, doi:10.1002/cbic.200700470 (2008).
204 Yuen, V. G. *et al.* Glucose lowering effect of montbretin A in Zucker Diabetic Fatty rats. *Molecular and Cellular Biochemistry* **411**, 373-381, doi:10.1007/s11010-015-2599-4 (2016).
205 Tysoe, C. R. *et al.* Synthesis of montbretin A analogues yields potent competitive inhibitors of human pancreatic α-amylase. *Chem Sci* **10**, 11073-11077, doi:10.1039/c9sc02610j (2019).
206 Rappé, M. S. & Giovannoni, S. J. The uncultured microbial majority. *Annu Rev Microbiol* **57**, 369-394, doi:10.1146/annurev.micro.57.030502.090759 (2003).
207 Maurice, C. F., Haiser, H. J. & Turnbaugh, P. J. Xenobiotics shape the physiology and gene expression of the active human gut microbiome. *Cell* **152**, 39-50, doi:10.1016/j.cell.2012.10.052 (2013).
208 Doud, D. F. R. *et al.* Function-driven single-cell genomics uncovers cellulose-degrading bacteria from the rare biosphere. *The ISME Journal* **14**, 659-675, doi:10.1038/s41396-019-0557-y (2020).
209 Nitta, N. *et al.* Raman image-activated cell sorting. *Nature Communications* **11**, doi:10.1038/s41467-020-17285-3 (2020).
210 Martinez-Garcia, M. *et al.* Capturing Single Cell Genomes of Active Polysaccharide Degraders: An Unexpected Contribution of Verrucomicrobia. *PLoS ONE* **7**, e35314, doi:10.1371/journal.pone.0035314 (2012).
211 Hehemann, J.-H. *et al.* Single cell fluorescence imaging of glycan uptake by intestinal bacteria. *The ISME Journal* **13**, 1883-1889, doi:10.1038/s41396-019-0406-z (2019).
212 Berry, D. & Loy, A. Stable-Isotope Probing of Human and Animal Microbiome Function. *Trends in Microbiology* **26**, 999-1007, doi:10.1016/j.tim.2018.06.004 (2018).
213 Berry, D. *et al.* Tracking heavy water (D2O) incorporation for identifying and sorting active microbial cells. *Proc Natl Acad Sci U S A* **112**, E194-203, doi:10.1073/pnas.1420406112 (2015).
214 Herrmann, E. *et al.* Determination of Resistant Starch Assimilating Bacteria in Fecal Samples of Mice by In vitro RNA-Based Stable Isotope Probing. *Frontiers in Microbiology* **8**, doi:10.3389/fmicb.2017.01331 (2017).

215 Kovatcheva-Datchary, P. *et al.* Linking phylogenetic identities of bacteria to starch fermentation in anin vitromodel of the large intestine by RNA-based stable isotope probing. *Environmental Microbiology* **11**, 914-926, doi:10.1111/j.1462-2920.2008.01815.x (2009).
216 Patnode, M. L. *et al.* Interspecies Competition Impacts Targeted Manipulation of Human Gut Bacteria by Fiber-Derived Glycans. *Cell* **179**, 59-73.e13, doi:10.1016/j.cell.2019.08.011 (2019).
217 Dridi, L., Altamura, F., Gonzalez, E., Lui, O., Kubinski, R., Pidgeon, R., Montagut, A., Chong, J., Xia, J., Maurice, C. F., Castagner, B. Identifying Glycan Consumers in Human Gut Microbiota using Metabolic Labeling Coupled to Fluorescence-Activated Cell Sorting. (2021).
218 Gonzalez, E., Pitre, F. E. & Brereton, N. J. B. ANCHOR: a 16S rRNA gene amplicon pipeline for microbial analysis of multiple environmental samples. *Environmental Microbiology* **21**, 2440-2468, doi:10.1111/1462-2920.14632 (2019).
219 Butta, H., Sardana, R., Vaishya, R., Singh, K. N. & Mendiratta, L. Bifidobacterium: An Emerging Clinically Significant Metronidazole-resistant Anaerobe of Mixed Pyogenic Infections. *Cureus* **9**, e1134-e1134, doi:10.7759/cureus.1134 (2017).
220 Taguer, M., Quillier, O. & Maurice, C. F. Effects of oxygen exposure on relative nucleic acid content and membrane integrity in the human gut microbiota. *PeerJ* **9**, 10602 (2021).
221 Fouhy, F. *et al.* The Effects of Freezing on Faecal Microbiota as Determined Using MiSeq Sequencing and Culture-Based Investigations. *PLOS ONE* **10**, e0119355, doi:10.1371/journal.pone.0119355 (2015).
222 Tang, Q. *et al.* Current Sampling Methods for Gut Microbiota: A Call for More Precise Devices. *Frontiers in Cellular and Infection Microbiology* **10**, doi:10.3389/fcimb.2020.00151 (2020).
223 Ringel, Y. *et al.* High throughput sequencing reveals distinct microbial populations within the mucosal and luminal niches in healthy individuals. *Gut microbes* **6**, 173-181 (2015).
224 Zmora, N. *et al.* Personalized Gut Mucosal Colonization Resistance to Empiric Probiotics Is Associated with Unique Host and Microbiome Features. *Cell* **174**, 1388-1405.e1321, doi:https://doi.org/10.1016/j.cell.2018.08.041 (2018).
225 Vandeputte, D. *et al.* Stool consistency is strongly associated with gut microbiota richness and composition, enterotypes and bacterial growth rates. *Gut* **65**, 57-62, doi:10.1136/gutjnl-2015-309618 (2016).
226 Duranti, S. *et al.* Genomic Characterization and Transcriptional Studies of the Starch-Utilizing Strain Bifidobacterium adolescentis 22L. *Applied and Environmental Microbiology* **80**, 6080-6090, doi:10.1128/aem.01993-14 (2014).
227 Zhou, Z., Zhang, Y., Zheng, P., Chen, X. & Yang, Y. Starch structure modulates metabolic activity and gut microbiota profile. *Anaerobe* **24**, 71-78, doi:https://doi.org/10.1016/j.anaerobe.2013.09.012 (2013).
228 Rios-Covian, D., Gueimonde, M., Duncan, S. H., Flint, H. J. & de los Reyes-Gavilan, C. G. Enhanced butyrate formation by cross-feeding between Faecalibacterium prausnitzii and Bifidobacterium adolescentis. *FEMS Microbiology Letters* **362**, doi:10.1093/femsle/fnv176 (2015).
229 Lopez-Siles, M. *et al.* Cultured Representatives of Two Major Phylogroups of Human Colonic Faecalibacterium prausnitzii Can Utilize Pectin, Uronic Acids, and Host-Derived

Substrates for Growth. *Applied and Environmental Microbiology* **78**, 420-428, doi:doi:10.1128/AEM.06858-11 (2012).
230 Benevides, L. *et al.* New Insights into the Diversity of the Genus Faecalibacterium. *Frontiers in Microbiology* **8**, doi:10.3389/fmicb.2017.01790 (2017).
231 Blanco, G., Sánchez, B., Fdez-Riverola, F., Margolles, A. & Lourenço, A. In silico Approach for Unveiling the Glycoside Hydrolase Activities in Faecalibacterium prausnitzii Through a Systematic and Integrative Large-Scale Analysis. *Frontiers in Microbiology* **10**, doi:10.3389/fmicb.2019.00517 (2019).
232 Cameron, E. A. *et al.* Multifunctional Nutrient-Binding Proteins Adapt Human Symbiotic Bacteria for Glycan Competition in the Gut by Separately Promoting Enhanced Sensing and Catalysis. *mBio* **5**, e01441-01414, doi:doi:10.1128/mBio.01441-14 (2014).
233 Newgard, C. B. *et al.* A Branched-Chain Amino Acid-Related Metabolic Signature that Differentiates Obese and Lean Humans and Contributes to Insulin Resistance. *Cell Metabolism* **9**, 311-326, doi:https://doi.org/10.1016/j.cmet.2009.02.002 (2009).
234 Bruslind, L. *Microbial Growth*, <https://bio.libretexts.org/@go/page/10667>

Abbreviations

ABC transporter: ATP-binding cassette transporter

ACN: acetonitrile

B. theta: *Bacteroides thetaiotaomicron*

BA: bile acid

BSH: bile salt hydrolase

cABB: custom anaerobe basal broth

CAZy database: Carbohydrate Active Enzymes database

CAZyme: carbohydrate-active enzyme

CBM: carbohydrate binding module

CD-F: fluorescein-conjugated cyclodextrin

CDI: *Clostridioides difficile* infection

DAA: differential abundance analysis

DF: dietary fiber

DMF: *N*,*N*-dimethyl formamide

DP: degree of polymerization

DT2: diabète de type 2

ESV: exact sequence variant

FACS: fluorescence activated cell sorting

FC: fold change

FISH: fluorescence in situ hybridization

FLA-PS: fluorescently-labeled polysaccharides

Fluorescein-NHS: 5/6-carboxyfluorescein *N*-hydroxysuccinimidyl ester

FSC: forward scatter

FXR: farnesoid X receptor

GF: germ-free

GH: glycosyl hydrolase

GH13: glycosyl hydrolase family 13

GIT: gastrointestinal tract

GLP-1: glucagon-like peptide 1

GM: gut microbiota

GPCR: G-protein coupled receptor

GUDCA: glycoursodeoxycholic acid

HDAC: histone deacetylase

HFD: high-fat diet

HPA: human pancreatic α-amylase

IBD: inflammatory bowel disease

LC-MS: liquid chromatography—mass spectrometry

LPS: lipopolysaccharide

MALDI-TOF: matrix-assisted laser desorption/ionization-time of flight

Mal-Fl: fluorescein-conjugated maltodextrin

MbA: montbretin A

MFI: median fluorescence intensity

MM: minimum medium

MRS medium: De Man, Rogosa and Sharpe medium

NaH: sodium hydride

NaOAc: sodium acetate

NYST-F: fluorescein-conjugated nystose

OD: optical density

OTU: operational taxonomic unit

PBS: phosphate buffered saline

PCR: polymerase chain reaction

PL: polysaccharide lyase

PUL: polysaccharide utilization locus

PYY: peptide YY

RDA: redundancy analysis

RNA-SIP: stable isotope probing coupled with 16S rRNA sequencing

RS: resistant starch

SCFA: short-chain fatty acid

SIP: stable isotope probing

SPF: specific-pathogen-free

SSC: side scatter

ssMRS medium: semi-synthetic De Man, Rogosa and Sharpe medium

Sus: starch utilization system

T2D: type 2 diabetes

TLR-4: toll-like receptor 4

Tregs: regulatory T cells

TSA: tryptic soy agar

Appendix A (Supplementary Methods)

LC-MS analysis of purified Mal-Fl fractions

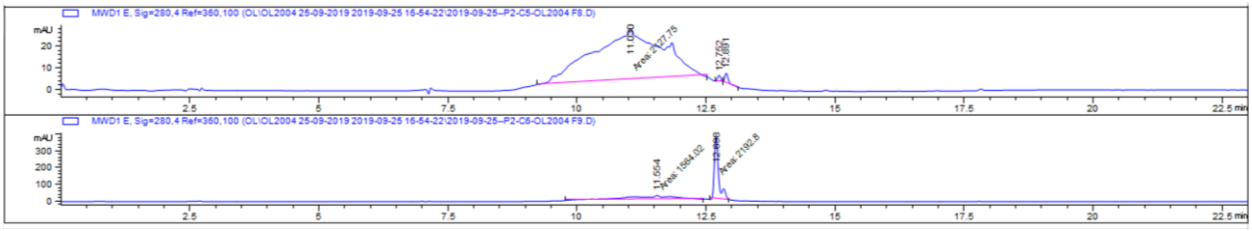

Figure 25. ***HPLC spectra of Mal-Fl fractions purified by size exclusion chromatography.*** *A broad peak is seen in fraction 8 (top) between 9.5 and 12.5 minutes, corresponding to the fluorescein-conjugated maltodextrins. The peak with a retention time between 12.5 and 13 minutes, seen in fraction 9 (bottom) corresponds to unconjugated fluorescein. Area under the peaks are integrated to calculate the approximate purity of the fraction.*

Flow cytometry gating approach

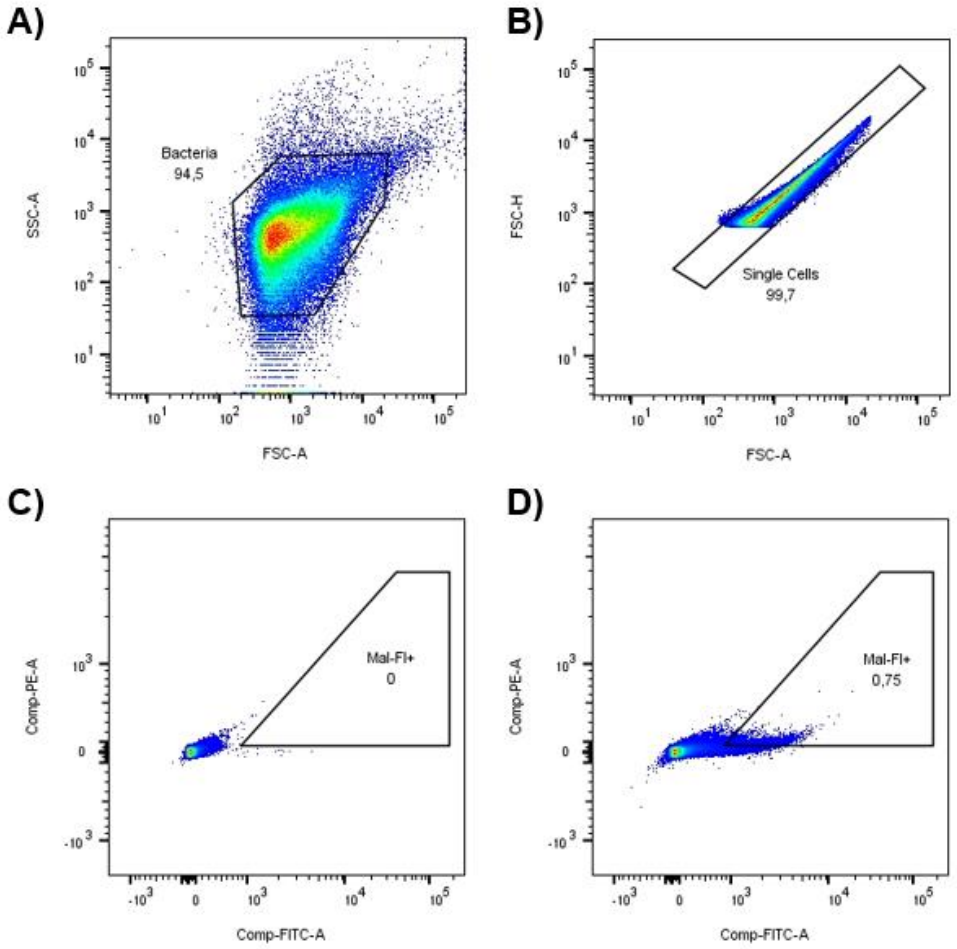

Figure 26. **Flow cytometry dot plots from Mal-Fl labeling assays.** A) SSC-A vs. FSC-A plot shows all events recorded in a sample. "Bacteria" gate includes the population of events considered to be bacteria. The percentage of the parent population is shown below the gate name. B) Within the "Bacteria" population, a "Single Cells" gate is designed in the FSC-H vs. HSC-A plot to include single cells and exclude doublets. C) Within the "Single Cells" population, a "Mal-Fl^{+}" gate is designed in the PE-A vs. FITC-A plot to include Mal-Fl labeled cells and exclude auto-fluorescent cells. A non-labeled negative control sample shows 0% of Single Cells are Mal-Fl^{+} cells. D) A labeled, non-treated control sample shows 0.75% of Single Cells are Mal-Fl^{+} cells.

Media

Custom Anaerobe Basal Broth (cABB)

Peptone (16 mg/mL), yeast extract (7 mg/mL), $NaHCO_3$ (4.8 mM), L-arginine (1 mg/mL), L-cysteine (0.5 mg/mL), dithiothreitol (1 mg/mL), NaCl (86 mM), sodium pyruvate (9 mM), sodium succinate (3 mM), sodium thioglycolate (4.4 mM), $FeSO_4 \cdot 7H_2O$ (15 μM), vitamin K1 (2.5 μg/mL) and hemin (6 μM).

Semi-synthetic DeMan, Rogosa and Sharpe (ssMRS)

Peptone (10 mg/mL), yeast extract (5 mg/mL), K_2HPO_4 (11.5 mM), $CH_3COONa \cdot 3H_2O$ (14.7 mM), triammonium citrate (2 mg/mL), $MgSO_4 \cdot 7H_2O$ (811 μM), $MnSO_4 \cdot H_2O$ (296 μM) and Tween-80 (1 μL/mL).

M2 Agar

Peptone (10 mg/mL), yeast extract (2.5 mg/mL), $NaHCO_3$ (47 mM), L-cysteine (1 mg/mL), dextrose (2 mg/mL), potato starch (2 mg/mL), KH_2PO_4 (3.3 mM), K_2HPO_4 (2.6 mM), $(NH_4)_2SO_4$ (6.8 mM), NaCl (15 mM), $MgSO_4 \cdot 7H_2O$ (365 μM), $CaCl_2 \cdot 2H_2O$ (809 μM), clarified rumen fluid (30% v/v) and agar (15 mg/mL).

Minimum Medium (MM)

$NaHCO_3$ (24 μM), L-cysteine (1 mg/mL), KH_2PO_4 (6.6 mM), NaCl (15 mM), $MgCl_2 \cdot 6H_2O$ (1 mM), $CaCl_2 \cdot 2H_2O$ (175 μM), $MnSO_4 \cdot H_2O$ (50 μM), $(NH_4)_2SO_4$ (5 mM), $FeSO_4 \cdot 7H_2O$ (15 μM), vitamin B12 (200 ng/mL), hemin (6 μM) and hematin (1.9 μM).

Appendix B (Supplementary Results)

MALDI mass spectra of non-functionalized maltodextrins

A)

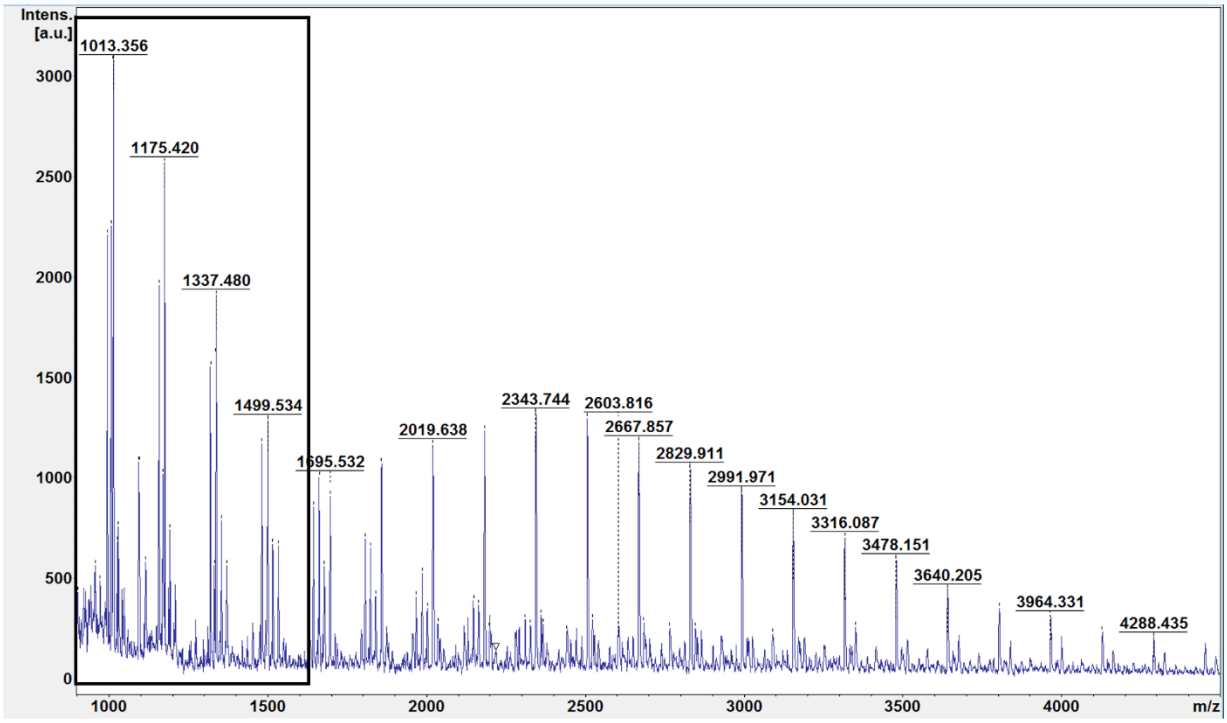

B)

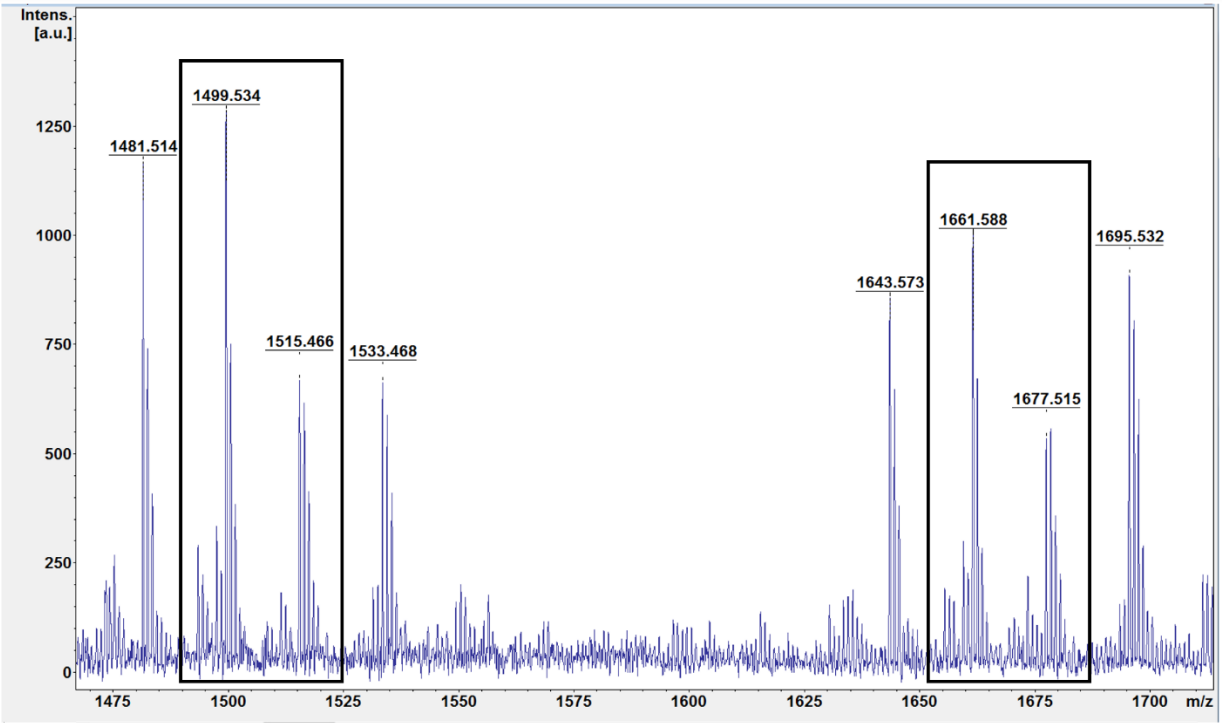

C)

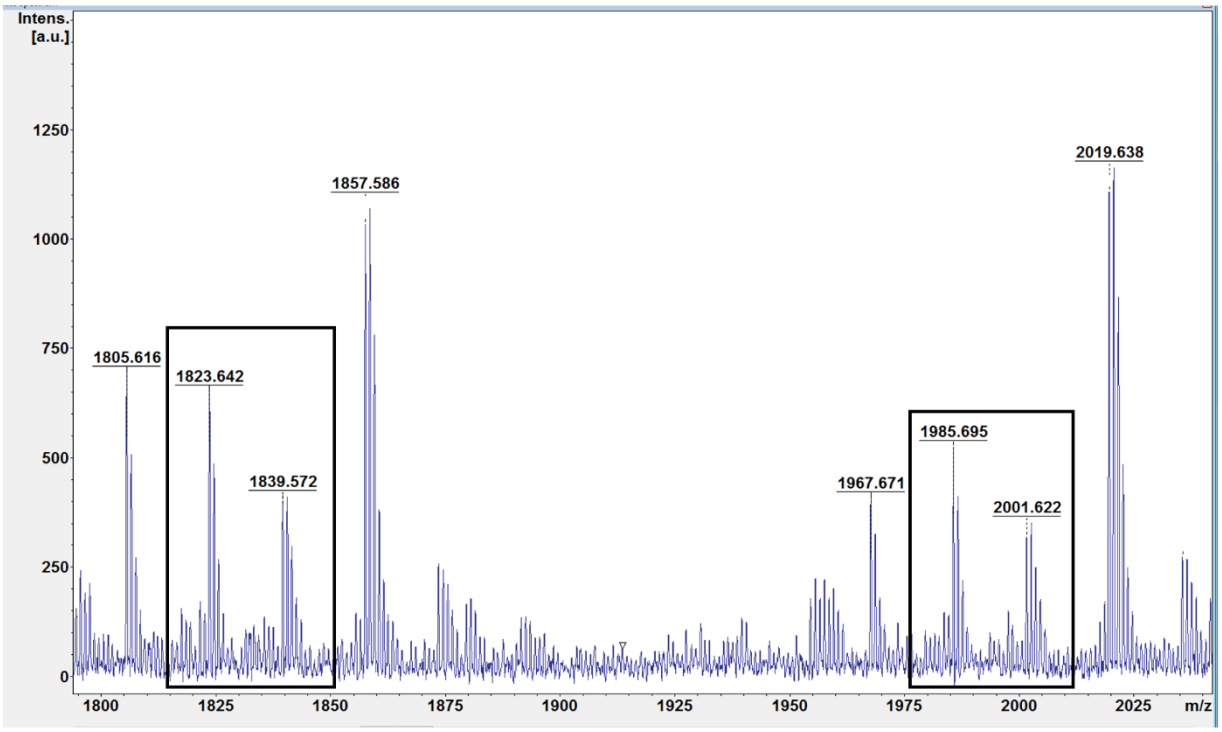

D)

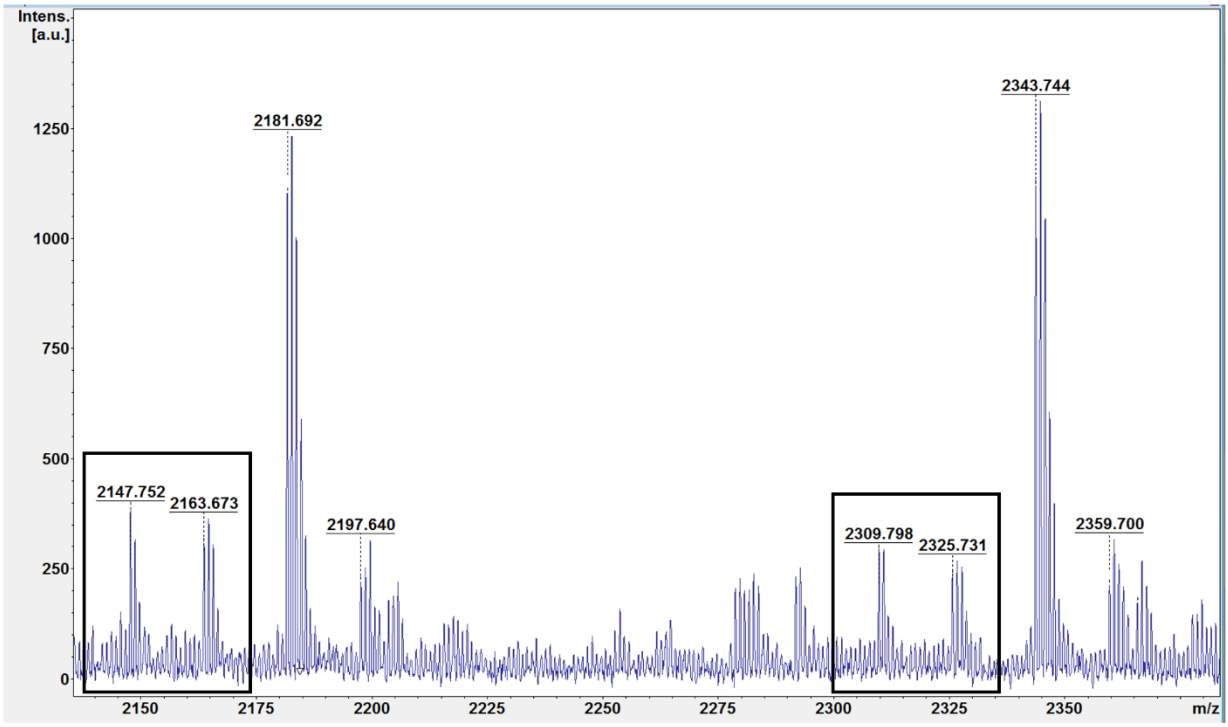

Figure 27. **MALDI mass spectra of purified Mal-Fl with identified m/z corresponding to non-functionalized maltodextrins with DP 6-14.** A) $(M+Na)^+$ of maltodextrins with DP 6-9. $(M+Na)^+$ and $(M+K)^+$ of maltodextrins with B) DP 9 and 10, C) DP 11 and 12, D) DP 13 and 14.

Table 5-1. **Specific masses of non-functionalized maltodextrins.**

Degree of polymerization	Chemical formula	m/z $(M+Na)^+$ calculated	m/z $(M+Na)^+$ found	m/z $(M+K)^+$ calculated	m/z $(M+K)^+$ found
6	$C_{36}H_{62}O_{31}$	1013.31	1013.356		
7	$C_{42}H_{72}O_{36}$	1175.37	1175.420		
8	$C_{48}H_{82}O_{41}$	1337.42	1337.480		
9	$C_{54}H_{92}O_{46}$	1499.47	1499.534	1515.44	1515.466
10	$C_{60}H_{102}O_{51}$	1661.52	1661.588	1677.49	1677.515
11	$C_{66}H_{112}O_{56}$	1823.58	1823.642	1839.55	1839.572
12	$C_{72}H_{122}O_{61}$	1985.63	1985.695	2001.60	2001.622
13	$C_{78}H_{132}O_{66}$	2147.68	2147.752	2163.65	2163.673
14	$C_{84}H_{142}O_{71}$	2309.73	2309.798	2325.70	2325.731

Growth metrics of bacterial isolates

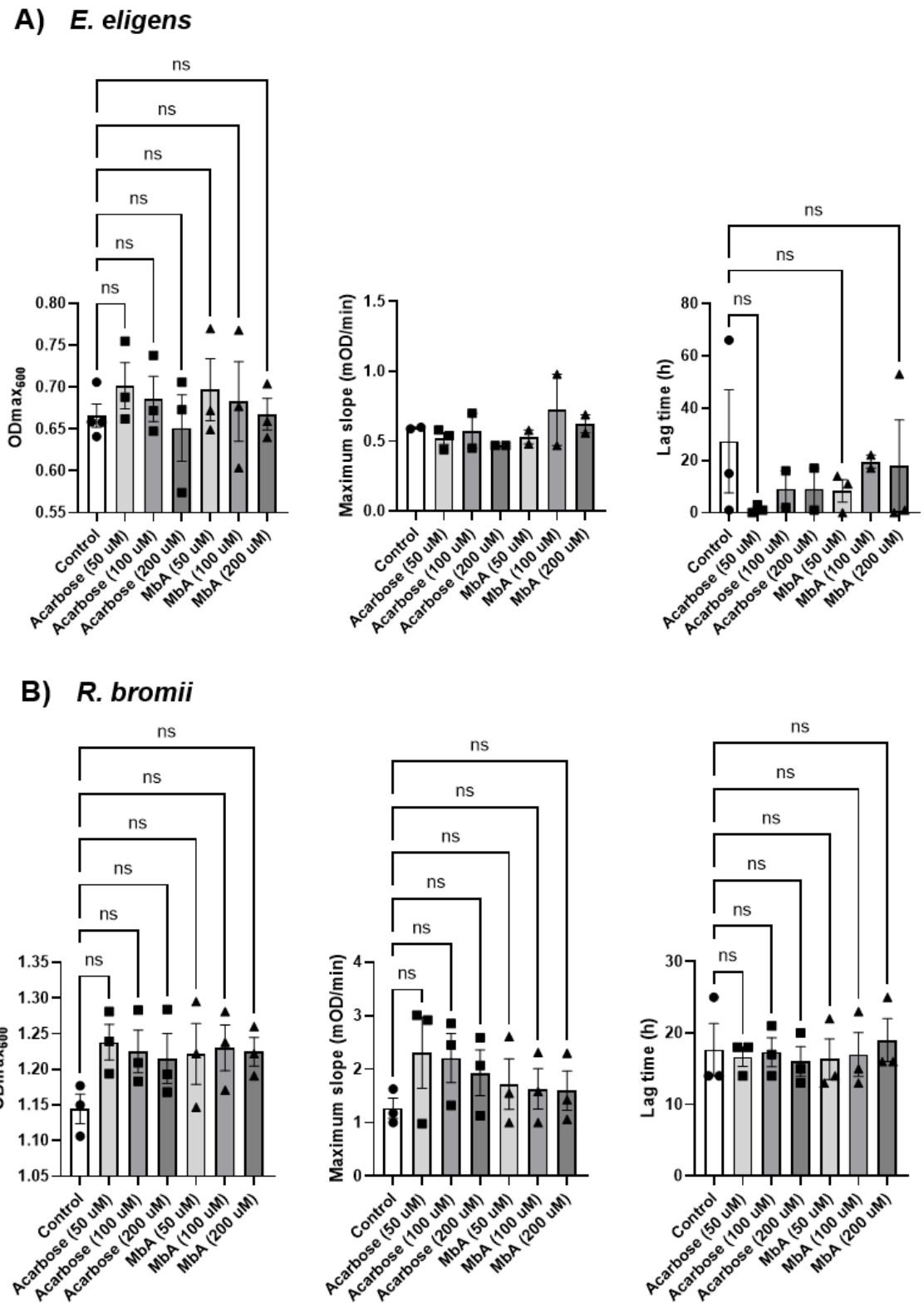

C) *B. vulgatus*

Maltodextrin

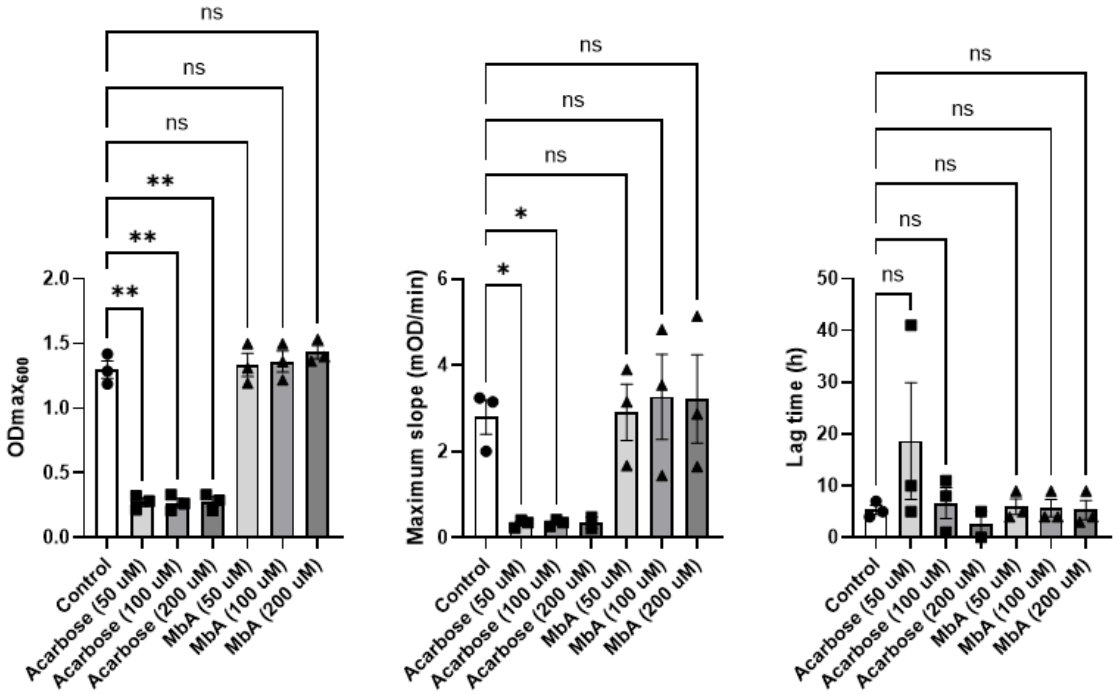

Glucose

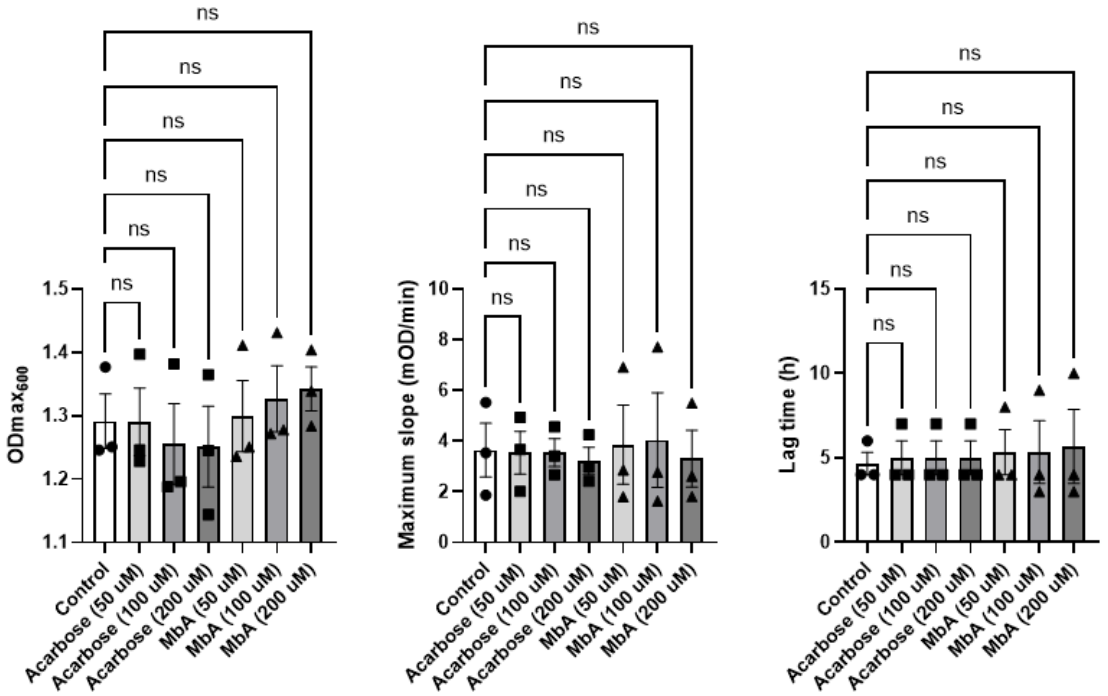

D) *A. rectalis*

Maltodextrin

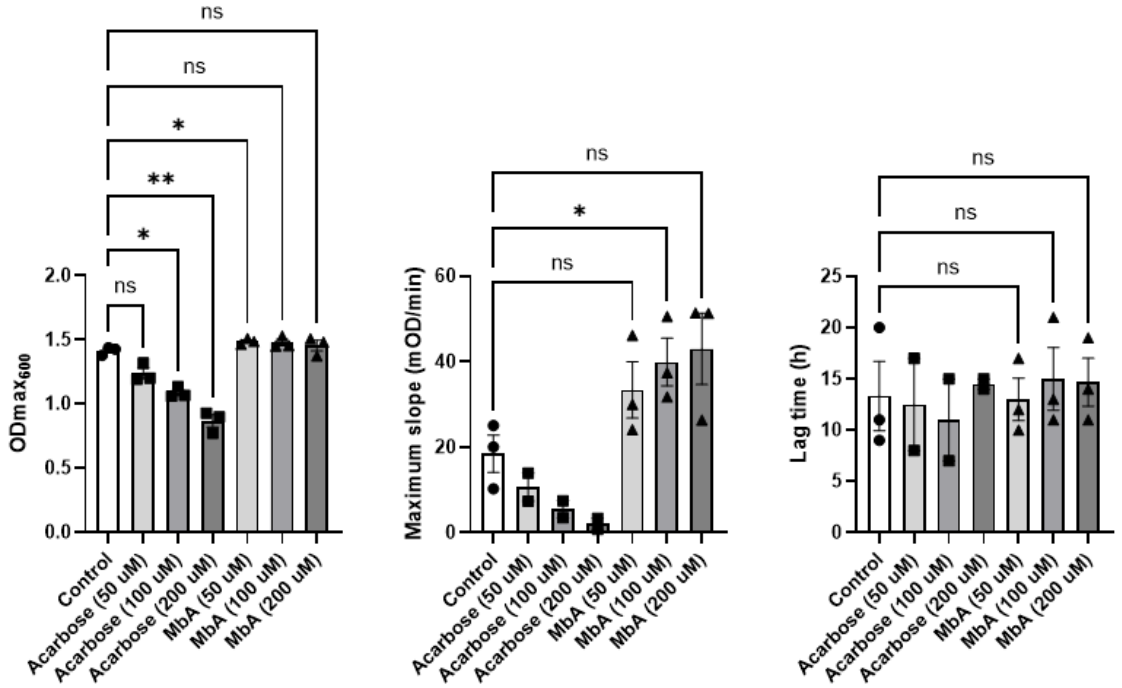

Glucose

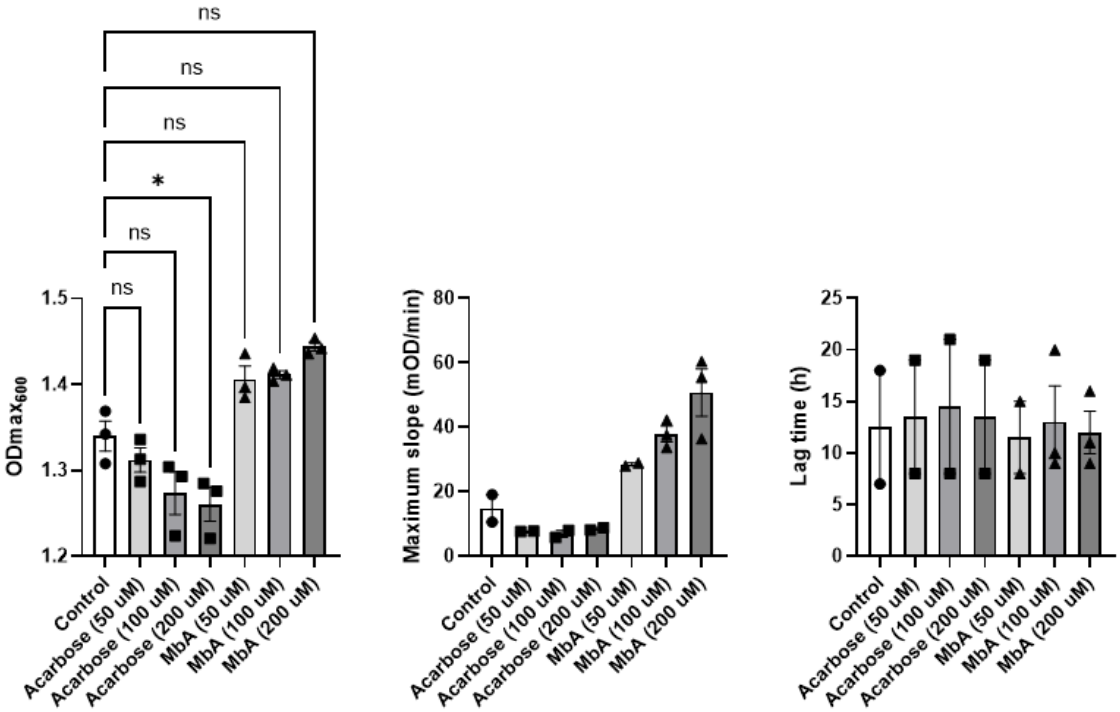

E) *B. xylanisolvens*

Maltodextrin

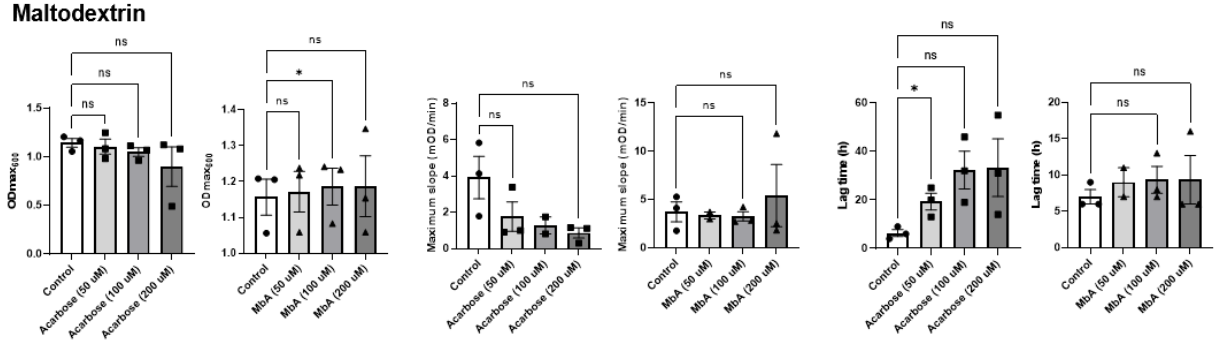

Glucose

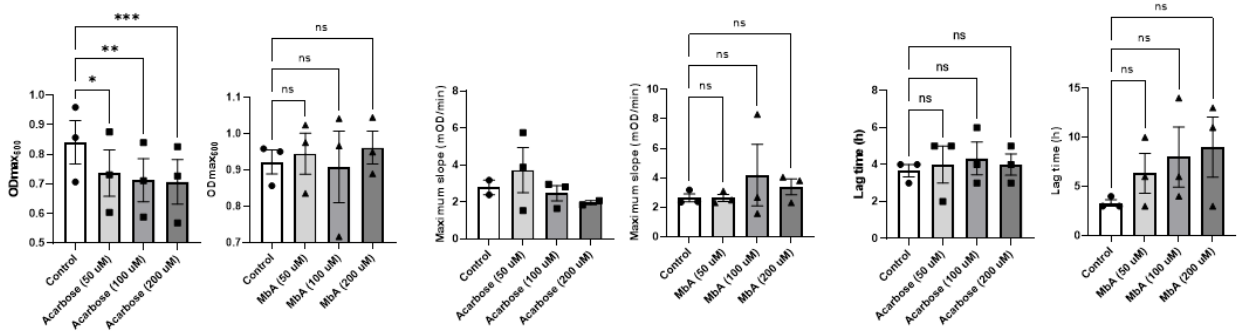

F) *B. adolescentis* DSM 20083

Maltodextrin

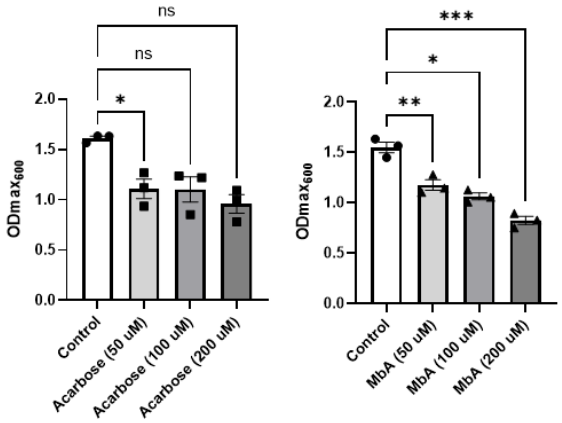

Glucose

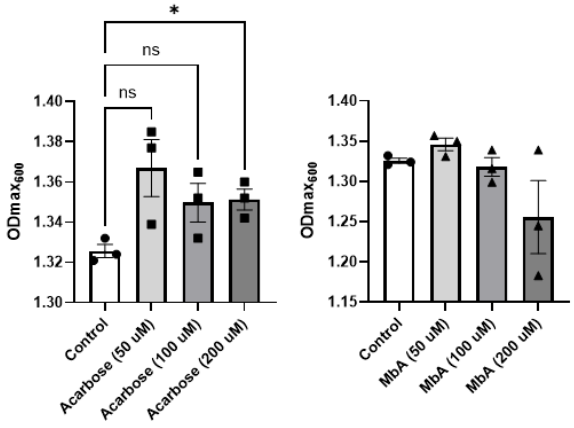

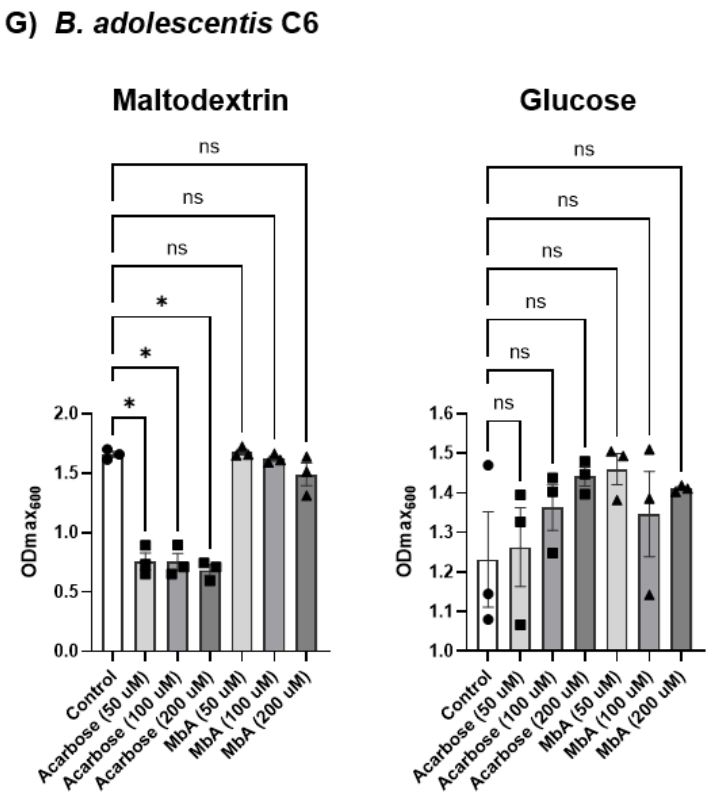

Figure 28. **Growth metrics of A) *E. eligens* ATCC 27750, B) *R. bromii* ATCC 27255, C) *B. vulgatus* ATCC 8482, D) *A. rectalis* ATCC 33656, E) *B. xylanisolvens*, F) *B. adolescentis* DSM 20083, and G) *B. adolescentis* C6.** Mean ± SEM are shown (n = 3). Repeated-measures ANOVA and Dunnett's multiple comparisons test were carried out for each metric; * $p < 0.05$, ** $p < 0.01$, *** $p < 0.001$. Some groups have missing values due to a negative value (i.e. for maximum slope), or an inappropriate value (i.e. lag time does not match the curve). Pairwise comparisons were not carried out for groups with missing values.

Gram staining of *B. adolescentis* strains

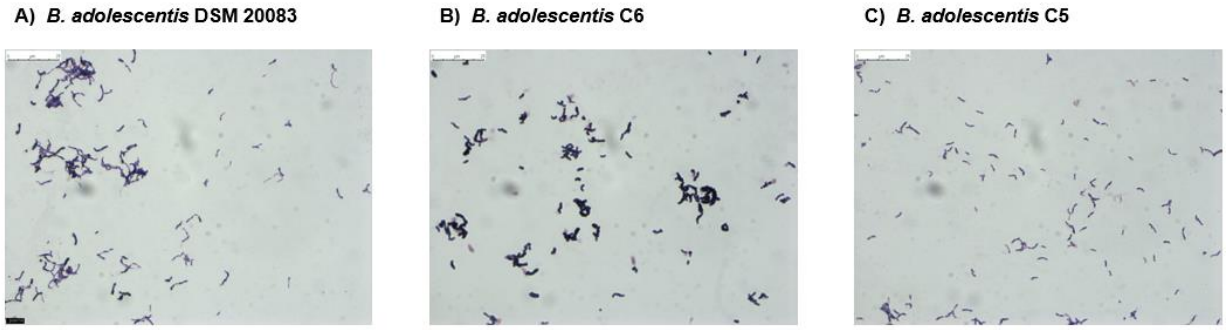

Figure 29. **Images of gram-stained smear of gram-positive *B. adolescentis* (100X, oil immersion).** A) DSM 20083, B) C6, C) C5.

Labeling of *B. vulgatus* ATCC 8482 with Mal-Fl

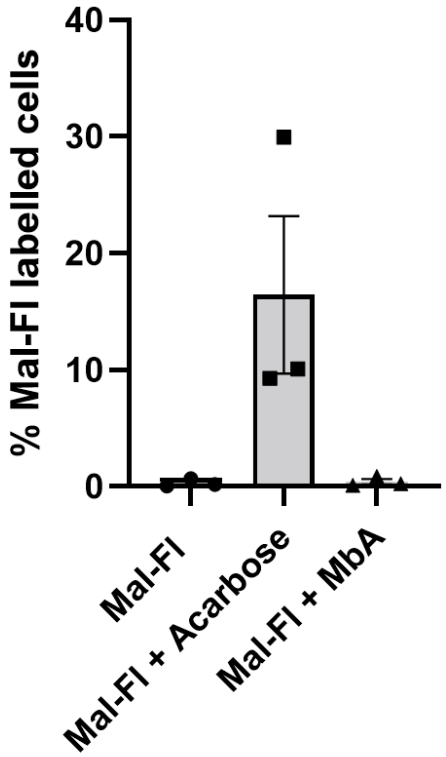

Figure 30. **Labeling of *B. vulgatus* ATCC 8482 with Mal-Fl in the absence and presence of amylase inhibitor.** Mean ± SEM (n = 3).